

On the coupling between the stratosphere and the troposphere

Citation for published version (APA):

Sigmond, M. (2003). *On the coupling between the stratosphere and the troposphere*. [Phd Thesis 1 (Research TU/e / Graduation TU/e), Applied Physics and Science Education]. Technische Universiteit Eindhoven. <https://doi.org/10.6100/IR570889>

DOI:

[10.6100/IR570889](https://doi.org/10.6100/IR570889)

Document status and date:

Published: 01/01/2003

Document Version:

Publisher's PDF, also known as Version of Record (includes final page, issue and volume numbers)

Please check the document version of this publication:

- A submitted manuscript is the version of the article upon submission and before peer-review. There can be important differences between the submitted version and the official published version of record. People interested in the research are advised to contact the author for the final version of the publication, or visit the DOI to the publisher's website.
- The final author version and the galley proof are versions of the publication after peer review.
- The final published version features the final layout of the paper including the volume, issue and page numbers.

[Link to publication](#)

General rights

Copyright and moral rights for the publications made accessible in the public portal are retained by the authors and/or other copyright owners and it is a condition of accessing publications that users recognise and abide by the legal requirements associated with these rights.

- Users may download and print one copy of any publication from the public portal for the purpose of private study or research.
- You may not further distribute the material or use it for any profit-making activity or commercial gain
- You may freely distribute the URL identifying the publication in the public portal.

If the publication is distributed under the terms of Article 25fa of the Dutch Copyright Act, indicated by the "Taverne" license above, please follow below link for the End User Agreement:

www.tue.nl/taverne

Take down policy

If you believe that this document breaches copyright please contact us at:

openaccess@tue.nl

providing details and we will investigate your claim.

On the coupling between the stratosphere and the troposphere

PROEFSCHRIFT

ter verkrijging van de graad van doctor aan de
Technische Universiteit Eindhoven, op gezag van de
Rector Magnificus, prof.dr. R.A. van Santen, voor een
commissie aangewezen door het College voor Promoties
in het openbaar te verdedigen op
maandag 27 oktober 2003 om 16.00 uur

door

Michael Sigmond

geboren te Arnhem

Dit proefschrift is goedgekeurd door de promotoren:

prof.dr. H. Kelder
en
prof.dr. F.W. Sluijter

Copromotor:
dr. P.C. Siegmund

Druk: Universiteitsdrukkerij Technische Universiteit Eindhoven

CIP-DATA LIBRARY TECHNISCHE UNIVERSITEIT EINDHOVEN

Sigmond, Michael

On the coupling between the stratosphere and the troposphere / by Michael Sigmond. –
Eindhoven : Technische Universiteit Eindhoven, 2003. – Proefschrift.

ISBN 90-386-1795-X

NUR 912

Trefw.: stratosfeer / troposfeer / atmosferische luchtstromingen / klimaatveranderingen /
stratosfeer-troposfeer uitwisseling

Subject headings: stratosphere / troposphere / atmospheric dynamics / climate change /
modelling / chemistry-climate interactions / stratosphere-troposphere coupling / stratosphere-
troposphere exchange

Voor mijn ouders en oma's

Cover:

Picture of the stratosphere and the troposphere.
The dark blue layer is the calm, dry stratosphere.
The clouds are situated in the turbulent troposphere.
Photograph: Anita van Kooten Niekerk

This PhD study has led to the following publications and manuscripts:

Sigmond, M., P.C. Siegmund, H. Kelder, and E. Manzini, 2003b: A simulation of the separate climate effects of middle atmospheric and tropospheric CO₂ doubling. *J. Climate*, submitted.

Chapter 2

Sigmond, M., P.C. Siegmund, and H. Kelder, 2003a: Analysis of the coupling between the stratospheric meridional wind and the surface level zonal wind during 1979-93 Northern Hemisphere extratropical winters. *Clim. Dyn.*, **21**, 211-219, doi: 10.1007/s00382-003-0328-2.

Chapter 3

Sigmond, M., J. Meloen, and P.C. Siegmund, 2000: Stratosphere-troposphere exchange in an extratropical cyclone, calculated with a Lagrangian method. *Ann. Geophys.*, **18**, 573-582.

Chapter 4

Fortuin, J.P.F., H.M. Kelder, M. Sigmond, R. Oemraw, and C.R. Becker, 2003: Inertial instability flow in the troposphere over Suriname during the South American Monsoon. *Geophys. Res. Lett.*, **30**, 1482, doi:10.1029/2002GL016754.

Meloen, J., P.C. Siegmund, and M. Sigmond, 2001: A Lagrangian computation of stratosphere-troposphere exchange in a tropopause folding event in the subtropical Southern Hemisphere. *Tellus*, **53**, 367-378.

Scaife, A.A., N. Butchart, M. Bourqui, J. de Grandpre, S. Hare, J. Kettleborough, U. Langematz, E. Manzini, F. Sassi, K. Shibata, D. Shindell and M. Sigmond, 2003: Model intercomparison of climate change in troposphere-stratosphere mass exchange, *in preparation*.

Contents

Samenvatting	1
1 Introduction	7
1.1 Vertical structure of the atmosphere.....	7
1.2 Influence of the troposphere on the stratosphere.....	9
1.3 Influence of the stratosphere on the troposphere.....	11
1.4 Arctic Oscillation.....	13
1.5 Stratosphere-troposphere exchange.....	14
1.6 Stratosphere-troposphere coupling and climate change.....	15
1.7 Stratospheric representation in general circulation models.....	17
1.8 Overview of this thesis.....	18
2 Simulation of the separate climate effects of middle atmospheric and tropospheric CO₂ doubling	21
2.1 Introduction.....	22
2.2 Model and set-up of the experiments.....	24
2.2.1 General Circulation Model.....	24
2.2.2 Experiments.....	24
2.3 Climate response to a uniform CO ₂ doubling.....	26
2.3.1 Control climate.....	26
2.3.2 Middle atmospheric response to uniform CO ₂ doubling.....	26
2.3.3 Tropospheric response to uniform CO ₂ doubling.....	32
2.4 Additivity of the non-uniform CO ₂ doubling responses.....	32
2.5 Middle atmospheric response to non-uniform CO ₂ doubling.....	35
2.5.1 Middle atmospheric response to tropospheric CO ₂ doubling (T-run).....	35
2.5.2 Middle atmospheric response to middle atmospheric CO ₂ doubling (M-run).....	37
2.6 Tropospheric response to non-uniform CO ₂ doubling.....	38
2.6.1 Tropospheric response to middle atmospheric CO ₂ doubling (M-run).....	38
2.6.2 Tropospheric response to tropospheric CO ₂ doubling (T-run).....	38
2.7 Additional experiments on the response of the troposphere to middle atmospheric CO ₂ doubling.....	39
2.7.1 Tropospheric response to middle atmospheric CO ₂ doubling without change of SSTs.....	40
2.7.2 Tropospheric response to CO ₂ doubling above 10 hPa.....	41

2.8	Discussion and conclusions.....	42
2.9	Appendix: Note on the tropical stratospheric vertical wind in MA-ECHAM.....	45
3	Analysis of the coupling between the stratospheric meridional wind and the surface level zonal wind during 1979-93 NH extratropical winters	49
3.1	Introduction.....	50
3.2	Data and method.....	51
3.3	Results.....	51
3.3.1	Meridional wind around 60°N.....	51
3.3.2	Meridional mass flux at 60°N and its effect on the polar cap mean surface pressure.....	54
3.3.3	Variations in the meridional surface pressure gradient and the zonal wind near the surface.....	59
3.3.4	Forces governing the meridional transport at 60°N.....	62
3.4	Summary and discussion.....	65
3.5	Appendix: Simple model of the upper and lower level meridional flow.....	67
4	Stratosphere-troposphere exchange in an extratropical cyclone, calculated with a Lagrangian method	71
4.1	Introduction.....	72
4.2	Method and data.....	74
4.2.1	Calculation of the air mass flux across a <i>PV</i> -surface.....	74
4.2.2	Trajectory model.....	76
4.2.3	ECMWF-data.....	77
4.3	Results.....	77
4.3.1	Synoptic situation.....	77
4.3.2	Geographical distribution of the flux across <i>PV</i> -surfaces.....	77
4.3.3	Decomposition of the flux.....	80
4.3.4	Vertical cross-sections of the air mass flux across <i>PV</i> -surfaces.....	80
4.3.5	Area-averaged upward and downward fluxes.....	84
4.4	Discussion.....	84
4.4.1	Parameterisation of <i>PV</i> -mixing in the ECMWF-model.....	84
4.4.2	Method for calculating the flux across a <i>PV</i> -surface.....	85
4.4.3	Comparison of F_{up}/F_{down} with previous studies.....	87
4.5	Conclusions.....	88

5 Summary and outlook	91
5.1 Summary.....	91
5.2 Outlook.....	94
References	99
Nawoord	109
Curriculum Vitae	111

Samenvatting

Deze samenvatting is speciaal geschreven voor de 'leek', in de hoop het onderzoek dat ik de afgelopen jaren heb uitgevoerd ook begrijpelijk te maken voor mensen buiten het klimaatonderzoek.

Inleiding

Traditioneel wordt de atmosfeer ingedeeld in verschillende lagen (zie figuur 1.1). De onderste laag wordt de troposfeer genoemd. Deze laag steekt zich uit vanaf het aardoppervlak tot ongeveer 15 kilometer hoogte. In deze laag vinden we het grootste gedeelte van de verschijnselen die we tezamen het weer noemen. In deze zelfde laag wonen en werken we. Daarom beïnvloeden de veranderingen van de troposfeer ons direct.

De laag boven de troposfeer wordt de stratosfeer genoemd. In deze laag, die zich uitstrekt vanaf de top van de troposfeer tot ongeveer 50 kilometer hoogte, vinden we de ozonlaag. Deze laag met verhoogde concentratie van ozon beschermt het leven op aarde voor schadelijke kortgolvlige zonnestraling. De ontdekking van het zogeheten Antarctische ozongat in de jaren '80 van de vorige eeuw was daarom reden tot zorg.

Het begrijpen van de koppeling tussen de troposfeer en de stratosfeer is belangrijk voor het begrijpen van het huidige klimaat én van klimaatverandering. Aan de ene kant heeft de troposfeer een grote invloed op de stratosfeer. In de troposfeer worden grootschalige atmosferische golven opgewekt door bergen en land-zeecontrasten, die zich vervolgens omhoog voortplanten naar de stratosfeer. Door de afname van de luchtdichtheid met de hoogte breken deze golven op een gegeven moment, net zoals zeegolven op het strand. Hierdoor wordt er in de stratosfeer een grootschalige circulatie aangedreven, die bestaat uit stijgende bewegingen in de tropen, poolwaartse beweging op gematigde breedten en dalende bewegingen boven de polen (zie ook figuur 1.2). Deze stratosferische circulatie wordt ook wel de Brewer-Dobsoncirculatie genoemd. Deze circulatie kan de waargenomen stratosferische verdelingen van diverse belangrijke chemische stoffen als waterdamp en ozon goed verklaren. Bovendien is het de belangrijkste aandrijver van de uitwisseling van lucht tussen de troposfeer en de stratosfeer.

Aan de andere kant heeft de stratosfeer ook invloed op de troposfeer. Het is bijvoorbeeld gebleken dat stofdeeltjes die na een grote vulkaanuitbarsting in de stratosfeer terechtkomen, een gedeelte van de zonnestraling tegenhouden en ervoor zorgen dat gedurende een aantal jaar de wereldgemiddelde temperatuur aan het aardoppervlak lager is dan normaal. Een onderwerp dat momenteel veel aandacht krijgt is de voortplanting van variaties in de westenwinden van de stratosfeer naar het aardoppervlak. Het blijkt dat variaties in de

stratosferische westenwinden in veel gevallen een paar weken later leiden tot soortgelijke variaties in de troposferische westenwinden. De sterkte van de laatstgenoemde winden is in de winter erg belangrijk voor het weer in bijvoorbeeld West-Europa. Een sterke westenwind zorgt dan voor transport van relatief warme, vochtige oceaanolucht naar West-Europa, waardoor het weer relatief zacht en nat is. Momenteel wordt onderzocht of het feit dat variaties in de stratosferische westenwinden voorbodes lijken te zijn van soortgelijke variaties in de troposfeer, uitgebuit kan worden om de weersverwachting op langere termijn (10-60 dagen) te verbeteren.

Dit proefschrift

De afgelopen jaren is de wintertemperatuur boven Europa en Azië toegenomen. Dit kan voor ongeveer de helft worden toegeschreven aan de toegenomen troposferische westenwinden. Het feit dat in ons huidige klimaat de westenwinden in de stratosfeer invloed lijken te hebben op de westenwinden in de troposfeer, doet vermoeden dat de stratosfeer ook een belangrijke rol kan spelen bij het versterken van de troposferische westenwinden. De waargenomen opwarming aan het oppervlak in Nederland zou dus deels veroorzaakt kunnen zijn door stratosferische processen.

Klimaatmodellen verwachten dat de toenemende concentratie van broeikasgassen als kooldioxide zal leiden tot een toename van de troposferische westenwinden op gematigde breedten. In **hoofdstuk 2** wordt onderzocht of deze toename van troposferische westenwinden toegeschreven kan worden aan troposferische of stratosferische processen. In verschillende experimenten met een numeriek klimaatmodel is de kooldioxideconcentratie verdubbeld in de gehele atmosfeer, in alleen de troposfeer en in alleen de stratosfeer. In overeenstemming met berekeningen met andere klimaatmodellen vinden we een toename van de troposferische westenwinden in het experiment waarin de kooldioxideconcentratie in de hele atmosfeer is verdubbeld. Deze toename vinden we ook in het experiment waarin alleen de stratosferische kooldioxide is verdubbeld, maar niet in het experiment met de troposferische kooldioxideverdubbeling. Deze resultaten suggereren dat niet de troposferische, maar de stratosferische kooldioxidetoe name de belangrijkste oorzaak is van de toegenomen troposferische westenwinden. Ze onderstrepen het belang van de stratosfeer voor het klimaat in de troposfeer, de laag waarin wij leven.

De meeste klimaatmodellen voorspellen een versterking van de Brewer-Dobsoncirculatie als gevolg van de toenemende broeikasgassen. Deze toename en de consequenties ervan voor de stratosferische temperatuur zullen vermoedelijk leiden tot een kleine versnelling van het herstel van de ozonlaag. Met behulp van de experimenten uit hoofdstuk 2 is vastgesteld dat deze versterking vooral veroorzaakt wordt door de troposferische kooldioxidetoe name. Dit resultaat is consistent met het feit dat de Brewer-

Dobsoncirculatie voornamelijk wordt aangedreven door grootschalige atmosferische golven die in de troposfeer worden opgewekt.

Lange tijd werd gedacht dat de toestand van de stratosfeer niet wezenlijk van invloed is op het weer aan het aardoppervlak en werd de stratosfeer niet of nauwelijks meegenomen in klimaatmodellen. Veel klimaatmodellen hadden een paar jaar geleden nog een top rond 30 kilometer hoogte (ergens halverwege de stratosfeer), terwijl tegenwoordig de top rond 85 kilometer hoogte ligt. De hierboven beschreven resultaten suggereren dat stratosferische klimaatverandering een grote invloed heeft op het klimaat in de troposfeer. In hoofdstuk 2 is onderzocht hoeveel van de invloed van de stratosferische klimaatverandering op de troposfeer wordt gemist door de oudere 'lagere' modellen. Hiertoe hebben we in ons klimaatmodel de kooldioxideconcentratie alleen verdubbeld in de laag tussen 30 en 85 kilometer hoogte (de top van het model). De resultaten laten zien dat kooldioxideverdubbeling in alleen al deze lagen leidt tot een significante versterking van de westenwinden op de gematigde breedten in de troposfeer in de winter. Als deze lagen niet meegenomen zouden worden in klimaatmodellen (zoals het geval is bij de oudere lagere modellen), zou dus een deel van de invloed van stratosferische klimaatverandering op de troposfeer worden gemist. Het ophogen van de modellen lijkt dus een belangrijk stap in het verbeteren van berekeningen van het toekomstige (troposferische) klimaat.

De koppeling tussen de troposfeer en de stratosfeer is verder bestudeerd door het onderzoeken via welk dynamisch mechanisme de stratosfeer invloed heeft op de troposfeer. Verschillende hypothesen voor een dergelijk mechanisme zijn geponeerd in de recente literatuur. In **hoofdstuk 3** hebben we één van die hypothesen getoetst door wind- en luchtdrukgegevens te analyseren van het Europese weercentrum voor de winters van 1979 tot 1993. Hierbij zijn verschillende aanwijzingen gevonden dat er op de gematigde breedten een koppeling bestaat tussen de noord-zuid (meridionale) component van de wind in de stratosfeer, en de oost-west (zonale) component van de wind in de troposfeer:

- Op gematigde breedten zijn de variaties in de meridionale component van de wind in de stratosfeer tegengesteld aan die in de troposfeer.
- Laagfrequente variaties in de meridionale component van de wind in de stratosfeer lopen gemiddeld ongeveer een dag voor op soortgelijke variaties in de troposfeer.
- Dit tijdsverschil heeft invloed op de luchtdrukverdeling aan de grond: als de stratosferische stroming toeneemt (d.w.z. sterker noordelijk of minder sterk zuidelijk), zal de troposferische stroming pas een dag later afnemen (sterker zuidelijk of minder sterk noordelijk). Gevolg is dat in die tussentijd de hoeveelheid lucht, ofwel de luchtdruk, in het gebied ten noorden van de gematigde breedten (de polaire kap) zal toenemen. (Het omgekeerde geldt als de stratosferische stroming afneemt)
- Het luchtdrukverschil tussen de polaire kap en het gebied ten zuiden daarvan blijkt voornamelijk bepaald te worden door de luchtdrukveranderingen in de polaire kap.

- Dit luchtdrukverschil is via een krachtenbalans gekoppeld aan de oost-west (zonale) component van de wind in de troposfeer.

Op deze manier lijkt het tijdsverschil tussen de variaties in de meridionale stromingen in de stratosfeer en de troposfeer invloed te hebben op de oost-west component van de wind in de troposfeer.

In **hoofdstuk 4** is de uitwisseling van lucht tussen de troposfeer en de stratosfeer onderzocht. Het berekenen van de grootte van deze luchtstromen door de tropopause (het grensvlak tussen de troposfeer en stratosfeer) op een bepaald moment op een bepaalde plaats uit wind- en temperatuurgegevens brengt de nodige complicaties met zich mee. Veel traditionele rekentechnieken zijn niet erg betrouwbaar, omdat die gebruik maken van formules die de grootte van de luchtstroom (de flux) beschrijven als de som van twee of meer termen. In het berekenen van deze termen zitten onzekerheden. Omdat in veel gevallen de netto flux klein is vergeleken met deze termen, leidt een kleine fout in de termen al gauw tot een grote relatieve fout in de netto flux. In hoofdstuk 4 hebben we een techniek geïntroduceerd die dit probleem omzeilt. Deze techniek maakt gebruik van trajectoriën (banen van luchtdeeltjes) en de grootte potentiële vorticititeit (een grootte waarin de stabiliteit en de draaiing van lucht is verwerkt). De formule voor de flux tussen de troposfeer en stratosfeer bestaat met deze rekentechniek uit slechts één term, waardoor de techniek geen last heeft van de hierboven beschreven problemen van de traditionele rekenmethoden. De rekentechniek is toegepast op een lagedrukgebied. In tropopauzevouw - gebieden waar de tropopauze relatief laag ligt - blijkt er een grote flux van lucht van de stratosfeer naar de troposfeer te zijn. In tropopauzeruggen - gebieden waar de tropopauze relatief hoog ligt - vinden we kleinere luchtstromen van de troposfeer naar de stratosfeer. De resultaten uit hoofdstuk 4 suggereren, samen met resultaten van een vergelijkingsstudie van rekentechnieken in Europees verband, dat de geïntroduceerde techniek betrouwbaar is.

Het onderzoek gepresenteerd in dit proefschrift heeft geleid tot een beter begrip van verschillende aspecten van de koppeling tussen de troposfeer en de stratosfeer. Met behulp van berekeningen met een klimaatmodel is aannemelijk gemaakt dat belangrijke circulatieveranderingen in de troposfeer toegeschreven kunnen worden aan veranderingen in de stratosfeer. Andersom hebben veranderingen in de troposfeer ook invloed op de stratosfeer, de laag waarin we de voor ons belangrijke ozonlaag vinden. Het ophogen van de klimaatmodellen opdat de stratosfeer volledig wordt meegenomen lijkt een belangrijke stap voorwaarts te zijn in de modellering van de troposfeer. Verder wijst het onderzoek op het bestaan van een dynamisch mechanisme waarbij de stratosfeer de troposfeer beïnvloedt via variaties in de stratosferische en troposferische noord-zuid (meridionale) stromingen. Tenslotte is er een nieuwe, meer betrouwbare rekenmethode geïntroduceerd voor het bepalen van de grootte van de luchtstroom tussen de troposfeer en de stratosfeer.

Chapter 1

Introduction

In this thesis several aspects of the coupling between the stratosphere and the troposphere are investigated. The understanding of this coupling is relevant for the understanding of the present climate and of climate change. For example, tropospheric waves drive the stratospheric meridional circulation that can explain much of the stratospheric water vapour and ozone distributions. Stratospheric zonal wind variations often precede similar variations in the troposphere, which could be exploited to improve long-range weather forecasts. It is believed that the increase of greenhouse gases concentrations has caused stratospheric zonal wind changes, which, in turn, could have induced tropospheric zonal wind changes. Since greenhouse gas concentrations will increase even further in the next century, the understanding of these processes is relevant for understanding future climate change. In this Introduction a concise summary on stratosphere-troposphere coupling is presented. First, the basic vertical structure of the atmosphere will be described, and the troposphere and stratosphere will be defined (section 1.1). Then, it will be described how tropospheric processes influence the stratosphere (section 1.2), and how stratospheric processes influence the troposphere (section 1.3). Thereafter, the Arctic Oscillation (or: Northern Annular Mode), the framework in which much of the recent research on stratosphere-troposphere coupling has been done, will be introduced (section 1.4). In section 1.5, some aspects of the exchange of air between the stratosphere and troposphere will be described. The importance of stratosphere-troposphere coupling for understanding climate change will be discussed in section 1.6. The stratospheric representation in General Circulation Models will be discussed in section 1.7. This chapter will be concluded by a description of the major research goals of this thesis.

1.1 Vertical structure of the atmosphere

Before investigating the coupling between the stratosphere and the troposphere, it should be clear what exactly is meant by the ‘stratosphere’ and the ‘troposphere’. The atmosphere is conventionally divided into several layers, according to the temperature distribution with height (Fig. 1.1). The lowermost layer extends from the surface to approximately 15 km altitude, and is called the troposphere. This is the layer in which almost all human activities and weather phenomena occur, and which contains about 85% of the atmospheric mass. Since the troposphere is mainly heated from the ground, the tropospheric temperature decreases with height. This implies a low static stability, leading to rapid vertical mixing on timescales

from hours to days. This basic property of the troposphere is reflected in its name: troposphere stems from the Greek word *tropos*, which means turning, or mixing.

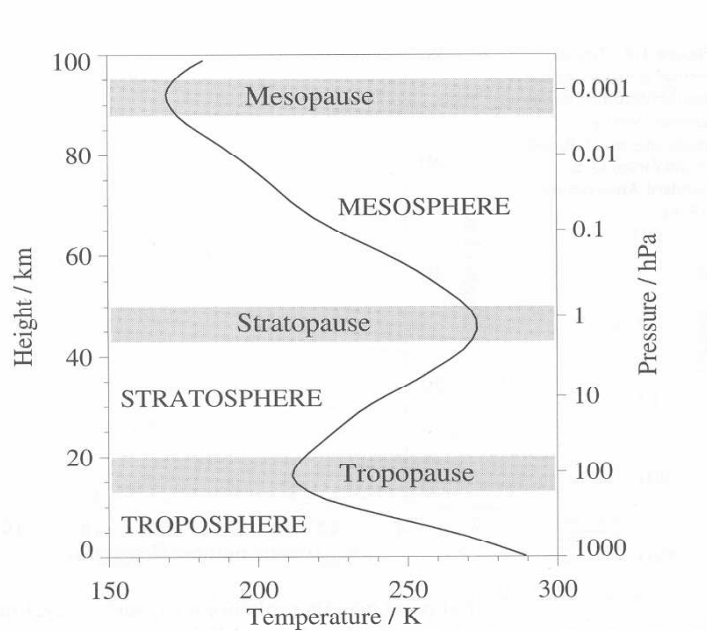


Fig. 1.1: A typical vertical temperature distribution in the lowest 100 km of the atmosphere. After Andrews (2000).

The upper boundary of the troposphere is called the tropopause. Two different definitions of the tropopause are widely used. The traditional definition is based on the difference between the tropospheric and stratospheric temperature lapse rate (the ‘thermal’ definition). The thermal tropopause is assigned to the lowest level at which the temperature lapse rate decreases to 2 K km^{-1} or less, provided that the average lapse rate between this level and the upper levels within 2 km does not exceed 2 K km^{-1} . An alternative way to define the tropopause is based on dynamical features, and is therefore referred to as the ‘dynamical’ definition. The dynamical tropopause is assigned to the level where the potential vorticity (PV) reaches a critical value, varying from 1.5 to 3.5 PVU ($1 \text{ PVU} = 1 \times 10^{-6} \text{ K m}^2 \text{ kg}^{-1} \text{ s}^{-1}$). The PV is defined as:

$$PV = -g(f + \zeta) \frac{\partial \theta}{\partial p}, \quad (1.1)$$

where g denotes the acceleration due to gravity, f is the Coriolis parameter, ζ is the relative vorticity, θ is the potential temperature and p is pressure. The tropopause separates low PV values in the troposphere from high PV values in the stratosphere. The advantage of the

dynamical definition is that it generally results in a better spatial and temporal continuity of the tropopause, because PV is conserved in adiabatic flows.

The layer extending from the tropopause to approximately 50 km altitude is the stratosphere. The stratospheric temperature increases with height, which is mainly due to the absorption of solar ultraviolet radiation by ozone. Because of the resulting large stratospheric static stability, rapid vertical motions are suppressed. The fact that in the stratosphere horizontal mixing is more important than vertical mixing is captured by its name: stratosphere stems from the Latin word *stratum*, which means layered. The stratosphere is bounded above by the stratopause. The mesosphere is situated on top of the stratosphere and extends from the stratopause to approximately 85 km altitude. The mesospheric temperature decreases with altitude owing to the reduced solar heating of ozone. The mesosphere is bounded above by the mesopause, where the lowest temperatures of the atmosphere occur. The stratosphere and mesosphere together are referred to as the middle atmosphere.

In the region above the mesosphere, commonly referred to as the upper atmosphere, ionisation processes become important, and the temperature increases dramatically with height. This thesis focuses on the lower and middle atmosphere, and in particular on the coupling between the stratosphere and the troposphere.

1.2 Influence of the troposphere on the stratosphere

Since the troposphere holds the largest part of the atmospheric mass, it is not surprising that it influences the stratospheric circulation. An important mechanism through which the troposphere influences the stratosphere involves atmospheric waves. Gravity and planetary waves excited in the extratropical troposphere propagate upward into the stratosphere where they break and exert a forcing on the stratospheric mean flow. The net result of wave breaking is a westward force on the zonal-mean zonal flow, creating an imbalance between the Coriolis force on the zonal-mean zonal wind and the meridional pressure gradient force, and driving an extratropical poleward flow. By mass continuity, this poleward flow is compensated by upward motions in the tropics and downward motions in the polar regions. The tropical upward motions are accompanied by expansion and adiabatic cooling, driving the temperature below the radiative equilibrium temperature, whereas the polar downward motions are accompanied by compression and adiabatic warming, driving the temperature above the radiative equilibrium temperature. This meridional overturning circulation is commonly referred to as the Brewer-Dobson, residual mean or diabatic circulation, and is schematically depicted by Fig. 1.2. The term ‘diabatic circulation’ may be a bit misleading. Although the meridional circulation is accompanied by radiative heating and cooling, it is not forced by it. Rather, the meridional circulation is a dynamical response to the wave forcing in the extratropical stratosphere driving the stratosphere from its radiatively determined state, thus *causing* the radiative heating and cooling patterns.

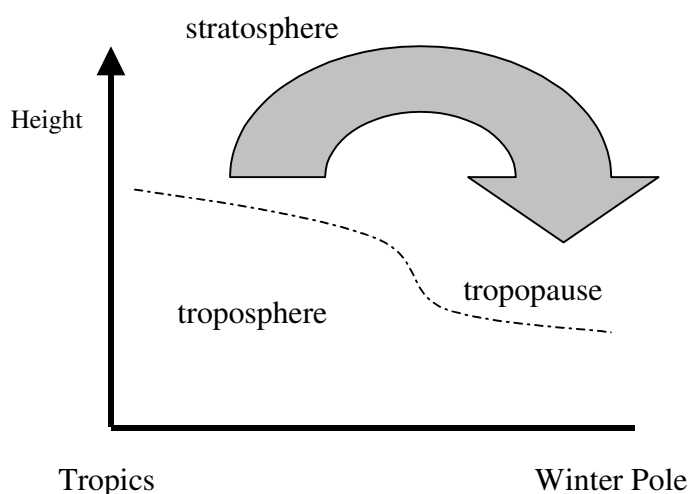


Fig. 1.2: Schematic representation of the stratospheric Brewer-Dobson circulation, which is mainly driven by breaking of troposphericly originated waves.

The stratospheric wave activity and associated wave forcing is largest during winter, which can be explained by linear wave theory first derived by Charney and Drazin (1961). They showed that the background wind should meet certain conditions for the planetary waves to propagate upward: the background wind should be westerly, but it should be less than a critical value. This critical value depends on the wavelength of the planetary waves, such that only the waves with the longest horizontal wavelengths can propagate upward. This so-called ‘Charney-Drazin criterion’ is only met during certain periods in winter. The stratospheric winter wave activity in the Northern Hemisphere is larger than that in the Southern Hemisphere, due to the larger zonal-asymmetries in land-sea thermal contrasts and orography in the Northern Hemisphere, which generate more planetary waves.

The Brewer-Dobson circulation is important for the stratospheric distribution of chemical species. It transports ozone from its primary photochemical source region, the tropical upper stratosphere, towards the winter pole and downward, from which it can be explained that the maximum ozone concentrations occur at high latitudes in the spring hemisphere at levels below 20 km. It can also explain the extreme dryness of the stratosphere: tropospheric air is pulled into the stratosphere through the extremely cold tropical tropopause, where it is thoroughly dehydrated.

The occurrence of the annually returning dramatic decrease of stratospheric ozone over the Antarctic since the 1980s (the so-called Antarctic ozone hole, Farman *et al.* 1985), and the absence of such a hole over the Arctic is connected to the strength of the stratospheric wave activity. The Southern Hemispheric (SH) winter stratospheric wave activity is smaller than that in the Northern Hemisphere, causing less poleward heat transport and lower winter temperatures in the Antarctic stratosphere than in the Arctic stratosphere. The weaker SH Brewer-Dobson circulation caused by less wave breaking is accompanied by less compression and adiabatic warming over Antarctica, which also contributes to the colder temperatures in

the Antarctic stratosphere. These colder temperatures support the formation of polar stratospheric clouds on which man-made chlorine- and bromine- containing substances are converted to photochemically active forms. The weaker SH wave forcing causes the SH polar vortex to be stronger, constituting a barrier and isolating this chemically modified air. Also, less ozone is transported poleward by the weaker SH Brewer-Dobson circulation. In the presence of sunlight in springtime, chlorine- and bromine-catalysed photochemical reactions destroy most of the stratospheric ozone, thus causing the so-called Antarctic ozone hole. Later in SH spring, the polar vortex breaks up due to changing meridional temperature gradients, allowing polar ozone-poor air to mix with extratropical ozone-rich air, and causing the ozone hole to fill up.

In the Northern Hemisphere, more troposphericly generated planetary waves transport more heat poleward, causing higher temperatures. However, occasionally also NH stratospheric temperatures are low enough to form polar stratospheric clouds. Sometimes, the westward force due to the wave breaking is large enough to cause a reversal of the polar zonal-mean zonal wind. This feature is known as a major stratospheric sudden warming, since it involves a rapid increase of the polar temperatures, with up to 80 K within a few days. During the SH winter 2002, this feature has been observed for the first time in the Southern Hemisphere (e.g., Eskes *et al.* 2003).

Troposphericly generated waves also play a crucial role in the Quasi-Biennial Oscillation, an alternating pattern of eastward and westward wind regimes in the equatorial stratosphere below 35 km. Equatorial waves are thought to be forced by geographically confined time variations in the large-scale cumulus convective heating in the equatorial troposphere (e.g., Andrews *et al.* 1987). They propagate upward to the stratosphere and deposit momentum to the zonal-mean zonal flow such that the successive regimes propagate downward at an average rate of about 1 km month⁻¹, and are repeated at intervals varying from about 22 to 34 months (e.g., Baldwin *et al.* 2001).

1.3 Influence of the stratosphere on the troposphere

In the previous section it has been argued that waves originating from the troposphere play a crucial role in the stratospheric circulation. The notion that stratospheric processes influence the tropospheric circulation is a less commonly held view, but has recently received increasing attention. A lot of observational evidence exists that stratospheric circulation anomalies often precede similar tropospheric anomalies. One of the first studies giving such evidence was that by Quiroz (1977), who noted that anomalies associated with the stratospheric sudden warming of January 1977 propagated to the Earth's surface. Large explosive volcanic eruptions bringing huge amounts of aerosols into the stratosphere are followed by a global cooling for 1-2 years (Kelly *et al.* 1996). Low-frequency zonal wind variations propagate from the upper stratosphere to the lower troposphere as has been noted

by, e.g., Kodera *et al.* (1990) and Christiansen (2001) (see Fig. 1.3). Baldwin and Dunkerton (1999) showed that large anomalies in the strength of the NH wintertime stratospheric polar vortex tend to propagate to the surface within several weeks. The induced tropospheric anomalies tend to persist during up to two months after extreme stratospheric circulation anomalies (Baldwin and Dunkerton 2001). It is currently being investigated whether the precedence of stratospheric disturbances relative to those in the troposphere can be exploited to improve long-range weather forecasts (Thompson *et al.* 2002).

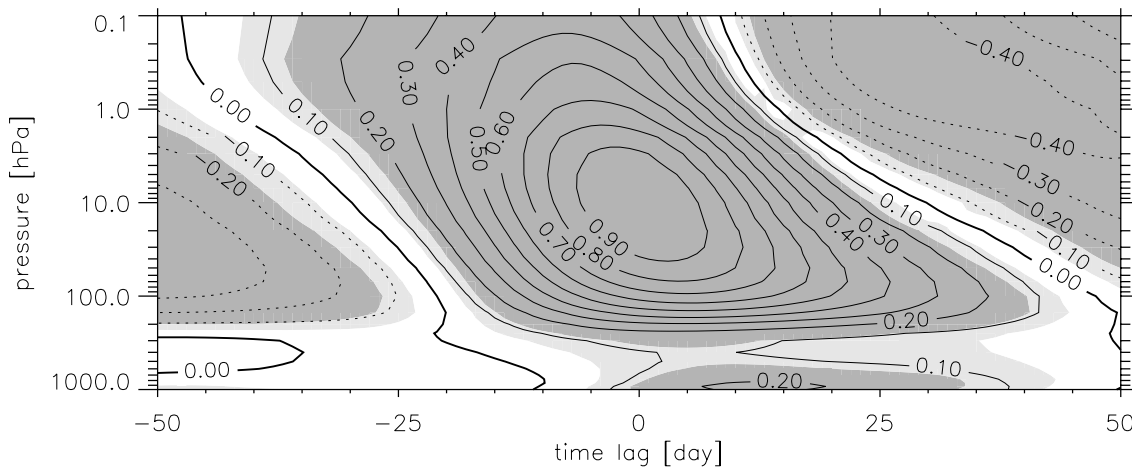


Fig. 1.3: Illustration of the downward propagation of zonal wind variations. Depicted is the correlation as function of height and time lag between the zonal-mean zonal wind at 10 hPa, 60°N and the zonal-mean zonal wind at other levels. Data have been band-passed filtered to include only timescales between 30 and 350 days. The plot is based on all 44 years (1958-2001) of the ERA-40 dataset. Light and dark shading identify regions where the correlations are significantly different from zero on two sigma and four sigma levels. (source: B. Christiansen, Danish Meteorological Institute)

The notion that the stratosphere influences the troposphere is supported by several modelling studies. Downward propagating variations have been noted in both relatively simple models (e.g., Holton and Mass 1976) and in the more complex General Circulation Models (e.g., Christiansen 2001). Boville (1984) showed that there are significant differences in the simulation of the troposphere when the stratospheric polar vortex is changed. Kodera *et al.* (1991) performed two model runs each of which had the same initial conditions in the troposphere, but with different stratospheric zonal wind conditions. They found that the zonal wind difference between the two runs propagated downward to the troposphere in the 45-day period after the initialisation.

The stratosphere can influence the troposphere through radiative and dynamical mechanisms. Aerosols emerging in the stratosphere after a major volcanic eruption decrease the amount of solar radiation that reaches the surface, and stratospheric ozone depletion reduces the amount of downwelling longwave radiation by the stratosphere, but increases the

amount of solar shortwave radiation that reaches the Earth's surface. Radiative changes associated with changes in the atmospheric composition (e.g., greenhouse gas increases, volcanic aerosols and ozone depletion) can induce stratospheric zonal wind changes, which through dynamical mechanisms can influence the tropospheric zonal wind (Shindell *et al.* 2001). Three dynamical mechanisms can be postulated by which the stratosphere influences the troposphere (Hartmann *et al.* 2000): (1) potential vorticity induction, (2) interaction between the zonal-mean flow and upward propagating waves, and (3) mass redistribution in the stratosphere. Hartley *et al.* (1998) show that lower stratospheric zonal wind variations (caused by, e.g., wave-mean flow interactions) are linked to potential vorticity anomalies that should induce significant changes in the tropopause height and tropospheric flow. The basic principle underlying the wave-mean flow interaction mechanism (e.g., Shindell *et al.* 2001) is that the zonal-mean zonal wind modulates the meridional propagation of the planetary waves, which in turn alters the locations where the planetary waves deposit momentum on the zonal-mean zonal flow. The net result is that zonal-mean zonal wind variations propagate downward. Baldwin and Dunkerton (1999) postulated that stratospheric meridional mass fluxes induced by wave forcing could influence the surface pressure distribution, which in turn is coupled to the lower tropospheric zonal wind. Evidence for such a mechanism will be presented in Chapter 3 of this thesis. It is important to note that stratospheric wave forcing, the initiator of these three dynamical mechanisms, is caused by waves that ultimately came from the troposphere. Therefore, it is erroneous to conclude that the stratosphere *drives* the troposphere through dynamical processes. Instead, these considerations suggest that a two-way dynamical coupling between the troposphere and the stratosphere exists, which can result in the precedence of stratospheric disturbances relative to those in the troposphere. A signature of this large two-way dynamical coupling is the phenomenon known as the Arctic Oscillation or the Northern Annular Mode.

1.4 Arctic Oscillation

Much of the recent research on the coupling between the troposphere and stratosphere has been done in the framework of the Arctic Oscillation (AO). The AO is the leading mode of variability of the NH wintertime circulation. It is an approximately zonally symmetric mode extending from the Earth's surface to the middle stratosphere (or higher). Because of its zonally symmetric (annular) character, it is sometimes referred to as the Northern Annular Mode. The AO emerges as the leading Empirical Orthogonal Function of the NH wintertime sea-level pressure (Fig. 1.4, Thompson and Wallace 1998) with associated regression patterns of the three-dimensional circulation and temperature fields. The AO is often considered as the hemispheric version of the North Atlantic Oscillation (Wallace 2000). The AO can be characterised by a seesaw of mass between low and high latitudes. By convention, a positive phase of the AO is associated with relatively low pressure over the polar cap and relatively

high pressure at middle latitudes, which causes the zonal wind around 55°N to be relatively strong. These circulation anomalies accompanying the phase of the Arctic Oscillation imply a strong dependence of the Northern Hemispheric winter weather on the phase of the AO (Thompson and Wallace 2001). The precedence of stratospheric circulation anomalies relative to those in the troposphere has been quantified in the AO framework by Baldwin and Dunkerton (1999). They showed that AO-anomalies often propagate down from the stratosphere to the surface level within several weeks.

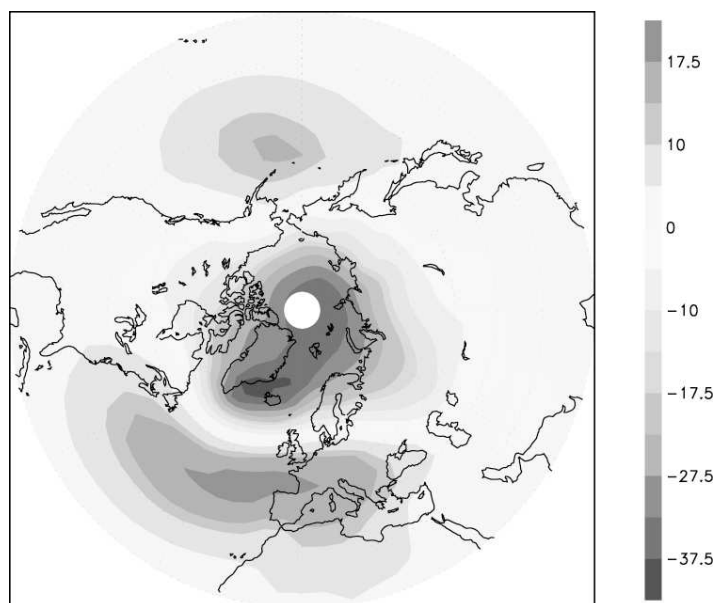


Fig. 1.4: Surface signature of the Arctic Oscillation. The Arctic Oscillation is defined here as the leading Empirical Orthogonal Function of NH monthly-mean 1000 hPa height anomalies. Units are meter per standard deviation of the Arctic Oscillation index. A positive phase of the Arctic Oscillation is associated with relatively low pressure over the polar cap and relatively high pressure at middle latitudes (source: D.W.J. Thompson, Colorado State University).

1.5 Stratosphere-troposphere exchange

In the previous sections, we have focussed on the coupling between the stratosphere and the troposphere through radiative processes and dynamical processes involving atmospheric waves. Atmospheric waves are able to transport information from one part of the atmosphere to the other, without a corresponding transport of mass. However, stratosphere-troposphere coupling can also occur directly through the transport of mass through the tropopause. The study of stratosphere-troposphere exchange (STE) is important for several reasons. For example, STE is important for the human impact on the atmosphere. The transport of CFC's from the ground to the stratosphere is believed to be the main cause of stratospheric ozone

depletion, whereas the increasing aircraft emissions in the tropopause region could have a substantial impact on climate and the atmospheric composition (IPCC 1999).

The global scale stratosphere-troposphere exchange (STE) is driven by the Brewer-Dobson circulation (see section 1.2). Wave forcing in the extratropical winter stratosphere drives a poleward circulation, hereby pulling tropospheric air through the tropical tropopause into the stratosphere, and pushing stratospheric air through the extratropical tropopause into the troposphere. At smaller scales, however, STE is not dominated by mean circulations, but by synoptic scale eddy processes, such as tropopause folds and cut-off lows. In the region commonly referred to as the ‘middle world’ (Holton *et al.* 1995), isentropes (isolines of potential temperature) intersect the tropopause, so that STE can occur adiabatically. Although the strength of the large-scale circulation ultimately determines the total mass transport across the tropopause, the smaller-scale processes strongly influence the time and space distribution of the transport. Gettelman and Sobel (2000) demonstrated that the knowledge of the instantaneous bi-directional cross-tropopause flux (CTF) rather than the time-mean net flux is, in the presence of a cross-tropopause gradient of a chemical species, necessary to determine the flux of this species across the tropopause.

Three-dimensional model fields of wind and temperature are often used to estimate the CTF. The CTF is often computed by applying one of the versions of the diagnostic formula derived by Wei (1987) to these data. However, this method often suffers from an almost cancellation of large terms, making it less reliable (Wirth and Egger 1999). Recently, a number of Lagrangian methods have been used to diagnose STE, one of which will be introduced and applied to an extratropical cyclone in Chapter 4 of this thesis.

1.6 Stratosphere-troposphere coupling and climate change

In the previous sections we focussed on the importance of stratosphere-troposphere coupling for understanding features in the present climate. In this section it is argued that stratosphere-troposphere coupling is also important for understanding climate change. Tropospheric climate change can induce stratospheric climate change, since tropospheric greenhouse gas increases can alter the excitation and propagation patterns of the atmospheric waves that drive the stratospheric Brewer-Dobson circulation. Rind *et al.* (1990) were one of the first to study the effect of CO₂ increase on the stratosphere with a three-dimensional climate model. They found that the Brewer-Dobson circulation strengthens in response to increasing CO₂ concentrations, a result that is supported by more recent modelling studies like Butchart and Scaife (2001), and Scaife *et al.* (2003). The author of this thesis has contributed to the latter study by providing results of doubled CO₂ simulations with a middle atmosphere General Circulation Model (GCM), and interpreting differences between these simulations and results from other GCM’s. A strengthening of the Brewer-Dobson circulation would have several implications, most of which would benefit the recovery of the ozone layer. Firstly, man-made

CFC's are transported faster into the stratosphere, leading to a quicker removal of CFC's out of the atmosphere and a faster recovery of the ozone layer (Butchart and Scaife 2001). Secondly, a stronger Brewer-Dobson circulation would transport more ozone from the tropical source regions to the poles. And thirdly, the resulting stronger downward motions in the polar regions are accompanied by more compression and adiabatic warming, causing higher temperatures. Consequently, less often the temperatures will be low enough to form polar stratospheric clouds, causing less (heterogeneous) stratospheric ozone depletion. On the other hand, higher temperatures would accelerate ozone depletion through (homogeneous) gas-phase reactions. Rind *et al.* (1990) also investigated the causes of the strengthening of the Brewer-Dobson circulation by performing experiments in which the CO₂ was doubled in either the middle atmosphere or the troposphere. They suggested that the strengthening of the Brewer-Dobson circulation is due to both the 'in situ' (stratospheric) and the 'remote' (tropospheric) CO₂ doubling. In Chapter 2 of this thesis, results from similar experiments with a different middle atmosphere GCM, and integrated over a much longer period will be presented.

Since the stratosphere is thought to influence the troposphere in the present climate, stratospheric climate change could also induce tropospheric climate change. During the last 30 years the AO-index has undergone a positive trend (Fig. 1.5), which can explain many observed Northern Hemispheric trends. An increased AO-index implies a stronger NH mid-latitude lower tropospheric zonal wind, which in NH winter transports relatively warm, moist air to Eurasia. The recent AO-index increase can explain about 50% of the observed surface temperature increase over the Eurasian continent (Thompson *et al.* 2000). Since the AO is related to the stratospheric mid-latitude zonal wind (e.g., Thompson *et al.* 2000), the observed warming may be partially due to changes in the stratospheric circulation.

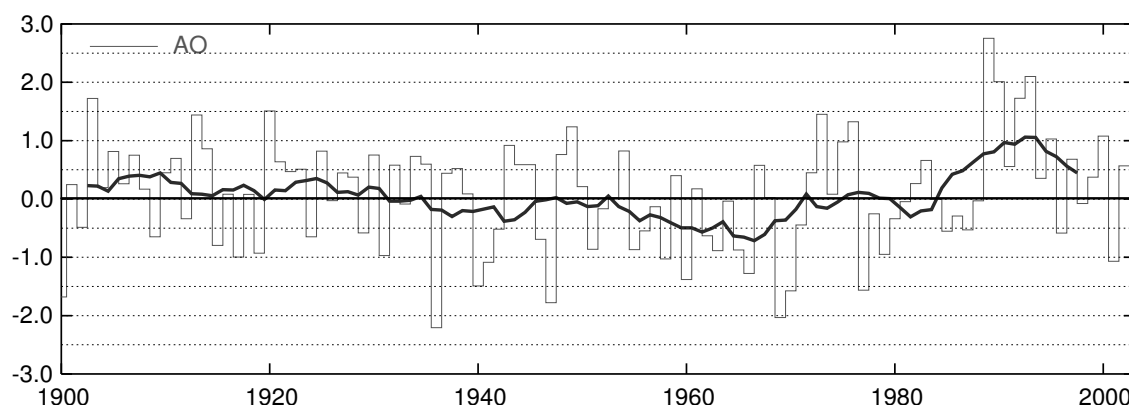


Fig. 1.5: Time series of the winter (December to March) Arctic Oscillation index. The thick line denotes the 10-year running average. Averaged over the last 30 years, a positive trend is observed. (Data source: D.W.J. Thompson, Colorado State University)

Several modelling studies predict a further increase of the NH mid-latitude lower tropospheric zonal wind (which is associated with a further increase of the AO-index) in response to increasing greenhouse gas concentrations (Shindell *et al.* 1999, Fyfe *et al.* 1999, Paeth *et al.* 1999, Gillett *et al.* 2002). The increase of greenhouse gases is believed to cool the polar stratosphere, and to warm the tropical upper troposphere and, consequently, to increase the meridional temperature gradient in the tropopause region. Therefore, the stratospheric zonal wind is, via the thermal wind relationship, also expected to increase. Shindell *et al.* (2001) argue that this could also strengthen the polar vortex, and that through the wave-mean-flow mechanism described in section 1.3, the increased stratospheric zonal wind could lead to an increased lower tropospheric zonal wind, and, consequently, to an increased AO-index. These considerations raise the question which part of the zonal wind increase in the NH mid-latitude lower troposphere can be attributed to enhanced greenhouse gas-induced changes in the stratosphere. This question will also be addressed in Chapter 2 of this thesis.

1.7 Stratospheric representation in general circulation models

Modelling the climate of the next century is currently perhaps the most challenging activity in atmospheric sciences. One of the most important tools for such studies are General Circulation Models (GCM's). The focus of the modelling studies has traditionally been on the troposphere, and in particular on surface climate change. This was mainly because of the limited availability of computer resources. Also, for a long time it has been assumed that, because of the relatively small part of the atmospheric mass it contains, the stratosphere needs not to be represented very accurately in GCM's to obtain accurate tropospheric climate predictions. Until recently most GCM's had an upper boundary around 10 hPa, so that only the troposphere and the lower stratosphere were represented adequately. With the increase of available computer resources and the increasing awareness of the strong coupling between tropospheric and stratospheric processes (and, consequently, the potentially large influence of stratospheric changes on the troposphere) during the last decade, more effort has been put into improving the stratospheric representation in GCM's. Nowadays, many state-of-the-art GCM's have an upper boundary around 0.01 hPa, which is around the mesopause. The necessity of the inclusion of a realistic stratosphere in GCM's for the prediction of the future surface climate is still matter of discussion, and has been the subject of several recent studies (Shindell *et al.* 1999, Gillett *et al.* 2002). The study presented in Chapter 2 of this thesis contributes to this discussion.

1.8 Overview of this thesis

This thesis describes several aspects of the coupling between the stratosphere and the troposphere.

The following questions will be addressed:

1. *What is the effect of CO₂ doubling in the troposphere on the middle atmosphere?*
2. *What is the effect of CO₂ doubling in the middle atmosphere on the troposphere?*
3. *How well has the middle atmosphere to be represented in General Circulation Models to capture the middle atmospheric influence on the tropospheric climate and climate change?*
4. *Through which dynamical mechanism does the stratosphere influence the troposphere?*
5. *How can Lagrangian methods be used to quantify stratosphere-troposphere exchange?*

The first three questions are related to stratosphere-troposphere coupling on climatological time-scales, and will be addressed in **Chapter 2**. Hereto, the separate climate effects of middle atmospheric and tropospheric CO₂ doubling have been simulated with the middle atmosphere version of the ECHAM4 global climate model. The CO₂ concentration has been separately doubled in the middle atmosphere, the troposphere, and the entire atmosphere, and the results will be compared to a control run. Thus, the dynamical response to radiative perturbations caused by CO₂ doubling in specific layers of the atmosphere can be investigated. Special emphasis will be put on the tropospheric response to middle atmospheric CO₂ doubling and to the middle atmospheric response to tropospheric CO₂ doubling. It will be investigated whether the response to a uniform CO₂ doubling can be regarded as the sum of the separate responses to tropospheric and middle atmospheric CO₂ doubling. In addition, it will be investigated to what extent CO₂ doubling between 10 hPa and 0.01 hPa influences the tropospheric climate. Chapter 2 has been submitted as Sigmond *et al.* (2003b). In the appendix to Chapter 2 the vertical wind in the experiments with the middle atmosphere GCM will be considered in more detail. It will be demonstrated that the pattern of the zonally and annually averaged vertical wind in the tropical stratosphere strongly depends on whether it is calculated with daily, 12-hourly or 6-hourly data. This result was used to explain differences between these simulations and results from other GCM's in the study by Scaife *et al.* (2003).

Question 4 and 5 address stratosphere-troposphere coupling issues in the present climate. **Chapter 3** will address question 4. Reanalysis data provided by the European Centre for Medium-Range Weather Forecasts (ECMWF) will be used to validate a mechanism by which the stratosphere influences the troposphere through variations in a meridional circulation cell. Chapter 3 has been published as Sigmond *et al.* (2003a).

Finally, in **Chapter 4** question 5 will be addressed. A new Lagrangian method to quantify stratosphere-troposphere exchange will be introduced and applied to an extratropical cyclone. Special emphasis will be put on the statistical significance of the calculated cross-tropopause fluxes. This method has been applied to a SH subtropical cyclone by Meloen *et al.* (2001), and was part of an intercomparison study of models and methods to quantify stratosphere-troposphere exchange (Meloen *et al.* 2003). Chapter 4 has been published as Sigmond *et al.* (2000).

Chapter 2

Simulation of the separate climate effects of middle atmospheric and tropospheric CO₂ doubling *

The separate climate effects of middle atmospheric and tropospheric CO₂ doubling have been simulated and analysed with the ECHAM middle atmosphere climate model. To this end, the CO₂ concentration has been separately doubled in the middle atmosphere, the troposphere, and the entire atmosphere, and the results have been compared to a control run. During NH winter, the simulated uniformly doubled CO₂ climate shows an increase of the stratospheric residual circulation, a small warming in the Arctic lower stratosphere, a weakening of the zonal winds in the Arctic middle atmosphere, an increase of the tropospheric NH mid-latitude westerlies, and a poleward shift of the tropospheric SH westerlies. The uniformly doubled CO₂ response is in most regions approximately equal to the sum of the separate responses to tropospheric and middle atmospheric CO₂ doubling. The increase of the stratospheric residual circulation can be attributed for about two thirds to the tropospheric CO₂ doubling and one third to the middle atmospheric CO₂ doubling. This increase contributes to the Arctic lower stratospheric warming and, through the thermal wind relationship, to the weakening of the Arctic middle atmospheric zonal wind. The increase of the tropospheric NH mid-latitude westerlies can be attributed mainly to the middle atmospheric CO₂ doubling, indicating the crucial importance of the middle atmospheric CO₂ doubling for the tropospheric climate change. Results from an additional experiment show that also the CO₂ doubling above 10 hPa, which is above the top of many current GCM's, causes significant changes in the tropospheric climate.

* This Chapter is a slightly revised version of: Sigmond, M., P.C. Siegmund, H. Kelder, and E. Manzini, 2003b: A simulation of the separate climate effects of middle atmospheric and tropospheric CO₂ doubling. *J. Climate*, submitted.

2.1 Introduction

The notion that the stratosphere influences the tropospheric dynamics has been supported by many recent studies. Low-frequency zonal wind variations propagate downward from the upper stratosphere to the lower troposphere (e.g., Kodera *et al.* 1990). Anomalies in the leading mode of variability of the Northern Hemispheric (NH) circulation (known as either the Arctic Oscillation (AO) or the Northern Annular Mode (NAM), Thompson and Wallace 1998) generally first appear in the stratosphere and propagate to the surface within several weeks (Baldwin and Dunkerton 1999). Several dynamical mechanisms for this downward propagation have been proposed: potential vorticity-induction (Hartley *et al.* 1998), wave-mean flow interactions (e.g., Shindell *et al.* 2001) and meridional mass redistribution (Sigmond *et al.* 2003a, cf. Chapter 3 of this thesis). During the last 30 years, the index corresponding to this leading mode of variability (the AO-index) has undergone a positive trend, which can explain about 50% of the observed surface temperature increase over the Eurasian continent (Thompson *et al.* 2000). Since the AO is related to the mid-latitude stratospheric zonal wind (e.g., Thompson *et al.* 2000), the observed warming may be partially due to changes in the stratospheric circulation. Several GCM studies predict an increased westerly circulation in the (lower) tropospheric NH mid-latitudes (associated with a further increase of the AO-index) in response to increasing CO₂ concentrations (Shindell *et al.* 1999, Fyfe *et al.* 1999, Paeth *et al.*, 1999, Gillett *et al.* 2002). The increase of greenhouse gases is believed to cool the polar stratosphere, to warm the tropical upper troposphere and, consequently, to increase the meridional temperature gradient in the tropopause region. Shindell *et al.* (2001) argue that this causes stratospheric zonal wind changes that in turn cause the increased westerly circulation in the tropospheric NH mid-latitudes through wave-mean flow interactions. Several other GCM studies also indicate this downward influence (Boville 1984, Rind *et al.* 2002).

Other recent studies have addressed the question of how well the stratosphere has to be represented in GCM's to capture this downward influence adequately. Shindell *et al.* (1999) show that their model only captures the observed AO-index increase if it includes the region between 10 hPa and 0.01 hPa. However, Fyfe *et al.* (1999) and Gillett *et al.* (2002) found an AO-index increase in response to increasing CO₂ concentrations in models with an upper boundary at, respectively, 12 hPa and 5 hPa. The latter result did not notably change when the upper boundary was raised to 0.01 hPa.

Greenhouse gas induced changes in the troposphere are expected to change the stratospheric circulation. Tropospheric waves propagate upward into the stratosphere, where they are dissipated and drive a meridional overturning circulation, known as the residual or Brewer-Dobson circulation (e.g., Holton *et al.* 1995). Tropospheric greenhouse gas increases can alter the sources and propagation patterns of the atmospheric waves that drive the stratospheric residual circulation. In a GCM experiment with increasing CO₂, Butchart and

Scaife (2001) found an increase of the strength of this circulation. They argued that such an increase would accelerate the removal of CFC's from the stratosphere and, consequently, accelerate the recovery of the ozone layer.

Rind *et al.* (1990) investigated the causes of the middle atmospheric response to a uniform doubling of CO₂, by performing experiments of one to three years in which the CO₂ was doubled in either the middle atmosphere or the troposphere. They suggested that the residual stratospheric circulation increase is due to both the 'in situ' (middle atmospheric) and the 'remote' (tropospheric) CO₂ doubling. The tropospheric response to CO₂ doubling in either the troposphere or middle atmosphere was not considered in this study.

In the present study, the separate climate effects of middle atmospheric and tropospheric CO₂ increase are investigated with the middle atmosphere version of the ECHAM global climate model. The control and uniformly doubled CO₂ climate have been simulated. In addition, experiments have been performed in which the CO₂ has been doubled in either the troposphere or the middle atmosphere. These idealized experiments have been performed to study the mechanisms leading to the changes in the simulated uniformly doubled CO₂ climate. Changes found in the uniformly doubled CO₂ climate will be attributed to either middle atmospheric or tropospheric CO₂ doubling. We will investigate whether this separation is allowed, which requires that the response to a uniform CO₂ doubling is approximately equal to the sum of the separate responses to tropospheric and middle atmospheric CO₂ doubling. We have performed 30-year equilibrium experiments to obtain statistically significant results. Since the stratosphere-troposphere coupling is strongest in NH winter, we will focus on this season.

This Chapter is organised as follows. In section 2.2 the model and the set-up of the experiments are described. In section 2.3 the control climate and the response to a uniform CO₂ doubling is described. In section 2.4 it is investigated to what extent the response to a uniform CO₂ doubling can indeed be regarded as the sum of the responses to tropospheric and middle atmospheric CO₂ doubling. The middle atmospheric and tropospheric responses to non-uniform (i.e., only tropospheric or middle atmospheric) CO₂ doubling are described in, respectively, sections 2.5 and 2.6. The downward influence of middle atmospheric CO₂ doubling on the troposphere is investigated in more detail in section 2.7. Finally, the results are summarized and discussed in section 2.8.

2.2 Model and set-up of the experiments

2.2.1 General Circulation Model

The GCM used in this study is MA-ECHAM4 (Manzini *et al.* 1997), which is the middle atmosphere version of the ECHAM4 model (Roeckner *et al.* 1996). The MA-ECHAM4 model has 39 levels from the surface up to 0.01 hPa (about 80 km). Gravity wave drag is parameterised for both orographic gravity waves (McFarlane 1987) and a spectrum of nonstationary gravity waves (Hines 1997a,b). Sensitivities to the specification of the gravity wave parameterizations are discussed by Manzini and McFarlane (1998). The simulations in this study are performed at T42 horizontal resolution (about $2.8^\circ \times 2.8^\circ$) and the integration timestep is set to 10 minutes. The ozone distribution (Brühl 1993) and the sea surface temperatures (SSTs) are prescribed.

2.2.2 Experiments

Six 30-year simulations have been performed, whose configurations are summarized in Table 1. The atmospheric CO₂ content has been doubled in the entire atmosphere from 353 ppmv in the control run (C-run) to 706 ppmv in the uniformly doubled CO₂ run (A-run). Two additional runs have been performed in which the CO₂ is separately doubled in the middle atmosphere (M-run) and the troposphere (T-run). A monthly mean, longitude and latitude dependent tropopause field was used to select the regions where CO₂ should be doubled in the M- and T-run. This climatology was calculated with the WMO tropopause definition and was taken from a control run of MA-ECHAM4.

	C-run	A-run	M-run	T-run	MC-run	H-run
Middle Atmosphere	1X CO ₂	2x CO ₂	2x CO ₂	1X CO ₂	2x CO ₂	2x CO ₂ (only above 10 hPa)
Troposphere	1X CO ₂	2x CO ₂	1X CO ₂	2x CO ₂	1X CO ₂	1X CO ₂
SST	Control	2x CO ₂	RF-calculation	RF-calculation	Control	Control

Table 2.1: Summary of the configurations of the experiments, see subsection 2.2.2.

The atmospheric GCM is not interactively coupled to an ocean model. Instead, monthly climatological SSTs are prescribed. In the C- and A-run these SSTs are taken from a control and a doubled CO₂ run of ECHAM4 coupled to a slab layer ocean. The appropriate SSTs in the M- and T-run were calculated from these climatologies and calculated radiative forcings. The radiative forcing (RF) is the net radiative flux change at the tropopause caused by a radiative perturbation (e.g., IPCC 2001), and is generally considered as a useful measure for the surface temperature change. It will be assumed here that the SST change due to uniform CO₂ doubling is the sum of the SST changes due to CO₂ doubling in the troposphere and the middle atmosphere, which in turn are assumed to be proportional to the radiative forcings due to CO₂ doubling in these layers:

$$\Delta SST_T = \Delta SST_A * frac , \quad (2.1a)$$

$$\Delta SST_M = \Delta SST_A *(1-frac) , \quad (2.1b)$$

where

$$frac = \frac{RF_T}{RF_T + RF_M} . \quad (2.1c)$$

The ΔSST_X is the change of SST compared to the control run due to the CO₂ doubling in region X (M for middle atmosphere, T for troposphere and A for the entire atmosphere) and RF_X is the radiative forcing in the X -run. To compute RF_X , we have performed two additional integrations with the configurations of the M- and T-run, except that the control SSTs are prescribed. RF_X is approximated by the global-mean net radiative flux change at the tropopause compared to the control run after one time step. From the results ($RF_M = 0.64$ W/m², $RF_T = 3.26$ W/m²) a value of 0.84 for $frac$ is obtained.

To investigate to what extent the imposed SST changes in the M-run influence the results, an additional run (denoted as the MC-run) has been performed, which is similar to the M-run, except that the control SSTs are prescribed.

To investigate the influence of the CO₂ doubling in the higher stratosphere and mesosphere on the tropospheric climate, a run has been performed in which the CO₂ is doubled only above 10 hPa (H-run). The radiative forcing due to the CO₂ doubling above 10 hPa is calculated in the same way as for the other runs, and was found to be very small (0.02 W/m²). Therefore, control SSTs could be imposed in the H-run.

2.3 Climate response to a uniform CO₂ doubling

2.3.1 Control climate

Figure 2.1a and 2.1b show, respectively, the zonally averaged temperature and zonal wind in the control climate in NH winter. The temperature distribution, the strength of the NH stratospheric polar vortex, the subtropical jet streams and the SH middle atmospheric easterlies compare reasonably well with reference climatologies (Manzini and McFarlane 1998). The residual mean stream function (computed following the transformed Eulerian mean formulation, Andrews *et al.* 1987) depicted in Fig. 2.1c shows the stratospheric residual circulation. This circulation is driven by the wave drag from planetary and gravity waves. The planetary waves are resolved by the model and their effect on the mean flow is quantified by $div\mathbf{F}/\rho_0$ (where $div\mathbf{F}$ is the divergence of the Eliassen-Palm flux and ρ_0 is the density), which is shown in Fig. 2.1d. In regions where $div\mathbf{F}/\rho_0$ is negative, the waves decelerate the zonal wind, thus causing an imbalance between the Coriolis force on the zonal-mean zonal wind and the meridional pressure gradient force, and driving a poleward flow. The surface zonal wind (Fig. 2.1e) is largest in the northern Atlantic and Pacific storm track regions, and in the SH mid-latitudes.

2.3.2 Middle atmospheric response to uniform CO₂ doubling

Figure 2.2a shows the zonally averaged temperature difference between the A-run and the C-run in NH winter (denoted as ΔT_A). As expected, the middle atmosphere generally cools in response to the uniform CO₂ doubling, which can be explained by radiative arguments (e.g., Fels *et al.* 1980, Shindell *et al.* 2001). The changes are statistically significant, except in some regions where the changes are small. The main exception to the middle atmospheric cooling is the Arctic lower stratosphere, which slightly warms. Figure 2.2b shows the zonally averaged zonal wind difference between the A- and the C-run in NH winter (Δu_A), which is physically consistent with Fig. 2.2a according to the thermal wind relationship. The warming of the Arctic lower stratosphere and the reduced cooling directly above this layer lead to a decrease of the meridional temperature gradient in the polar stratosphere, which is consistent with the weakening of the Arctic middle atmospheric zonal winds. The zonal wind in the NH subtropical middle atmosphere strengthens significantly, with up to 9 m s⁻¹ near the stratopause and just above the NH subtropical jet stream. The position of the maximum wind speed in the polar vortex has shifted equatorward from 60°N in the C-run to 40°N in the A-run, and its value has decreased from 38 m s⁻¹ in the C-run to 34 m s⁻¹ in the A-run (*not*

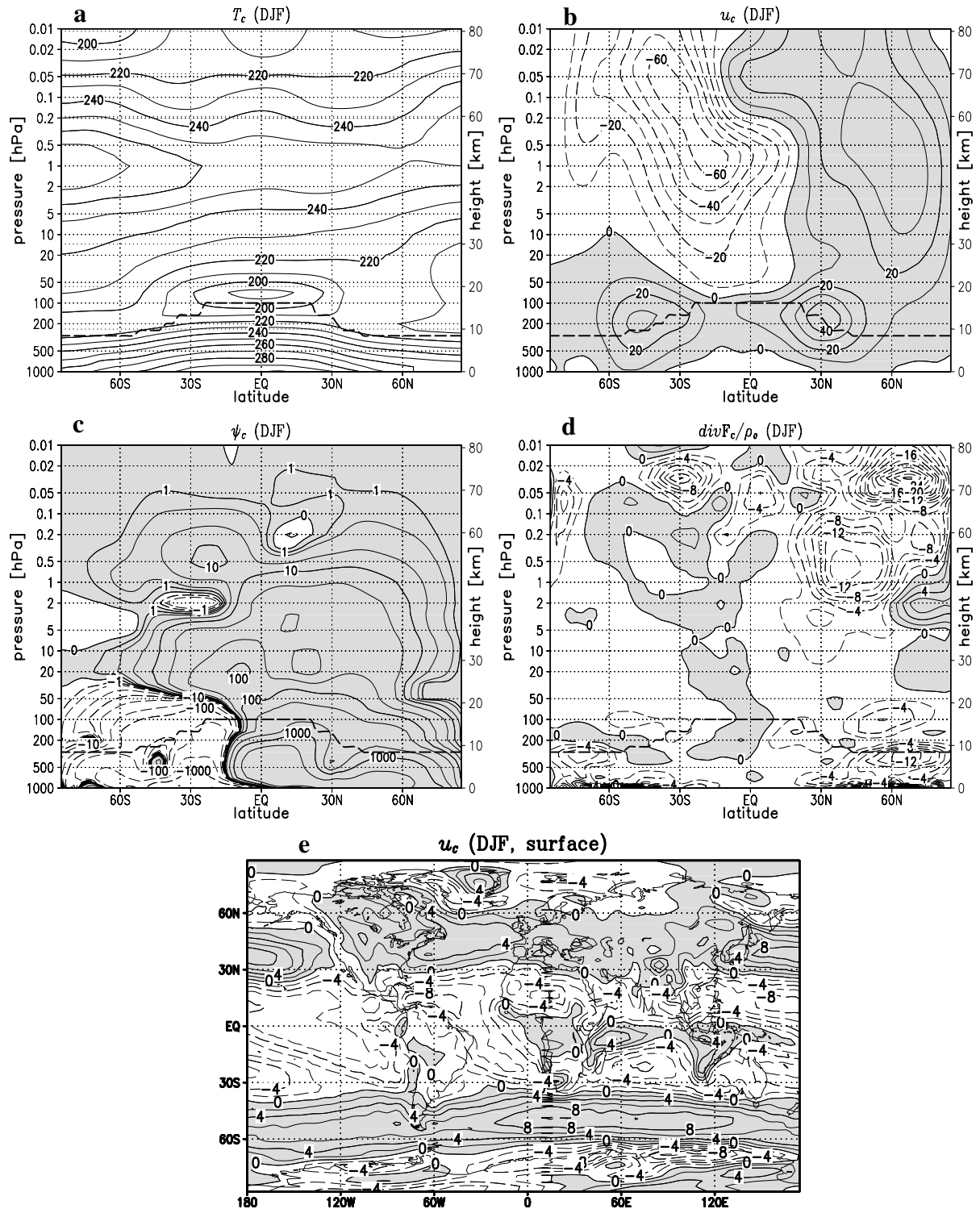


Fig. 2.1a-e: The zonally averaged temperature (a) and zonal wind (b), the residual streamfunction (c), the divergence of the EP-flux divided by density (d), and the surface level zonal wind (e) in the C-run. Results are averages over 30 years for the DJF-season, and shading indicates positive values. The contour interval is, respectively, 10 K (a), 10 m s^{-1} (b), 2 m s^{-1} day $^{-1}$ (d) and 2 m s^{-1} (e). The contour lines in Fig. 1c are at 0, ± 1 , ± 2 , ± 5 , ± 10 , ± 20 , ± 50 etc. $kg\ m^{-1}\ s^{-1}$. The bold dashed line in Figs. 1a-d denotes the position of the zonally averaged tropopause.

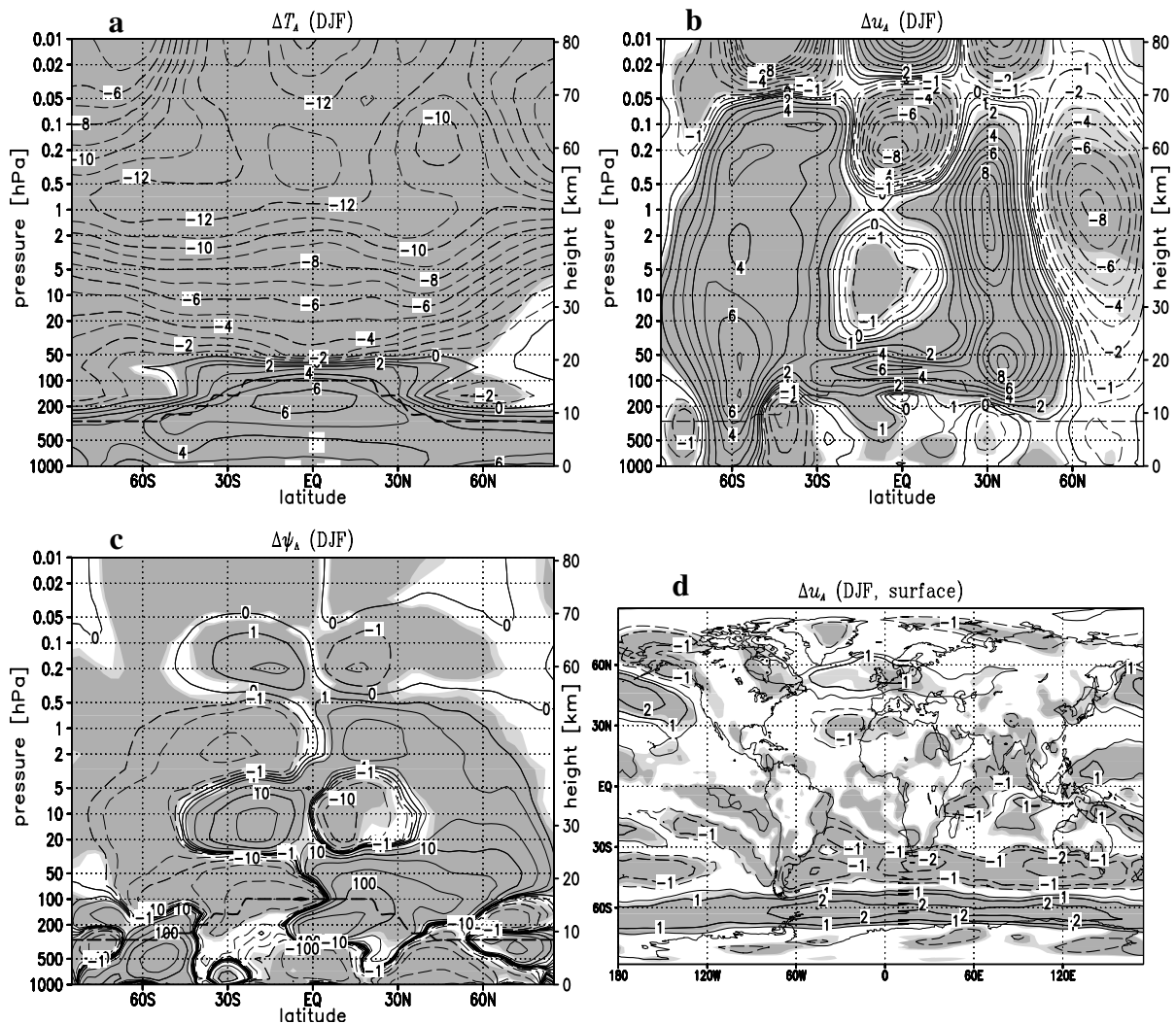


Fig. 2.2a-d: Fig. 2.2a-c,d as in Fig. 2.1a-c,e, except for the difference between the A- and C-run, and light (dark) shaded areas indicate regions where the difference is statistically significant at 95% (99%) level. The contour interval is 1 K (a), the contour lines are at 0, ± 0.5 , ± 1 , ± 2 , ± 3 etc. $m s^{-1}$ (b,d), and at 0, ± 1 , ± 2 , ± 5 , ± 10 , ± 20 , ± 50 etc. $kg m^{-1} s^{-1}$ (c). The zero contour line in Fig. 2.2d has been omitted.

shown). In the Southern Hemisphere, the value of the middle atmospheric extratropical zonal wind increases significantly (i.e., the easterlies significantly decrease in magnitude).

Figure 2.2c shows the change of the residual stream function in the A-run compared to the C-run ($\Delta\psi_A$). The strength of the stratospheric residual circulation generally increases significantly, except in the tropical middle stratosphere. The maximum of the NH residual streamfunction, which is located between 15° and $18^\circ N$ and is a measure for the NH extratropical mass flux from the stratosphere to the troposphere (e.g., Rosenlof and Holton 1993), significantly increases with 33% at 50 hPa and with 39% at 100 hPa. Associated with this increase, also the descending motions near the North Pole increase. While adiabatically heating the air they contribute to the temperature increase shown in Fig. 2.2a.

Figure 2.3a shows for the A-run the change of the residual meridional wind, from which the stream function change depicted in Fig. 2.2c has been computed. This residual meridional wind is defined as (Andrews *et al.* 1987, Eq. 3.5.1a):

$$v^* \equiv \bar{v} - \rho_0^{-1} \frac{\partial (\rho_0 \bar{v}' \theta' (\partial \bar{\theta} / \partial z)^{-1})}{\partial z}, \quad (2.2)$$

where ρ_0 is the density, v is meridional wind, and θ is the potential temperature. The overbar denotes the zonal-mean value, the prime denotes the deviation from that value. Figure 2.3a shows that in most of the NH stratosphere v^* increases in the doubled CO₂ climate (except in the tropical middle stratosphere), which corresponds to the increased residual circulation. The v^* is decomposed into v^* due to resolved planetary waves (denoted as $v^{*,resolved}$) and v^* due to the unresolved processes like gravity waves (denoted as $v^{*,gravity}$). The $v^{*,resolved}$ has been computed by applying the continuity equation to the vertical velocity due to planetary wave driving assuming “downward control” (Haynes *et al.* 1991). Assuming quasi-geostrophy and stationarity, this vertical velocity can be written as:

$$w^{*,resolved} = \frac{1}{a \rho_0 \cos \phi} \frac{\partial}{\partial \phi} \left\{ \int_z^\infty \left\{ \frac{\cos \phi \operatorname{div} \mathbf{F}}{f} \right\}_{\phi=const.} dz' \right\}, \quad (2.3)$$

where a is the radius of the Earth, ϕ is latitude and f is the Coriolis parameter.

The v^* due to the unresolved processes will be calculated here as a residual:

$$v^{*,gravity} \equiv v^* - v^{*,resolved}. \quad (2.4)$$

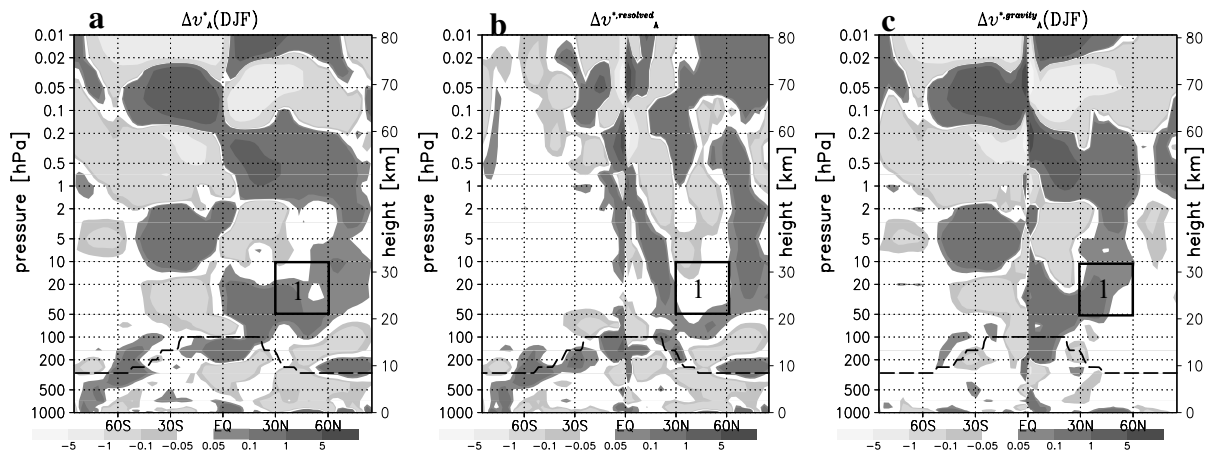


Fig. 2.3a-c: The difference between the A- and C-run of v^* (a), $v^{*,resolved}$ (b) and $v^{*,gravity}$ (c), for NH winter. See section 2.3.2 for the meaning of the symbols.

Comparison of Fig. 2.3b and Fig. 2.4a for the resolved waves shows that the structure of $\Delta v_A^{*resolved}$ is opposite to that of $\Delta div\mathbf{F}_A/\rho_0$. The decreased (i.e., more negative) $div\mathbf{F}_A/\rho_0$ in the large part of the NH stratosphere implies that the wave drag due to the resolved waves on the zonally averaged zonal flow increases, and that the resolved waves strengthen the poleward flow (i.e., $v_A^{*resolved}$ increases). Figure 2.3 shows that in the tropical and NH mid-latitude stratosphere the part of Δv_A^* that is due to gravity waves ($\Delta v_A^{*gravity}$, Fig. 2.3c), is comparable to the Δv_A^* due to resolved waves ($\Delta v_A^{*resolved}$). In some stratospheric regions (e.g., region 1) the increase of v_A^* is even mainly due to the increase of $v_A^{*gravity}$. Therefore, it is concluded that changes in both the resolved planetary and gravity waves drive the increased stratospheric residual circulation in the doubled CO₂ climate. In the mesosphere, planetary wave activity is very small due to absorption of these waves at lower levels, which can explain why in this region $\Delta v_A^{*resolved}$ is generally smaller than $\Delta v_A^{*gravity}$. Thus, the mesospheric Δv_A^* is mainly determined by gravity waves drag changes.

Figure 2.4a shows that in the NH stratosphere the pattern of the $\Delta div\mathbf{F}_A/\rho_0$ is similar to that of Δu_A (Fig. 2.2b): they both decrease in the polar region and increase around 40°N. This finding is consistent with the fact that $div\mathbf{F}/\rho_0$ is a force on the zonal-mean zonal wind. The changes in the resolved waves are investigated in more detail by decomposing $div\mathbf{F}/\rho_0$ in its horizontal and vertical components $div\mathbf{F}^y/\rho_0$ and $div\mathbf{F}^z/\rho_0$, where:

$$div\mathbf{F}^y = \frac{\partial}{\partial y} F^y, \quad (2.5a)$$

$$div\mathbf{F}^z = \frac{\partial}{\partial z} F^z, \quad (2.5b)$$

$$F^y = -\rho_0 \overline{u'v'}, \quad (2.5c)$$

$$F^z = \rho_0 f a \cos \phi \overline{v'\theta'} \left(\frac{\partial \bar{\theta}}{\partial z} \right)^{-1}. \quad (2.5d)$$

F^y and F^z are, respectively, the horizontal and vertical component of the Eliassen-Palm flux vector, which direction is the direction of the wave activity. F^z is generally positive, which corresponds to an upward propagation of the wave activity, and a positive F^y corresponds to a poleward propagation of wave activity. Figure 2.4 shows that in the NH upper stratosphere (region I) and in the NH subtropical lower stratosphere (region II) the structure of $\Delta div\mathbf{F}_A/\rho_0$ (Fig. 2.4a, shaded) is mainly determined by $\Delta div\mathbf{F}_A^y/\rho_0$ (Fig. 2.4b, shaded), whereas in the NH mid-latitude middle stratosphere (region III) it is mainly determined by $div\mathbf{F}_A^z/\rho_0$ (Fig. 2.4c, shaded). Changes in $div\mathbf{F}_A^y/\rho_0$ are related to changes in F^y and, consequently, to changes in the meridional refraction of wave activity. For example, in the middle of region II F^y (Fig. 2.4b,

contours) decreases, implying that waves are refracted more to the equator (see arrow), leading to decreases of $div\mathbf{F}^y/\rho_0$ at the equatorward side of region II and increases of $div\mathbf{F}^y/\rho_0$ at the poleward side of region II. Changes in $div\mathbf{F}^z/\rho_0$ are related to changes in F^z and, consequently, to changes in the vertical propagation of the wave activity. Just below region III F^z (Fig. 2.4c, contours) increases, which corresponds to more upward propagating wave activity (see upward arrow). This increased wave activity is dissipated in region III, causing a decrease of $div\mathbf{F}^z/\rho_0$. In summary, the structure of $\Delta div\mathbf{F}_A/\rho_0$ is mainly determined by changes in the meridional refraction of the wave activity in the NH upper stratosphere (region I) and in the NH subtropical lower stratosphere (region II), and by the increase of vertical wave activity in the NH mid-latitude lower stratosphere (just below region III). Considering that the tropospheric vertical wave activity is decreased (see Fig. 2.4c), the lower stratospheric increase can have two causes: (1) the NH mid-latitude tropopause is more ‘transparent’ for tropospheric wave activity, or (2) more wave activity is produced near the NH mid-latitude tropopause.

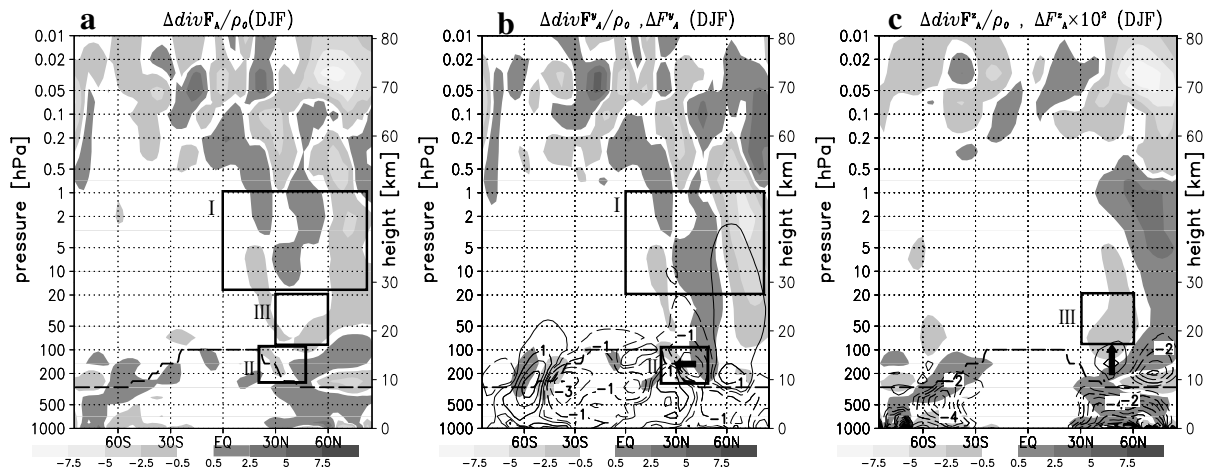


Fig. 2.4a-c: The difference between the A- and C-run in NH winter of $div\mathbf{F}/\rho_0$ (2.4a), $div\mathbf{F}^y/\rho_0$ (shaded, 2.4b) and F^y (contours, 2.4b), $div\mathbf{F}^z/\rho_0$ (shaded, 2.4c), and $F^z \times 10^2$ (contours, 2.4c). See text for the meaning of the symbols. $div\mathbf{F}/\rho_0$ in $m s^{-1} day^{-1}$. The contour lines of F^y are at $\pm 0.2, \pm 1, \pm 2, \pm 3$ etc. Pa, and the contour interval of F^z is 0.01 Pa. The zero contour lines for both F^y and F^z and are omitted. The arrows indicate the directions of the changes of the wave propagation discussed in the text.

The Arctic lower stratospheric warming and the associated weakening of the polar vortex in response to CO₂ increase (Figs. 2.2a,b) have been reported in several GCM studies (e.g., Rind *et al.* 1990, 1998, 2002, Mahfouf *et al.* 1994, Gillett *et al.* 2003a). An exception is the study of Shindell *et al.* (1998) who report a strengthening and cooling of the polar vortex (see Gillett *et al.* (2003a) for a discussion). In the present study the Arctic lower stratospheric

warming is attributed to an increased residual circulation due to increased planetary and gravity wave driving. It should be noted that the change in the upward propagation of vertical wave energy quantified by ΔF_A^{∞} at 100 hPa was found to be largest in November, causing a huge deceleration of the polar vortex compared to the control run, and influencing the strength of the polar vortex in the succeeding winter. Thus, the strength of the DJF polar vortex is not only influenced by the DJF wave activity, but also by that in November. The increase of the NH mid-latitude lower stratospheric wave driving in NH winter is consistent to what has been found by, e.g., Butchart and Scaife (2001) and Gillett *et al.* (2003a). In the NH subtropical lower stratosphere, the increased wave driving is due to the equatorward refraction of wave activity, which is consistent with the results of, e.g., Rind *et al.* (2002).

2.3.3 Tropospheric response to uniform CO₂ doubling

Figure 2.2a shows that the troposphere generally warms in response to a uniform CO₂ doubling, with a maximum warming of more than 6 K in the tropical upper troposphere. Figure 2.2b shows that the zonally averaged zonal wind in the tropospheric NH mid-latitudes increases with 0.5 to 1 m s⁻¹. This increase is statistically significant, except in the upper troposphere. At the surface (Fig. 2.2d), statistically significant zonal wind increases are found in the storm track regions above the oceans. Above the northern Atlantic, the zonal wind increases with more than 1.5 m s⁻¹, which is about 20% of the zonal wind in the C-run. The increase of the tropospheric NH mid-latitude westerlies has been reported in several previous GCM studies (see section 2.1). The decrease of the zonal wind around 40°S and the increase around 60°S throughout the troposphere imply that the SH summer westerlies are shifted poleward.

To summarize, the simulated uniformly doubled CO₂ climate is characterized by a generally cooler middle atmosphere, an increased stratospheric residual circulation (caused by increased planetary and gravity wave driving) that is consistent with warmer temperatures in the Arctic lower stratosphere and a weakening of the zonal winds in the Arctic middle atmosphere. Furthermore, the troposphere warms and the tropospheric NH mid-latitude westerlies increase.

2.4 Additivity of the non-uniform CO₂ doubling responses

Experiments in which the CO₂ is doubled non-uniformly (i.e., only in the troposphere or in the middle atmosphere) have been performed to study the mechanisms leading to the changes in the simulated uniformly doubled CO₂ climate. Changes found in the uniformly doubled CO₂ climate are attributed to either middle atmospheric or tropospheric CO₂ doubling. This separation is only allowed when the responses are additive, i.e., when the response to a

uniform CO₂ doubling can be regarded as the sum of the responses to CO₂ doubling in the middle atmosphere and in the troposphere. In other words, the following relationship should apply:

$$\Delta Q_A = \Delta Q_M + \Delta Q_T, \quad (2.6)$$

where ΔQ_X is the response to CO₂ doubling in region X (i.e., the difference between the X -run and the C-run) of the quantity Q . Relationship (2.6) will generally not be satisfied exactly due to non-linear middle atmosphere-troposphere interactions. It will be assumed that the responses are additive if relationship (2.6) applies at a more than 95% confidence level. A Student's t -test is applied to $(\Delta Q_M + \Delta Q_T - \Delta Q_A)$ to test whether this quantity significantly differs from zero. Significant non-additivities arise in regions where the value of $(\Delta Q_M + \Delta Q_T - \Delta Q_A)$ is large or where its interannual variability is small.

Figure 2.5 shows for NH winter the zonally averaged temperature response to middle atmospheric CO₂ doubling (ΔT_M , Fig. 2.5a) and to tropospheric CO₂ doubling (ΔT_T , Fig. 2.5b). Figure 2.5c shows that the temperature changes satisfy additiveness (i.e., $\Delta T_M + \Delta T_T - \Delta T_A \approx 0$) in most regions, except in some regions (shaded when not additive), which include the tropical and part of the NH extratropical stratosphere, the tropical upper troposphere and the polar troposphere. Note that the temperature responses are additive in the Arctic lower and middle stratosphere.

Figure 2.6 shows the zonally averaged zonal wind response to middle atmospheric CO₂ doubling (Δu_M , Fig. 2.6a) and to tropospheric CO₂ doubling (Δu_T , Fig. 2.6b) in NH winter. In the middle atmosphere, Δu_T is similar to Δu_A (Fig. 2.2b). In the tropospheric NH mid-latitudes, Δu_M is similar to Δu_A . The shaded regions in Fig. 2.6c indicate regions where the zonal wind responses are not additive. Note that the zonal wind responses are additive in the tropospheric NH mid-latitudes.

Figure 2.7 shows the zonal wind responses at the surface. Figure 2.7c shows that the surface zonal wind responses are additive above the entire northern Atlantic. In this region, both Δu_M (Fig. 2.7a) and Δu_T (Fig. 2.7b) are positive. The zonal wind responses are not additive in large parts of the northern Pacific. In this region, the pattern of Δu_T is similar to that of Δu_A , whereas the pattern of Δu_M is completely different. In the mid-latitudes of the Southern Hemisphere the zonal wind responses are additive, and the patterns of both Δu_M and Δu_T are similar to that of Δu_A .

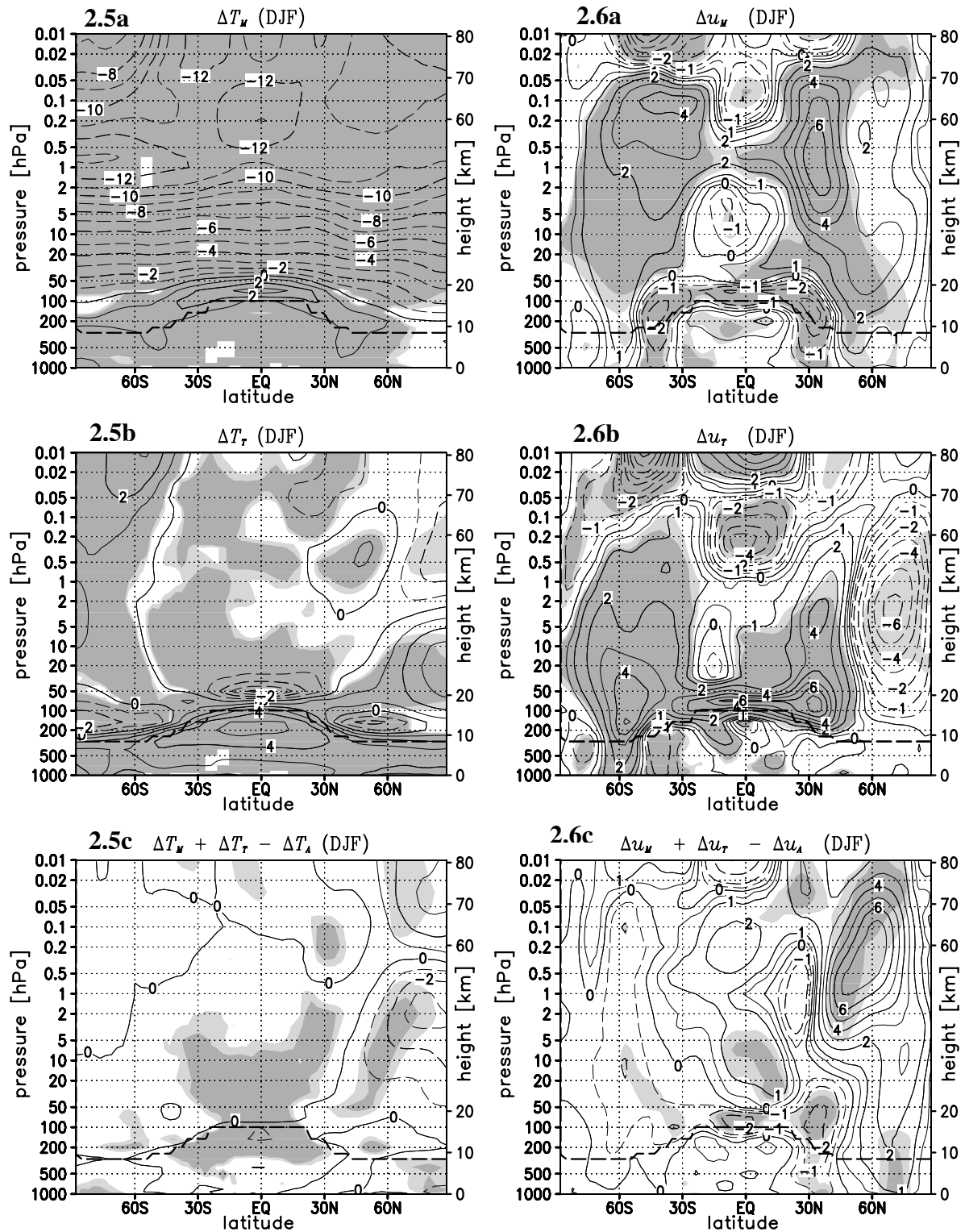


Fig. 2.5a-c (left): The difference of the zonally averaged temperature between the M- and C-run (a), and between the T- and C-run (b) for the DJF season. Fig. 2.5c shows the degree of non-additivity of the temperature (i.e., $\Delta T_M + \Delta T_T - \Delta T_A$, see text). Light (dark) shade denotes significance at 95% (99%) level and the contour interval is 1 K. The bold dashed line denotes the position of the tropopause.

Fig. 2.6a-c (right): As in Fig. 2.5a-c, except for the zonally averaged zonal wind. The contour lines are at 0, ± 0.5 , ± 1 , ± 2 , ± 3 etc. $m s^{-1}$.

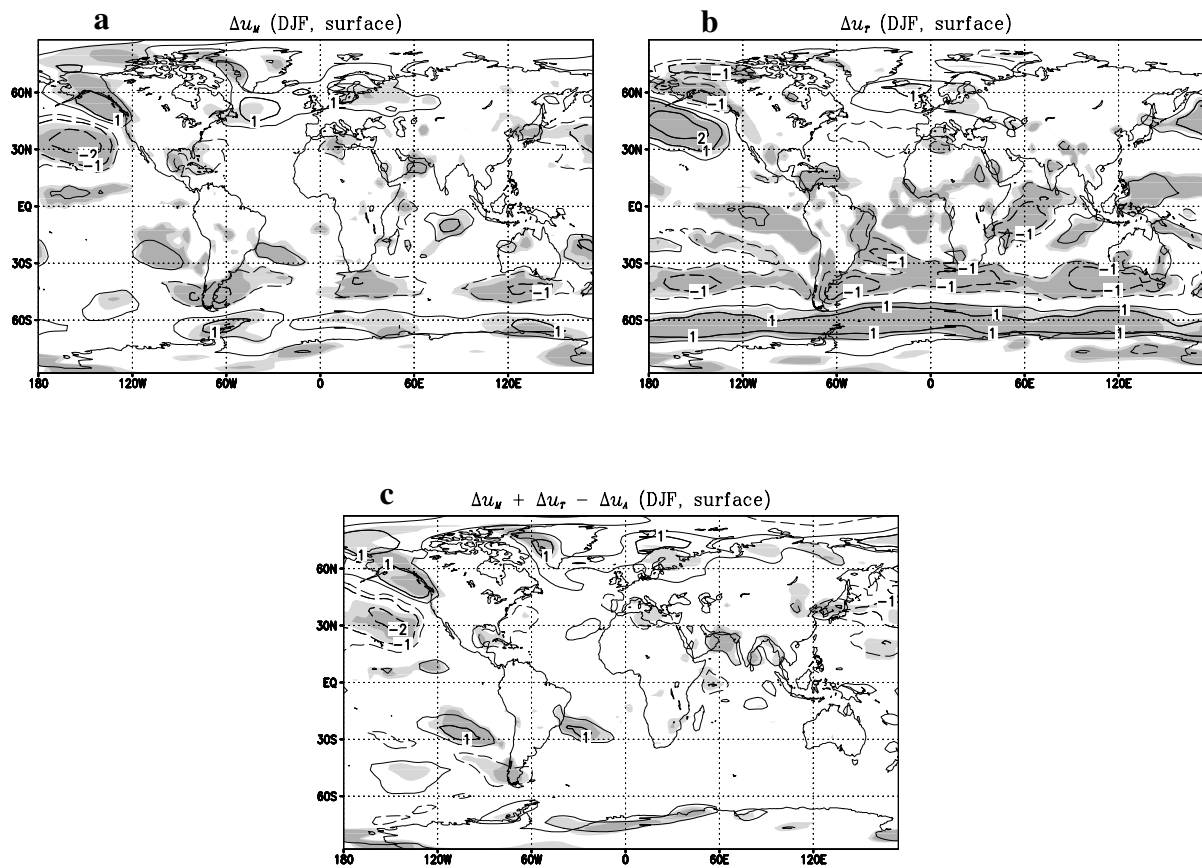


Fig. 2.7a-c: As in Fig. 2.5a-c, except for the surface zonal wind. The contour lines are at ± 0.5 , ± 1 , ± 2 , ± 3 etc. $m s^{-1}$, and the zero contour line has been omitted.

2.5 Middle atmospheric response to non-uniform CO₂ doubling

2.5.1 Middle atmospheric response to tropospheric CO₂ doubling (T-run)

Figure 2.5b shows that in the largest part of the middle atmosphere the temperature response to tropospheric CO₂ doubling (ΔT_T) is small. This is not surprising considering that the CO₂ concentration in the T-run is not doubled in the middle atmosphere, so that direct radiative effects are absent. However, a statistically significant warming of more than 3 K in the Arctic lower stratosphere (maximum at 20 hPa) and a statistically significant cooling of more than 2 K in the tropical lower stratosphere (maximum at 50 hPa) is found. Figure 2.6b shows that in the T-run the middle atmospheric zonal wind weakens in the Arctic and increases in the subtropics. These changes are statistically significant at a more than 95% confidence level.

Figure 2.8b shows the change in the residual stream function in the T-run. Similar to what was found in the A-run, the residual circulation in the T-run strengthens in most of the NH lower and middle stratosphere. However, different from what was found in the A-run, the residual streamfunction does not increase in the NH upper stratosphere and mesosphere. The maximum of the NH residual streamfunction significantly increases with 18% at 50 hPa and with 26% at 100 hPa. These changes are approximately two thirds of the increases found in the A-run. Associated with this increase, the downward motions near the North Pole increase too, leading to adiabatic heating and causing the temperature increase shown in Fig. 2.5b. Similarly, the upward motions in the tropical lower stratosphere increase, causing adiabatic cooling and a temperature decrease in the tropical lower stratosphere.

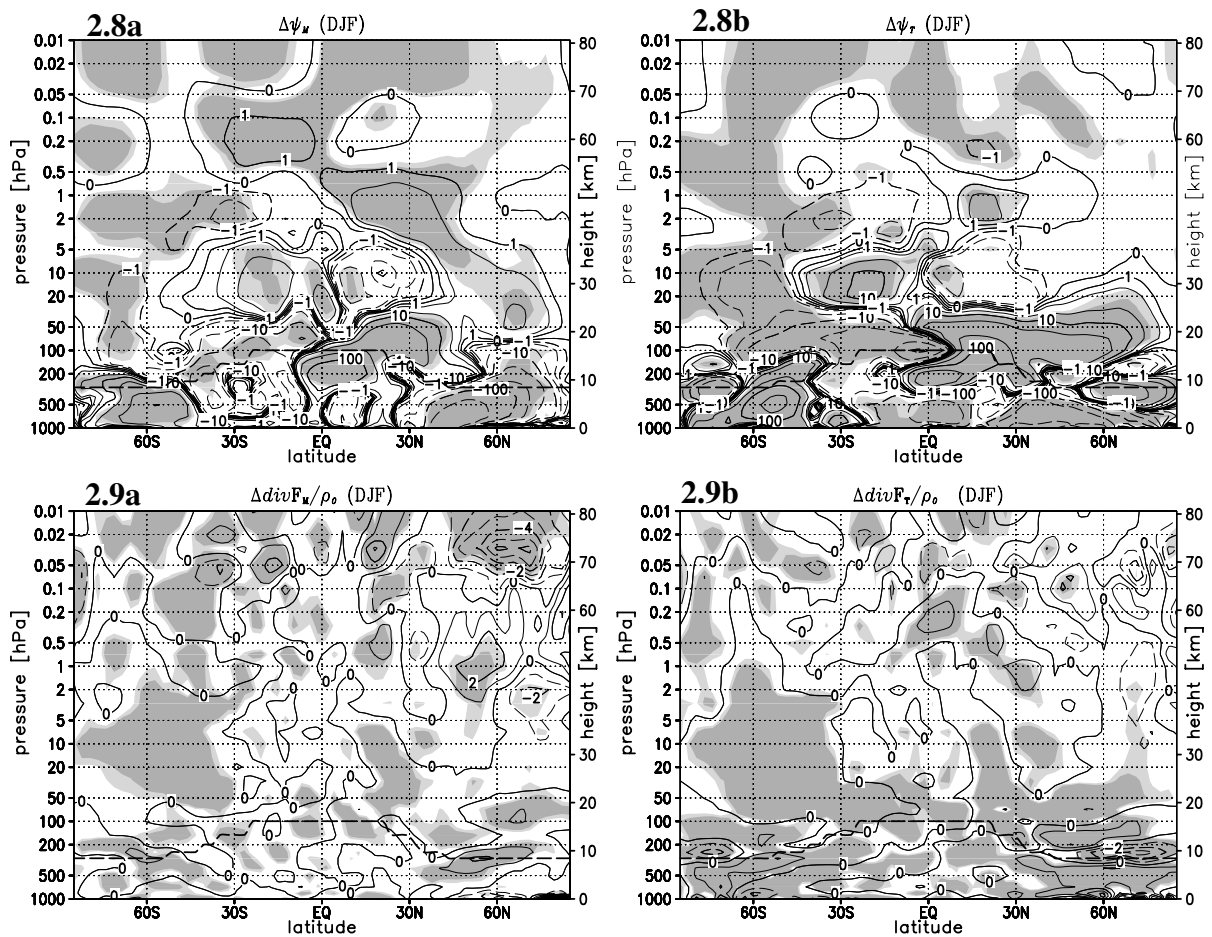


Fig. 2.8a+b: As in Fig. 2.5a+b, except for the residual stream function. Contour lines are at 0, ± 1 , ± 2 , ± 5 , ± 10 , ± 20 , ± 50 etc. $\text{kg m}^{-1} \text{s}^{-1}$.

Fig. 2.9a+b: As in Fig. 2.5a+b, except for $\text{div}F/\rho_0$. The contour interval is $1 \text{ m s}^{-1} \text{day}^{-1}$.

Also similar to what was found in the A-run, the increased stratospheric residual circulation is driven by the increased wave driving by both resolved (planetary) waves and unresolved (gravity) waves. The effect of the resolved waves on the zonal-mean flow is quantified by $div\mathbf{F}_T/\rho_0$. The causes of $\Delta div\mathbf{F}_T/\rho_0$ (Fig. 2.9b) are similar to the causes of $\Delta div\mathbf{F}_A/\rho_0$ described in subsection 2.3.2: the negative values of $\Delta div\mathbf{F}_T/\rho_0$ in the NH mid-latitude lower stratosphere are again mainly caused by dissipation of increased upward propagating wave activity in the lower stratosphere, and the pattern of $\Delta div\mathbf{F}_T/\rho_0$ in the NH subtropical lower stratosphere and in the NH upper stratosphere is again mainly determined by changes in the meridional refraction of the planetary waves (*not shown*).

To summarize, the patterns and causes of the middle atmospheric changes in the T-run are similar to those in the A-run, with the exception that in the T-run the middle atmosphere does not cool due to the radiative effects of CO₂ doubling. The residual circulation increase in the T-run is about two thirds of the increase in the A-run.

2.5.2 Middle atmospheric response to middle atmospheric CO₂ doubling

(M-run)

Figure 2.5a shows that the middle atmosphere cools in response to middle atmospheric CO₂ doubling, which can be explained by radiative arguments. Since the temperature responses in the Arctic lower stratosphere are additive (Fig. 2.5c), it is tempting to conclude that the positive ΔT_A in the Arctic stratosphere (Fig. 2.2a) is a small residual of a negative ΔT_M due to radiative cooling and a somewhat larger positive ΔT_T due to dynamical heating. However, a more detailed investigation of the responses in the M-run reveals that ΔT_M itself is a result of both radiative cooling and dynamical heating. Figure 2.8a shows that, similar to what was found in the A-run, the stratospheric residual circulation in the M-run generally increases, with the exception of the tropical middle stratosphere. The amplitude of this increase is approximately one third of that in the A-run; the maximum of the residual streamfunction in the M-run significantly increases with 7% at 50 hPa and with 13% at 100 hPa. Similar to what was found in the A- and the T-run, this increase is associated with stronger downward motions in and a warming of the Arctic lower stratosphere. Since ΔT_M is negative in this region, it can be concluded that in the M-run the radiative cooling is larger than the dynamical heating. The patterns of $\Delta div\mathbf{F}_M/\rho_0$ (Fig. 2.9a), $\Delta div\mathbf{F}_M^y/\rho_0$ and $\Delta div\mathbf{F}_M^z/\rho_0$ (*not shown*) are similar to those in the T- and A-run, but the amplitudes are smaller.

In summary, the simulated Arctic lower stratospheric warming in the uniformly doubled CO₂ climate is a small residual of radiative cooling and dynamical heating. The dynamical heating is caused by increased downward motions associated with the increase of the stratospheric residual circulation, which is caused by the increase of both the resolved and

unresolved wave driving. The stratospheric residual circulation increase can be attributed for about two thirds to the (remote) tropospheric CO₂ doubling and for about one third to the (in situ) middle atmospheric CO₂ doubling.

2.6 Tropospheric response to non-uniform CO₂ doubling

2.6.1 Tropospheric response to middle atmospheric CO₂ doubling (M-run)

Figure 2.5a shows that in the largest part of the troposphere the temperature response to middle atmospheric CO₂ doubling (ΔT_M) is small. This is not surprising since in the M-run the CO₂ is not doubled in the troposphere, so that direct radiative effects are absent. The tropospheric ΔT_M is characterized by a ‘tongue’ of increased positive ΔT_M in both the NH and SH mid-latitudes. Figure 2.6a shows that in the M-run the tropospheric zonal wind increases in the region north of 45°N. This increase is largest around 55°N and is generally statistically significant between 45° and 70°N. The amplitude of Δu_M is here comparable to that of Δu_A , implying that this tropospheric zonal wind response to middle atmospheric CO₂ doubling is substantial. Since the zonal wind responses were shown to be non-additive in the regions around 35°N and 70°N, the negative Δu_M near 35°N and the positive Δu_M north of 65°N will not be further discussed. The poleward shift of the SH westerlies in the A-run also occurs in the M-run. In this region, Δu_M is about one third of Δu_A .

Figure 2.7a shows the surface zonal wind response to middle atmospheric CO₂ doubling. The positive Δu_M in the western part of the northern Atlantic is statistically significant, and only slightly smaller than Δu_A (Fig. 2.2d). Since the surface zonal wind responses were shown to be non-additive above the northern Pacific (Fig. 2.7c), the pattern of Δu_M in this region will not be discussed.

2.6.2 Tropospheric response to tropospheric CO₂ doubling (T-run)

Figure 2.5b shows that the troposphere significantly warms in response to tropospheric CO₂ doubling, which is due to the radiative effects of the increased CO₂ concentration. In the troposphere, ΔT_T is about 80% of ΔT_A . Since the imposed SST increases in the T-run are 84% of those in the A-run (see subsection 2.2.2), this result suggests that the strength of the tropospheric warming is also influenced by the imposed SSTs. The structure of ΔT_T is similar to that of ΔT_A : the largest values (more than 5 K) occur in the tropical upper troposphere.

In the NH mid-latitude troposphere Δu_T (Fig. 2.6b) is very small and not statistically significant, in contrast to Δu_M (Fig. 2.6a). Since the zonal wind responses are additive in this region, this result indicates that not the tropospheric CO₂ doubling, but the remote middle

atmospheric CO₂ doubling is the main cause of the increased tropospheric NH mid-latitude westerlies in the uniformly doubled CO₂ climate. It indicates that the downward influence of the middle atmospheric CO₂ increase on the tropospheric climate is quite pronounced, at least in the NH mid-latitudes. Figure 2.6b shows that the poleward shift of the SH westerlies also occurs in the T-run. In this region, the amplitude of Δu_T is about two thirds of that of Δu_A . As the zonal wind responses are additive in this region, this suggests that the poleward shift of the SH westerlies in the uniformly doubled CO₂ climate is mainly due to tropospheric CO₂ doubling. In contrast to the tropospheric zonal mean Δu_T , the surface Δu_T (Fig. 2.7b) is statistically significant in some parts of the NH mid-latitudes. The surface zonal wind above the northern Atlantic increases in response to tropospheric CO₂ doubling, but this increase is only significant in a small region in the east part of the northern Atlantic.

To summarize, the middle atmospheric CO₂ doubling causes significant increases in the tropospheric NH mid-latitude westerlies, in contrast to the tropospheric CO₂ doubling. Since the zonal wind responses are additive in this region, it can be concluded that the middle atmospheric CO₂ doubling is the main cause of the increased tropospheric NH mid-latitude westerlies in the uniformly doubled CO₂ climate.

2.7 Additional experiments on the response of the troposphere to middle atmospheric CO₂ doubling

In subsection 2.6.1 it has been shown with the M-run that the middle atmospheric CO₂ doubling causes significant increases in the tropospheric NH mid-latitude westerlies during DJF. To account for the effect of the radiative forcing of middle atmospheric CO₂ doubling on the SSTs, the imposed SST increase in the M-run is 16% of that in the A-run (see subsection 2.2.2). Two questions arise which will be addressed in this section:

- 1) Which part of the tropospheric response in the M-run is caused by the imposed SST changes, and which part is caused by the middle atmospheric CO₂ doubling?
- 2) How well has the middle atmosphere to be represented in GCM's to capture the middle atmospheric influence on the troposphere?

The first question will be addressed in subsection 2.7.1, where results will be presented from an experiment (denoted as the MC-run) with the same configurations as the M-run, except that the control SSTs are prescribed. The second question will be addressed in subsection 2.7.2, where results will be presented from an experiment in which the CO₂ is doubled only above 10 hPa. The responses found in this experiment will give an indication of how much of the middle atmospheric CO₂ doubling influence on the troposphere is not captured in GCM's with an upper boundary around 10 hPa.

2.7.1 Tropospheric response to middle atmospheric CO₂ doubling without change of SSTs

Figure 2.10a shows that the tropospheric pattern of the temperature response in the MC-run (denoted as ΔT_{MC}) is similar to that in the M-run (Fig. 2.5a) in the Northern Hemisphere, but different from that in the M-run in the Southern Hemisphere: in the MC-run the ‘tongue’ of increased temperatures is only found in the Northern Hemisphere. The ΔT_{MC} is 0.3-1 K smaller than ΔT_M . These results show that the imposed SST-changes in the M-run cause a rather uniform tropospheric warming and a ‘tongue’ of additional warming in the SH mid-latitudes. Similar conclusions can be drawn for the tropospheric zonal wind (Fig. 2.10b): the significant mid-latitude zonal wind increases in the M-run only occur in the MC-run in the mid-latitudes of the Northern Hemisphere. The tropospheric Δu_{MC} is even larger than the Δu_M , suggesting that in the M-run the imposed SSTs weaken the tropospheric zonal wind response to middle atmospheric CO₂ doubling. Similar results are found for the surface zonal wind: above the northern Atlantic the surface Δu_{MC} (Fig. 2.10c) is about twice larger than the

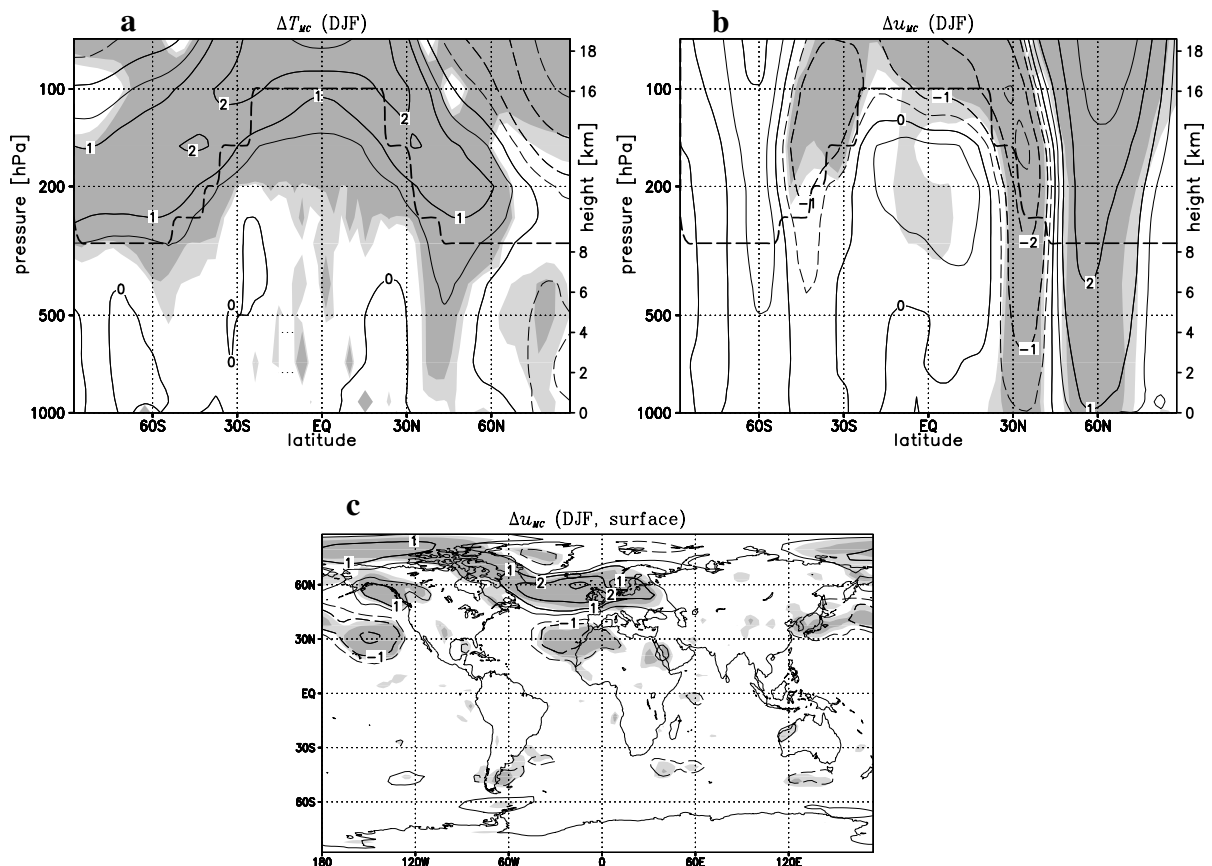


Fig. 2.10a-c: The difference of the zonally averaged temperature (a) and zonal wind (b), and the surface zonal wind (c) between the MC- and C-run in the DJF season. The contour lines in Fig. 2.10a are at 0, ± 0.5 , ± 1 , ± 2 , ± 3 etc. K. Contour lines in Fig. 2.10(b+c) same as in Fig. 2.2(b+d). Light (dark) shade denotes significance at 95% (99%) level.

surface Δu_M . It can thus be concluded that in the M-run, the increased NH westerlies are not caused by the imposed SSTs, but by the middle atmospheric CO₂ doubling. From this result and the results presented in section 2.6, it can be concluded that the middle atmospheric CO₂ doubling and not the imposed SSTs or tropospheric CO₂ doubling is the main cause of the increased NH westerlies in the uniformly doubled CO₂ climate. On the other hand, the poleward shift of the SH westerlies in the M-run is not found in the MC-run, suggesting that the SH response in the M-run is caused by the imposed SST changes. It is concluded that not the middle atmospheric CO₂ doubling, but the tropospheric CO₂ doubling and the imposed SSTs cause the poleward shift of the SH mid-latitude westerlies in the uniformly doubled CO₂ climate.

2.7.2 Tropospheric response to CO₂ doubling above 10 hPa

Now that it has been demonstrated that the middle atmospheric CO₂ doubling is important for the tropospheric and surface climate response in the uniformly doubled CO₂ climate, one may wonder how well the middle atmosphere has to be represented in GCM's to capture this downward influence. As described in section 2.1, several authors have addressed this issue previously. Gillett *et al.* (2002) and Shindell *et al.* (1999) compared the AO-responses to increasing greenhouse gases in a high (upper boundary around 0.01 hPa) and a low (upper boundary around 10 hPa) version of their models, and found contrasting results. Instead of varying the upper boundary of the GCM, we investigate the importance of changes in the region above 10 hPa with a slightly different approach. An additional run has been performed in which the CO₂ is doubled between 10 hPa and 0.01 hPa to investigate directly the influence of CO₂ changes above 10 hPa on the surface climate. SSTs from the control run are imposed in this run, which will be referred to as the H-run.

Figure 2.11a shows that the tropospheric temperature response to CO₂ doubling above 10 hPa (ΔT_H) is generally small. The tropospheric zonal wind response in the NH mid-latitudes (Δu_H , Fig. 2.11b) is surprisingly large: Δu_H is not much smaller than Δu_m (Fig. 2.6a) and about 50% of Δu_{MC} (Fig. 2.10b). Like in the M- and MC-run, the zonal wind decreases significantly around 35°N. The zonal wind in the SH troposphere does not change significantly in the H-run. The structure of the surface Δu_H is again similar to that of Δu_{MC} (Fig. 2.10c) and Δu_M (Fig. 2.7a), whereas the amplitude is slightly smaller than the amplitude of Δu_M and about 50% of the amplitude of Δu_{MC} . These results suggest that CO₂ doubling above 10 hPa significantly contributes to the strengthening of the tropospheric NH mid-latitude westerlies in the uniformly doubled CO₂ climate.

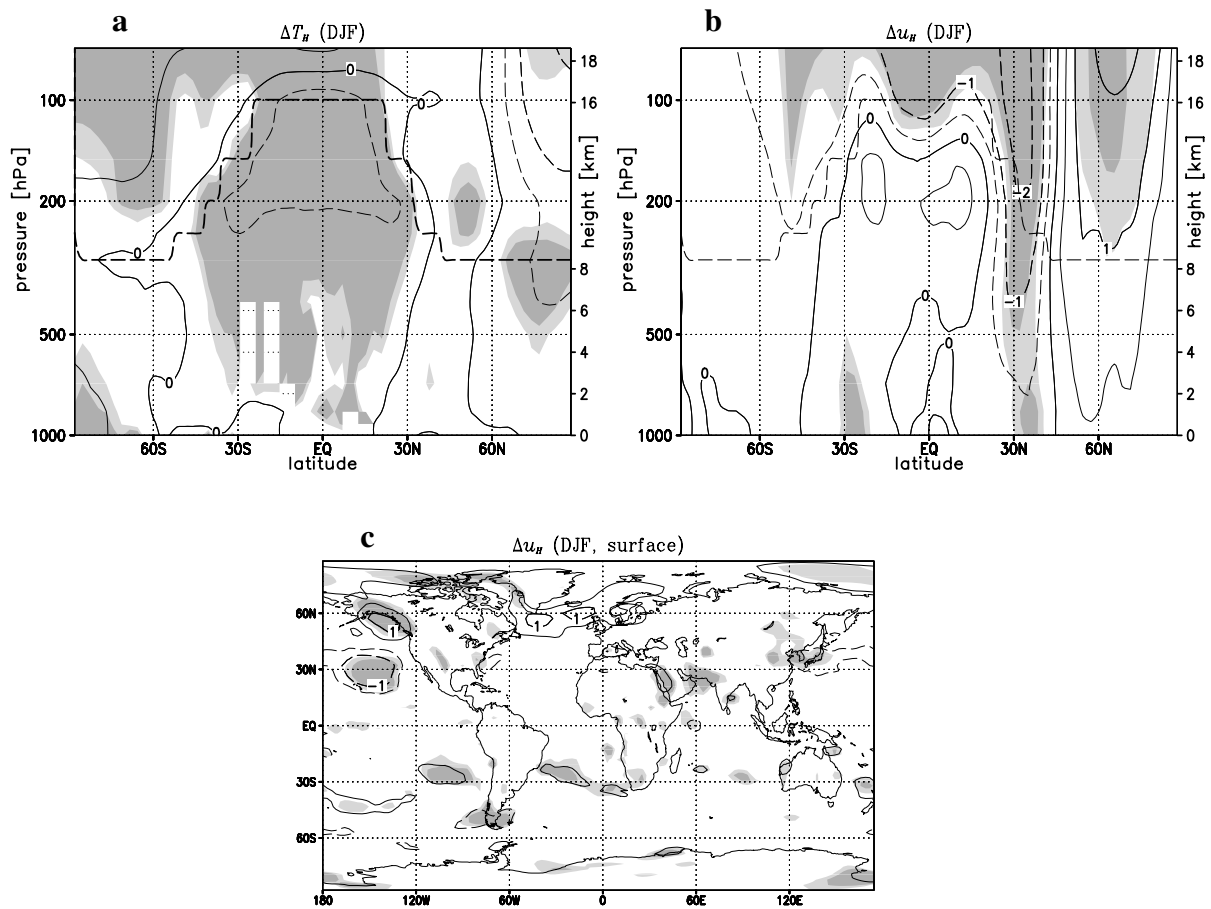


Fig. 2.11a-c: As in Fig. 2.10a-c, except for the difference between the H- and C-run.

2.8 Discussion and conclusions

In this Chapter, the separate climate effects during NH winter of tropospheric and middle atmospheric CO_2 doubling have been studied with the middle atmosphere version of the ECHAM global climate model. It has been investigated to what extent the changes in the uniformly doubled CO_2 climate can be considered as the sum of the separate tropospheric and middle atmospheric CO_2 doubling responses. Thereafter, changes in the uniformly doubled CO_2 climate have been attributed to either tropospheric or middle atmospheric CO_2 doubling. In addition, the question how well the middle atmosphere has to be represented in GCM's to acquire reliable tropospheric climate predictions, has been addressed.

Since planetary waves originating from the troposphere are dissipated in the stratosphere and drive a meridional circulation, and the stratosphere is thought to exert a significant downward influence on the troposphere, the coupling between the middle

atmosphere and the troposphere is anticipated to be important for understanding the changes in the doubled CO₂ climate (section 2.1). In the doubled CO₂ climate the Arctic lower stratosphere slightly warms, causing a decrease of the meridional temperature gradient and, consequently, a weakening of the Arctic middle atmospheric zonal wind (section 2.3). The small warming is thought to be caused by increased downward motions associated with an increased residual circulation. In the Arctic lower stratosphere the temperature response in the uniformly doubled CO₂ climate can be regarded as the sum of the responses to CO₂ doubling in the middle atmosphere and in the troposphere (section 2.4). The increased residual circulation contributing to the small Arctic lower stratospheric warming in the uniformly doubled CO₂ climate can be attributed for about two thirds to the tropospheric CO₂ doubling and about one third to the middle atmospheric CO₂ doubling (section 2.5). These results are consistent with those presented by Rind *et al.* (1990), who with much shorter experiments found that both the middle atmospheric and tropospheric CO₂ doubling contribute to the increase of the residual circulation. However, the increase of the stratospheric residual circulation and the resulting dynamical heating due to ‘in situ’ middle atmospheric CO₂ doubling is probably larger in their study. In their STRAT-run, which can be compared to our M-run, the dynamical heating due to the stratospheric residual circulation increase exceeds the radiative cooling, resulting in an upper stratospheric warming (their Fig. 4). In our M-run the dynamical heating is smaller than the radiative cooling, resulting in a cooling in the entire middle atmosphere (Fig. 2.5a). However, the STRAT-run was integrated for one winter, whereas our M-run was integrated for 30 years. Therefore, the different results may be due to model differences, but also due to differences in the length of the integration.

In the uniformly doubled CO₂ climate the tropospheric NH mid-latitude westerlies increase and the SH westerlies shift poleward (section 2.3). The zonal wind responses were shown to be additive in these regions (section 2.4). The increased tropospheric NH mid-latitudes westerlies are mainly caused by the (remote) middle atmospheric CO₂ doubling and not by the tropospheric CO₂ doubling. The middle atmosphere contains only ~15% of the total atmospheric mass. If we consider the zonal wind response in terms of response per kg CO₂ increase, the zonal wind response to middle atmospheric CO₂ doubling is even more dominant over that due to tropospheric CO₂ doubling. In contrast, the poleward shift of the SH tropospheric westerlies has been attributed to the tropospheric CO₂ doubling.

It has been concluded that in NH winter the middle atmospheric CO₂ doubling has an important effect on the NH tropospheric climate change. The question of how well the middle atmosphere has to be represented in GCM’s to capture this downward influence has been addressed in subsection 2.7.2. It has been shown that CO₂ doubling above 10 hPa already causes significant increases of the tropospheric NH mid-latitude westerlies.

The question of which mechanisms are responsible for the downward influence of the middle atmosphere in the doubled CO₂ climate is still under debate. Shindell *et al.* (1999) argue that the change in the meridional temperature gradient in the mid-latitude tropopause region in response to increasing greenhouse gases causes changes in the stratospheric circulation that could influence the tropospheric circulation through wave-mean flow interactions. The attribution of the tropospheric NH mid-latitude zonal wind increase to middle atmospheric CO₂ doubling, and the attribution of the poleward shift of the tropospheric SH summer westerlies to tropospheric CO₂ doubling are consistent with this hypothesis. The middle atmospheric zonal wind in NH winter is easterly in the SH, constituting a barrier for the transport of tropospheric wave activity into the middle atmosphere (Charney and Drazin 1961). Because of the lack of wave activity in the middle atmosphere, the middle atmosphere can not influence the tropospheric climate through wave-mean flow interactions. Therefore, the changes in the SH summer troposphere in the doubled CO₂ climate are expected to be the result of changes in the troposphere itself, and not from the coupling with the middle atmosphere. In the northern winter hemisphere, the middle atmospheric zonal wind is westerly, allowing tropospheric wave activity to propagate into the stratosphere, which, through wave-mean flow interactions can influence the troposphere. Shindell *et al.* (1999) found a strengthening of the Arctic vortex in response to increasing greenhouse gases, and argued that it induces a strengthening of the (lower) tropospheric westerlies through wave-mean flow interactions. Our results do not support this argument, since we also find a strengthening of the tropospheric NH mid-latitude westerlies, but a weakening of the stratospheric Arctic zonal winds (both results are also found in other models, see Gillett *et al.* 2003a). This does not contradict the hypothesis that the tropospheric NH mid-latitude zonal wind changes are induced by stratospheric zonal wind changes through wave-mean flow interactions, but the exact mechanism remains unclear.

In summary, in this Chapter the importance of the tropospheric climate change for the increase of the stratospheric residual circulation and associated middle atmospheric responses (small Arctic lower stratospheric warming and weakening of zonal wind in the Arctic middle atmosphere) in the uniformly doubled CO₂ climate has been shown. In addition, the results indicate the crucial role of the middle atmospheric climate change in the increase of the tropospheric NH mid-latitude westerlies in the uniformly doubled CO₂ climate. Finally, the need to include the region above 10 hPa in GCM's to acquire realistic climate predictions has been advocated.

2.9 Appendix: Note on the tropical stratospheric vertical wind in MA-ECHAM

The model simulations presented in this Chapter have been used in the study of Scaife *et al.* (2003), who intercompared the strength of the upward branch of the stratospheric residual circulation (commonly referred to as the tropical pipe) and its response to greenhouse gas increases in several GCM's. The zonally and annually averaged vertical motions in our 30-year climatologies were found to be downward in some parts of the tropical pipe, in contrast to the results from other models.

To investigate these differences, a sensitivity study has been done by performing several one-year control integrations. The structure of the zonally and annually averaged vertical velocity field in the tropical stratosphere was found to be insensitive to horizontal resolution and gravity wave parameterisation. However, it is very sensitive to whether it is calculated from daily, 12-hourly, or 6-hourly data. The plot based on daily data (at 12 GMT) shows that in large regions the vertical motions in the tropical pipe region are downward (Fig. 2.12a), whereas the downward motions are less pronounced in the plot based on 12-hourly data (Fig. 2.12b). The downward motions in the tropical stratosphere are absent in the plot calculated from 6-hourly data (Fig. 2.12c). The plots calculated from 3-hourly and 1-hourly data are almost identical to the plot calculated from 6-hourly data (*not shown*). These results indicate a large daily cycle in the modelled zonally averaged vertical velocity.

The vertical velocity plot of our runs in Scaife *et al.* (2003) is based on daily data, whereas the results from other GCM's are calculated from 12-hourly or 6-hourly data. Therefore, the strong sensitivity of the annually averaged vertical wind in the tropical pipe to the frequency of the data can explain the difference between our tropical pipe structure and that found by others. It would be interesting to investigate whether this sensitivity is also large in other models. If this would be the case, this would imply that in model intercomparison studies the time-averaged vertical velocity should always be calculated from data with the same frequency. The results presented in this Appendix indicate that a data frequency of 6 hours would be sufficient. It would also be interesting to repeat this analysis using observational data.

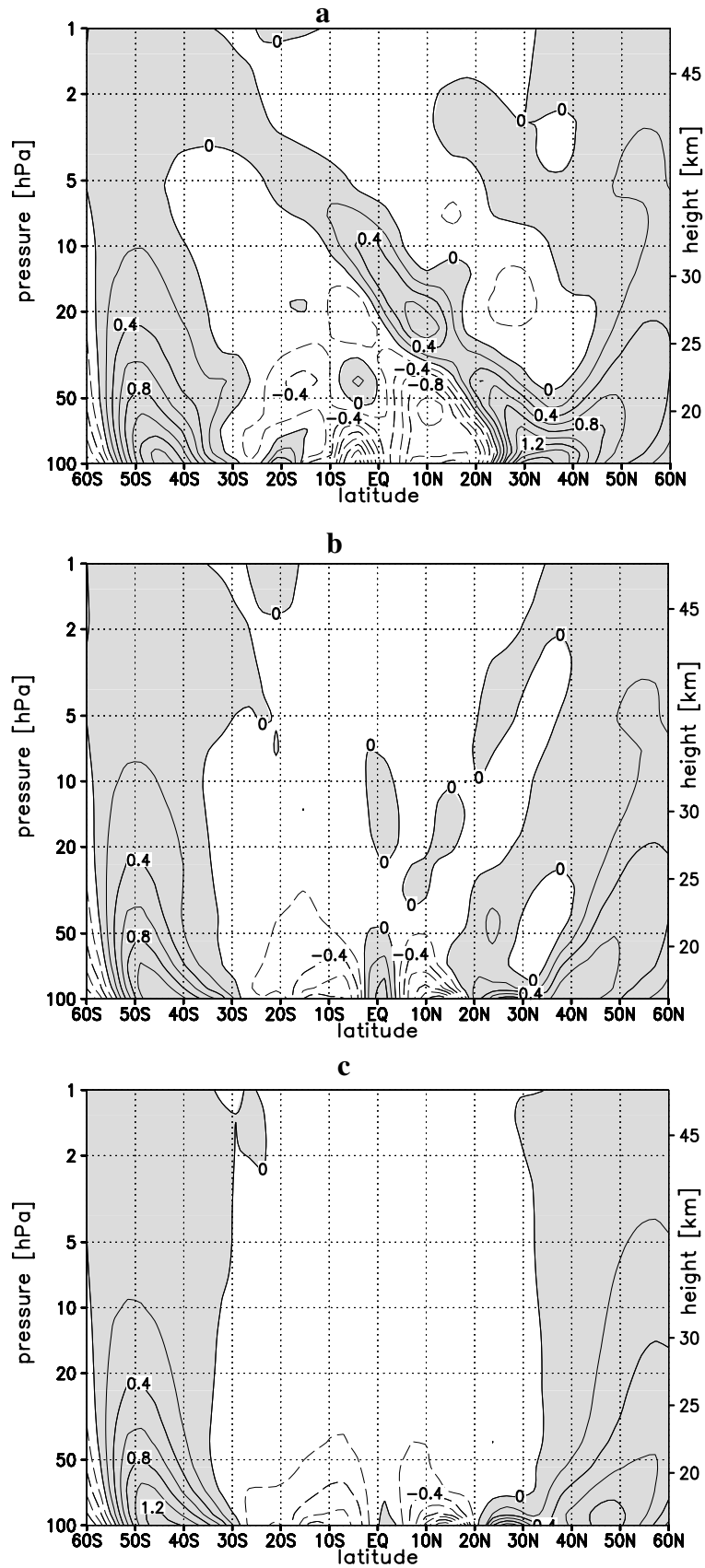


Fig. 2.12a-c: The annually and zonally averaged vertical wind ω (mPa s^{-1}) of a one-year control run, calculated from daily (a), 12-hourly (b) and 6-hourly (c) data. Negative values of ω denote upward motion.

Acknowledgements

The authors would like to thank Hans Cuijpers (KNMI) for extensive model support, Peter van Velthoven and Rob van Dorland (both KNMI), Frans Sluiter (Eindhoven University of Technology), and Neal Butchart and Adam Scaife (both UK Meteorological Office) for helpful comments and suggestions, Kleareti Tourpali (University of Thessaloniki) for providing the tropopause climatology, and Erich Roeckner (Max-Planck-Institut für Meteorologie) for providing the SST climatologies for the C- and A-run.

Chapter 3

Analysis of the coupling between the stratospheric meridional wind and the surface level zonal wind during 1979-93 Northern Hemisphere extratropical winters *

The coupling between the stratosphere and the troposphere has been investigated by analysing low-frequency variations in (1) the meridional mass flux into the polar cap (north of 60°N), computed separately for the stratosphere and the troposphere, (2) the polar cap mean surface pressure, and (3) the surface level meridional pressure gradient and zonal wind around 60°N. The analysis has been done for the 1979-93 Northern Hemisphere (NH) winters, using ECMWF reanalysis data. The results show that for all winters the meridional mass flux variations in the stratosphere precede those in the troposphere, by about one day. This result can also be obtained qualitatively with a very simple model, based on the zonally averaged zonal and meridional momentum equations. The lag is not very sensitive to the latitude of the southern boundary of the polar cap. The analysed variations in the polar cap mean surface pressure associated with variations in the meridional mass flux, determine most of the variability in the analysed meridional surface pressure gradient and the associated surface zonal wind around 60°N. The results also show that in the stratosphere the Coriolis force associated with the zonal-mean meridional wind is in near-balance with the convergence of the eddy momentum flux, and in the lower troposphere with the zonal frictional force. In summary, the results indicate that in the extratropical northern winter hemisphere, low-frequency variations in the meridional wind in the stratosphere induce low-frequency variations in the zonal wind near the surface.

* This Chapter is a slightly revised version of: Sigmond, M., P.C. Siegmund, and H. Kelder, 2003a: Analysis of the coupling between the stratospheric meridional wind and the surface level zonal wind during 1979-93 Northern Hemisphere extratropical winters. *Clim. Dyn.*, **21**, 211-219, doi: 10.1007/s00382-003-0328-2.

3.1 Introduction

Since the troposphere holds most of the atmospheric mass, it is not surprising that the troposphere influences the stratospheric circulation. Planetary waves generated in the troposphere can, under certain conditions, propagate upward to the stratosphere where they dissipate (Charney and Drazin 1961, Matsuno 1970) and drive the stratospheric circulation away from its radiatively determined state (e.g., Holton 1992).

The view that the stratosphere can influence the tropospheric circulation is less commonly held (Hartmann *et al.* 2000). An important manifestation of this downward influence is the propagation of low-frequency zonal wind variations from the upper stratosphere to the lower troposphere, which has been noted, e.g., by Kodera *et al.* (1990), Kuroda and Kodera (1999) and Christiansen (2001). Much of the recent research on stratosphere-troposphere coupling has been done in the framework of the Arctic Oscillation (AO). The AO is the leading mode of variability in the NH wintertime circulation (Thompson and Wallace 1998). Baldwin and Dunkerton (1999) noted that low-pass filtered AO-signature variations propagate downward from the stratosphere to the lower troposphere in most winters from 1958 to 1997. The induced tropospheric anomalies tend to persist during up to two months after extreme circulation anomalies in the northern extratropical stratosphere (Baldwin and Dunkerton 2001). Stratosphere-troposphere coupling is often studied in the framework of the AO since it has the advantage of explaining, by definition, the maximum of variance of circulation patterns. However, since the AO is not a variable in the primitive equations, its usefulness for searching for mechanisms of stratosphere-troposphere coupling is limited. Therefore, in this Chapter the coupling is investigated in terms of quantities that are part of these equations, such as the zonal and meridional wind.

Several authors have suggested mechanisms by which the stratosphere could dynamically influence the troposphere. Hartmann *et al.* (2000) noted that three such mechanisms can be postulated: potential vorticity induction (Hartley *et al.* 1998, Black 2002), interaction between the zonal-mean flow and upward propagating waves (Haynes *et al.* 1991, Christiansen 1999, Shindell *et al.* 2001) and mass redistribution in the stratosphere (Baldwin and Dunkerton 1999, Shindell *et al.* 2001). This last mechanism will be the subject of the present study.

Baldwin and Dunkerton (1999) suggested that an anomalous zonal body force in the stratosphere induces a meridional circulation whose stratospheric branch is thought to be not entirely compensated by a tropospheric return flow due to friction (Haynes and Shepherd 1989). Consequently, the total mass (and thus the mean surface pressure) in the polar cap would change which, in turn, would affect the meridional surface pressure gradient and the (geostrophically) coupled zonal wind around the southern boundary of the polar cap. However, whether this mechanism indeed occurs is still unclear. The aim of the present study is to investigate the existence of such a mechanism by analysing variations in the stratospheric and tropospheric meridional mass flux into or out of the polar cap, and the associated

variations in the polar cap mean surface pressure and in the lower tropospheric meridional pressure gradient and zonal wind. For this purpose ECMWF reanalysis data for the NH extratropical winters from 1979 to 1993 have been used.

This Chapter is organised as follows. In section 3.2, the applied ECMWF-data are described. In section 3.3, the mass flux into the polar cap is computed separately for the troposphere and the stratosphere. The total stratospheric plus tropospheric mass flux into the polar cap is compared with the tendency of the polar cap mean surface pressure and with the meridional surface pressure gradient and the zonal wind near the surface. Furthermore, the forces governing the meridional motions in the stratosphere and the troposphere are studied. Finally, the results are discussed in section 3.4.

3.2 Data and method

For this study data from the ECMWF 15-year reanalysis project (ERA15, see Gibson *et al.* 1997) at 0, 6, 12 and 18 GMT from November to March, for the winters 1979-80 to 1992-93 are used. The data used are on a $2.5^\circ \times 2.5^\circ$ horizontal grid at 31 hybrid sigma-pressure levels, extending from the surface up to 10 hPa. To filter out synoptic disturbances, the data have been low-pass filtered using an 11-day running mean filter. Variations remaining in the time-series after application of this filter will hereafter be called 'low-frequency'.

3.3 Results

3.3.1 Meridional wind around 60°N

Figure 3.1 shows the zonal-mean meridional wind between 50 and 70°N averaged over all winters between 1979 and 1993, and corresponds closely with the meridional wind climatology of e.g., Peixoto and Oort (1992). The Ferrel cell, which is characterised by relatively large equatorward (negative) winds at tropopause level and relatively large poleward (positive) winds below 850 hPa, is situated south of 60°N . North of 60°N , the largest equatorward winds are found near the top of the model (10 hPa), and the average poleward wind between 700 and 900 hPa is equatorward (negative), which corresponds to the lower branch of polar meridional circulation. The average level of transition from poleward to equatorward winds varies from about 650 hPa in the Ferrel cell to about 50 hPa at 70°N . At 60°N , this level of zero meridional wind is very close to the zonally and DJF averaged tropopause height, which is at approximately 270 hPa (Hoinka 1998). The meridional flows at this latitude, which is also the latitude at which the positive correlation between the Arctic Oscillation index and the zonal wind is maximal (Baldwin and Dunkerton 1999), are investigated in this section.

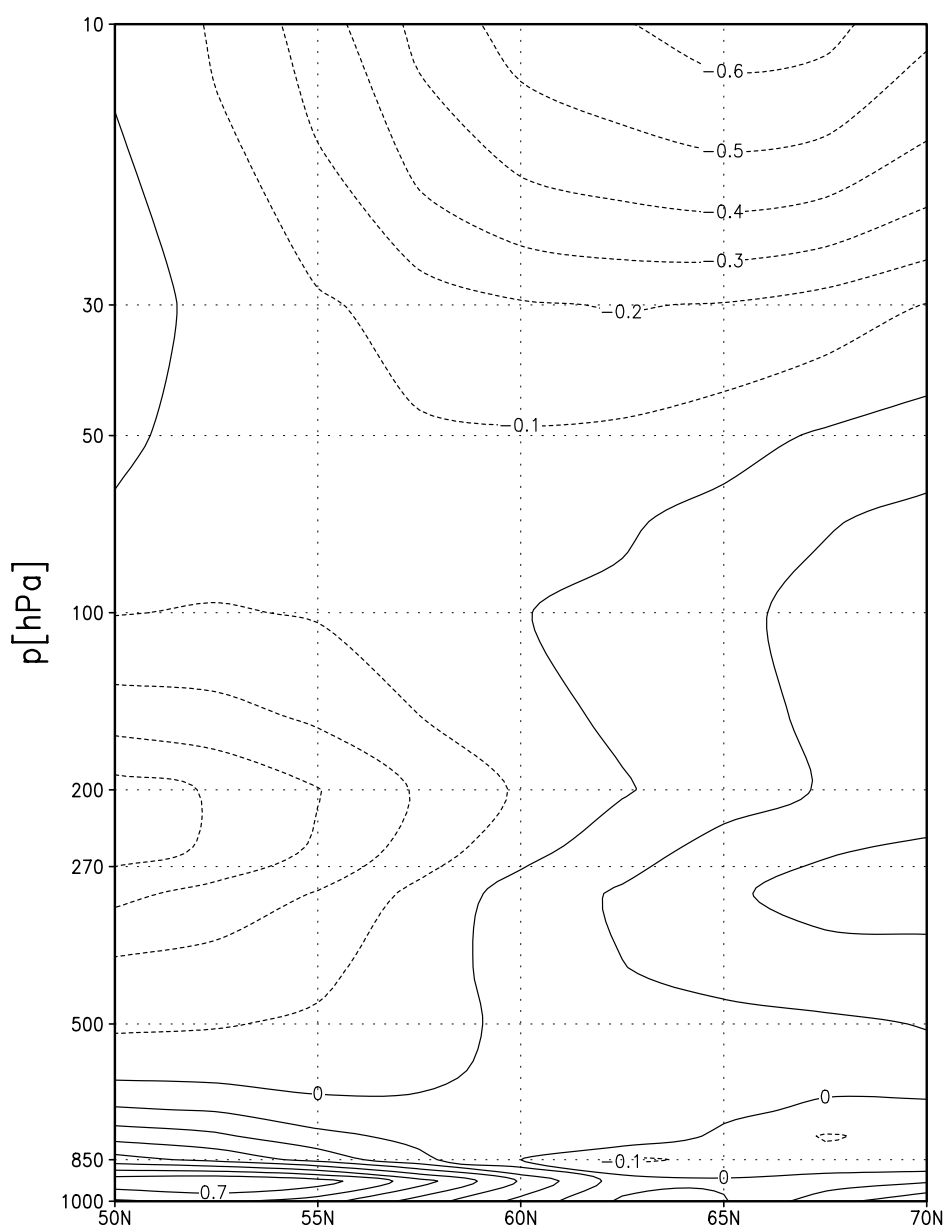


Fig. 3.1: The zonal-mean meridional wind between 50 and 70°N averaged over all winters (DJF) between 1979 and 1993.

Figure 3.2 shows the winter (DJF) mean of the zonal-mean meridional wind at 60°N as a function of pressure and winter. It shows that this wind is generally equatorward (negative) in the stratosphere and generally poleward (positive) in the troposphere. The difference between the equatorward mass flux out of the polar cap (i.e., the region north of 60°N) and the poleward mass flux into the polar cap causes a change in the total atmospheric mass in the polar cap and thus in the surface pressure averaged over the polar cap. Such a change may lead to a different meridional surface pressure gradient, and, by geostrophical balance, to a different zonal wind near the surface around the southern boundary of the polar cap (60°N). In this way, variations in the stratospheric meridional wind could be coupled to variations in the

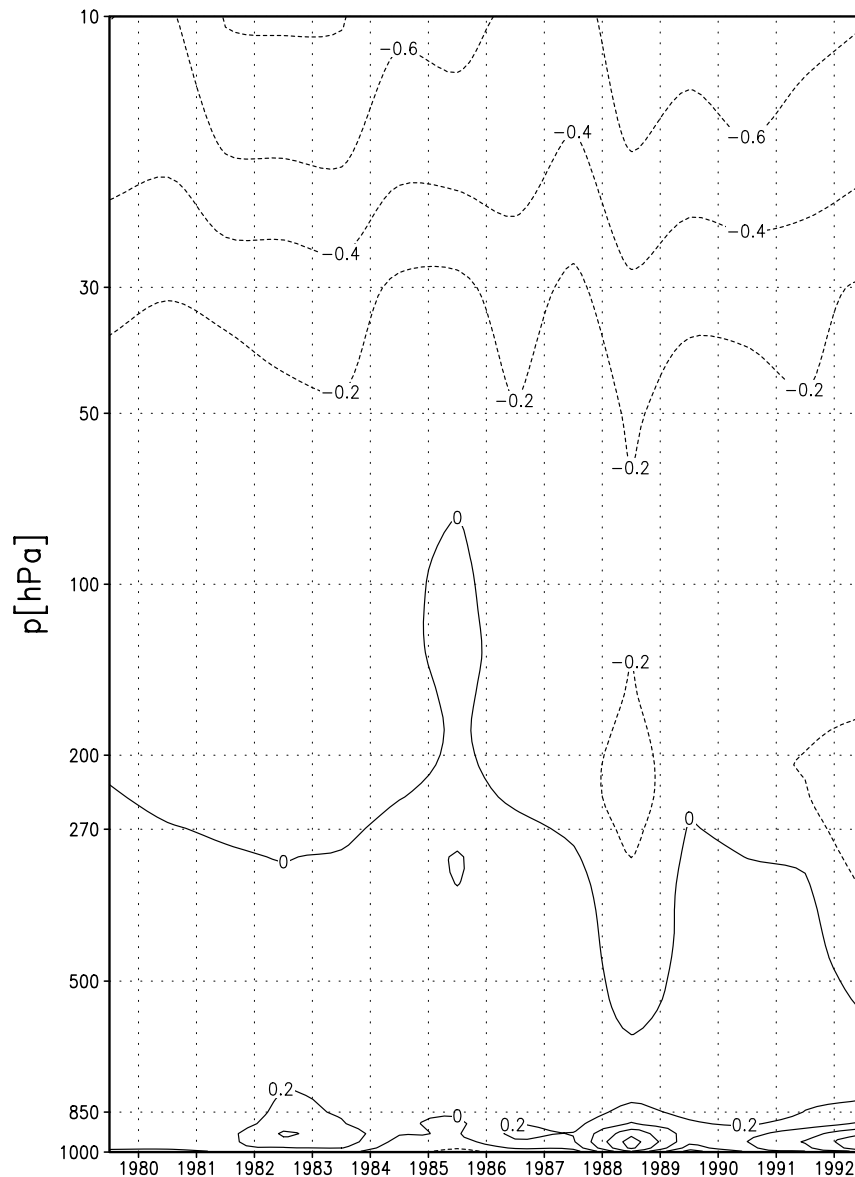


Fig. 3.2: The DJF-mean of the zonal-mean meridional wind at 60°N as a function of pressure and winter. Note that the value for, e.g., the winter 1980-81 is plotted between 1980 and 1981.

zonal wind near the surface. This possible connection between the stratosphere and the troposphere will be investigated for all NH winters from 1979 to 1993.

The low-frequency variations in the meridional mass flux and the related polar cap mean surface pressure variations will be investigated in subsection 3.3.2. The associated variations in the meridional surface pressure gradient around 60°N and the connection with variations in the zonal wind near the surface around 60°N will be discussed in subsection 3.3.3. Finally, the forces governing the meridional mass fluxes at 60°N will be investigated in subsection 3.3.4.

3.3.2 Meridional mass flux at 60°N and its effect on the polar cap mean surface pressure

In this subsection the meridional mass flux into the polar cap is computed separately for the troposphere and the stratosphere. The total mass flux across the southern boundary of the polar cap can be expressed as (e.g., Peixoto and Oort 1992, p.132):

$$\Phi = \int_{\lambda=0}^{\lambda=2\pi} \int_{z=0}^{z=\infty} (\rho v_{bpc} \cos(\varphi_{bpc}) a) dz d\lambda, \quad (3.1a)$$

where λ is longitude, a is the radius of the Earth, ρ is the density of the air, φ_{bpc} is the latitude of the southern boundary of the polar cap and v_{bpc} is the meridional wind at this latitude. Assuming hydrostatic equilibrium, Eq. (3.1a) can be written as:

$$\Phi = g^{-1} \int_{\lambda=0}^{\lambda=2\pi} \int_{p=0}^{p_0(\lambda)} (v_{bpc} \cos(\varphi_{bpc}) a) dp d\lambda, \quad (3.1b)$$

where g is the acceleration due to gravity, p is pressure and p_0 is surface pressure. The meridional mass flux has been decomposed into a stratospheric (Φ_S) and a tropospheric (Φ_T) part. A typical model level for the tropopause at 60°N, which is at approximately 270 hPa, is used tentatively as the boundary between the troposphere and the stratosphere. The stratosphere extends from this model level to 0 hPa. The vertical integration over pressure is done with the trapezium method, where v between 10 and 0 hPa was calculated using linear extrapolation of v at the two highest model levels. First the winter of 1988-89 will be investigated as an example, after which the analysis will be extended to all NH winters from 1979 to 1993.

winter 1988-89

Figure 3.3a shows the time series of the 11-day running mean of the tropospheric (Φ_T) and the opposite of the stratospheric (Φ_S) part of the meridional mass flux at 60°N for the winter 1988-89. Both $-\Phi_S$ and Φ_T are positive, implying that averaged over the stratosphere mass is transported out of the polar cap, and that averaged over the troposphere mass is transported into the polar cap.

The correlation coefficient of $-\Phi_S$ and Φ_T is calculated for time lags between the two time series that are multiples of the sampling period (i.e., multiples of 0.25 day). A maximal correlation is found when the time series of $-\Phi_S$ is shifted by +0.25 day. This implies that, in

the winter 1988-89, low-frequency variations in the stratospheric mass flux out of the polar cap generally precede similar variations in the tropospheric mass flux into the polar cap, by about 0.25 day. A more accurate value of this lag is obtained by fitting a second order polynomial through the time-lag dependent correlation coefficients for the lags of +0, +0.25 and +0.50 day, and calculating the lag at which this polynomial maximizes, resulting in a lag value of +0.32 day for this winter. Later it will be shown that this value is small compared to the lag values found for other winters, and that the average of all winter values is significantly positive.

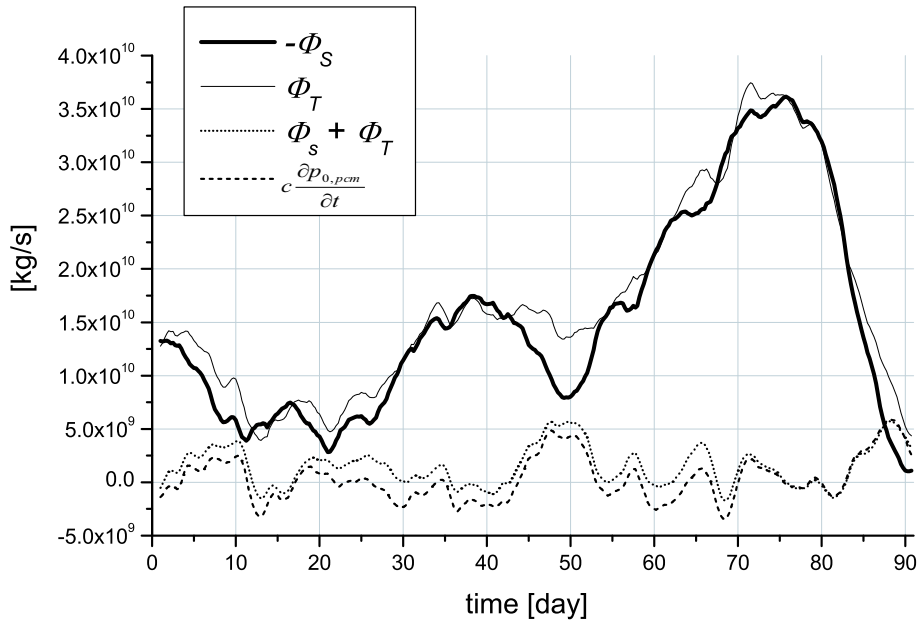


Fig. 3.3a: The time series of the 11-day running mean of $-\Phi_S$, Φ_T , the sum of Φ_S and Φ_T and the product of c and $\partial p_{0,pcm}/\partial t$ for the winter 1988-89 (note: data are plotted every 6 hours; day 1.0: 1 December 1988 0 GMT; day 1.25: 1 December 1988 6 GMT; day 32: 1 January 1989; day 63: 1 February 1989). For the meaning of the symbols see subsection 3.3.2.

The conservation of mass requires that the net mass flux into the polar cap atmosphere (i.e., the difference between the stratospheric outflow and tropospheric inflow) is equal to the net change of mass in the polar cap, and thus proportional to the tendency of the polar cap mean surface pressure:

$$\Phi_S + \Phi_T = c \frac{\partial p_{0,pcm}}{\partial t}, \quad (3.2a)$$

where

$$c = 2\pi a^2 g^{-1} (1 - \sin \phi_{bpc}), \quad (3.2b)$$

and $p_{0,pcm}$ is the polar cap mean surface pressure.

The time series of the 11-day running mean of both the lhs and the rhs of Eq. (3.2a) are also plotted in Fig. 3.3a. It shows that, although the analysed lhs term (the mass flux) is larger than the analysed rhs term (the ‘tendency term’), the correlation between these terms is very high (0.93). An imbalance between the mass flux and the tendency term can be due to the lack of mass conservation in the circulation data used (Trenberth 1991), a mass flux out of the polar cap atmosphere to the polar cap surface (in particular: precipitation minus evaporation), and to numerical errors in the calculation of the tendency term or errors in the vertical integration of the meridional wind. A large source of this difference is probably related to the upper boundary condition of the vertical integration method. The negative zonal-mean meridional wind at 60°N shown in Fig. 3.2 could increase more than linearly with height above 10 hPa. However, in the calculation of the mass flux, the meridional wind between 10 and 0 hPa was calculated using linear extrapolation of data at the two highest model levels. Therefore, $-\Phi_S$ is likely to be underestimated, leading to an overestimation of $\Phi_S + \Phi_T$. This explanation for overestimating the mass flux is supported by the fact that the absolute difference between the mass flux and the tendency term at 50°N averaged over all winters between 1979 and 1993 is two times smaller than this difference at 60°N (*not shown*). As shown in Fig. 3.1, the zonal-mean meridional wind at 50°N does not vary much with height near the top, so that the application of the linear extrapolation method gives a more realistic Φ_S at this latitude.

Due to the difference between the mass flux and the tendency term, it is not possible to analyse exactly the tendency of the polar cap mean surface pressure used in terms of the difference between the stratospheric outflow and tropospheric inflow. To better understand the influence of the lag between low-frequency variations in the stratospheric outflow and in the tropospheric inflow on the polar cap mean surface pressure, it is instructive to consider also a mass flux that balances the tendency term. Since the stratospheric part of the mass flux is likely to be underestimated, a balanced Φ_S is defined such that Eq. (3.2a) applies exactly. This balanced Φ_S is defined as:

$$\Phi_{S,bal} \equiv c \frac{\partial p_{0,pcm}}{\partial t} - \Phi_T \quad (3.3)$$

Figure 3.3b shows the time series of the 11-day running mean of $-\Phi_{S,bal}$, Φ_T and the sum of $\Phi_{S,bal}$ and Φ_T for the winter 1988-89. In some periods, the strength of the balanced stratospheric outflow, $-\Phi_{S,bal}$, increases (e.g., day 21-24, day 26-34 and day 58-71). During

these periods, the tropospheric inflow Φ_T also tends to increase. The $\partial p_{0,pcm}/\partial t$ tends to be negative during these periods, implying that the tropospheric inflow is slightly smaller than the stratospheric outflow. The opposite occurs during several other periods (e.g., day 3-8, day 16-21, day 39-50 and day 75-90). In these periods, both the strength of the balanced stratospheric outflow and tropospheric inflow tends to decrease. The $\partial p_{0,pcm}/\partial t$ tends to be positive, implying that in these periods the tropospheric inflow is larger than the balanced stratospheric outflow.

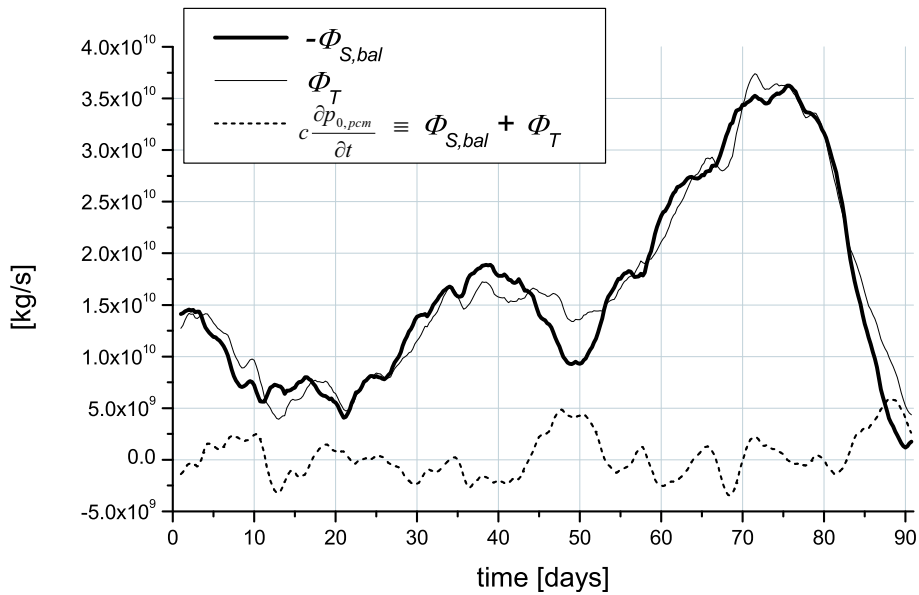


Fig. 3.3b: The time series of the 11-day running mean of $-\Phi_{S,bal}$, Φ_T and the product of c and $\partial p_{0,pcm}/\partial t$ for the winter 1988-89.

Correlating the time series of the 11-day running mean of $-\Phi_{S,bal}$ and Φ_T in the winter 1988-89 with different time lags indicates that variations in the balanced stratospheric outflow precede the variations in the tropospheric inflow. A maximal correlation is found when the time series of $-\Phi_{S,bal}$ is shifted by +0.8 day. Later it will be shown that the difference between this lag and the lag between Φ_S and Φ_T variations is much smaller for all other winters between 1979 and 1993.

It is not possible to conclude whether the lag between Φ_S and Φ_T variations or the lag between $\Phi_{S,bal}$ and Φ_T variations is the best measure for the lag between the stratospheric and tropospheric meridional mass flux in the real atmosphere. However, the fact that both lags are positive indicates that, in the winter 1988-89, low-frequency variations in the stratospheric mass flux out of the polar cap precede similar variations in the tropospheric mass flux into the polar cap.

winters 1979-1993

The generality of the results found for the winter 1988-89 is investigated by applying the described analysis for all NH winters from 1979 to 1993 (see Table 3.1). The time lag at which a maximal correlation is found between $-\Phi_S$ and Φ_T (denoted as $lag(s,t)$) is positive in all winters, implying that low-frequency variations in $-\Phi_S$ generally precede those in Φ_T . The 14-winter average of $lag(s,t)$ and its standard deviation (i.e., the sample standard deviation divided by $\sqrt{14}$) are, respectively, 0.8 and 0.1 day. Although in all winters the total mass flux is larger than the tendency term (Eq. 3.2), the average correlation between these terms is very high (0.92). The lag of maximal correlation between $-\Phi_{S,bal}$ and Φ_T (denoted as $lag(s_{bal},t)$) is positive in all winters too. Except for the winter 1988-89, the difference between $lag(s,t)$ and $lag(s_{bal},t)$ is less than 0.3 days. The 14-winter average of $lag(s_{bal},t)$ and its standard deviation are, respectively, 0.8 and 0.1 day. The values of the average of both $lag(s,t)$ and $lag(s_{bal},t)$ are significantly positive at a more than 99% level.

winter	$lag(s,t)$ (60°N) [days]	$lag(s_{bal},t)$ (60°N) [days]	$lag(s,t)$ (55°N) [days]	$lag(s,t)$ (65°N) [days]
1979-80	1.1	1.1	1.1	0.8
1980-81	0.9	0.9	0.9	0.6
1981-82	0.7	0.7	0.7	0.8
1982-83	0.7	0.7	0.7	0.3
1983-84	0.7	0.7	0.7	0.4
1984-85	0.6	0.5	0.6	0.9
1985-86	1.5	1.5	1.5	0.7
1986-87	0.4	0.4	0.4	1.1
1987-88	0.8	0.5	0.8	0.8
1988-89	0.3	0.8	0.3	0.2
1989-90	1.5	1.6	1.5	1.4
1990-91	1.0	0.9	1.0	0.9
1991-92	1.0	1.0	1.0	1.0
1992-93	0.3	0.3	0.3	0.1
Average (standard deviation)	0.8 (0.1)	0.8 (0.1)	0.8 (0.1)	0.7 (0.1)

Table 3.1 The time lag of maximal correlation between the time series of the 11-day running mean of $-\Phi_S$ and Φ_T ($lag(s,t)$) at 55, 60 and 65°N and of $-\Phi_{S,bal}$ and Φ_T ($lag(s_{bal},t)$) at 60°N, for the NH winters 1979-93, the 14-winter average and its standard deviation. For the meaning of the symbols see subsection 3.3.2

Sensitivity of the lag to latitude

Table 3.1 also shows $lag(s,t)$ for 55 and 65°N for all NH winters from 1979 to 1993. The separation level between the stratosphere and the troposphere is at 270 hPa, as at 60°N. The value of $lag(s,t)$ is positive in all winters at 55, 60 and 65°N and the average of $lag(s,t)$ for the winters between 1979 and 1993 is almost independent on latitude between 55 and 65°N.

In summary, the results of this subsection indicate that in all winters from 1979 to 1993, low-frequency variations in the stratospheric mass flux out of the polar cap and the tropospheric mass flux into the polar cap are not simultaneous, but that instead the variations in the stratospheric mass flux out of the polar cap are *followed* by variations in the tropospheric mass flux into the polar cap, with an average lag of about one day. The results are not very sensitive to the latitude of the southern boundary of the polar cap. A very simple model of the lag between the upper level and lower level meridional transport is presented in section 3.5.

3.3.3 Variations in the meridional surface pressure gradient and the zonal wind near the surface

The results presented in the previous subsection show that low-frequency variations in the meridional mass transport in the stratosphere are generally followed by similar variations in the troposphere, with a lag of about one day. This lag implies a difference between the strength of the stratospheric out- and tropospheric inflow, which in turn causes variations in the mass of the polar cap atmosphere and thus in the polar cap mean surface pressure. In this subsection the influence of the low-frequency variations in the polar cap mean surface pressure on those variations in the meridional pressure gradient and the zonal wind near the surface around 60°N will be investigated.

Figure 3.4 shows the time series of the 11-day running mean of the surface pressure averaged over the polar cap (denoted as $p_{0,pcm}$), and that of the surface pressure averaged over the region south of the polar cap between 47.5°N and 60°N (denoted as $p_{0,47.5-60N}$). The southern boundary of the latter region is chosen such that the area of this region is almost the same as the area of the polar cap. Figure 3.4 also shows the time series of the 11-day running mean of $p_{0,pcm} - p_{0,47.5-60N}$, which will be denoted as Δp . The figure shows that the variations in $p_{0,pcm}$ contribute more to variations in Δp than the variations in $p_{0,47.5-60N}$. This observation is quantified by the ratio of the standard deviations of the time series of $p_{0,pcm}$ and $p_{0,47.5-60N}$ (denoted as r), which is 1.2 for the winter 1988-89. This value is small compared to the values for the other NH winters from 1979 to 1993, as is shown in Table 3.2. The 14-winter average and the sample standard deviation of the ratio r are, respectively, 1.9 and 0.7. In the next subsection it will be shown that Δp can be interpreted as a good measure for the meridional

surface pressure gradient around 60°N. From these results it can be concluded that in all NH winters from 1979 to 1993 the variations in Δp (and, consequently, in the meridional surface pressure gradient around 60°N) are mainly due to the variations in $p_{0,pcm}$ (that are associated with the meridional mass flux variations).

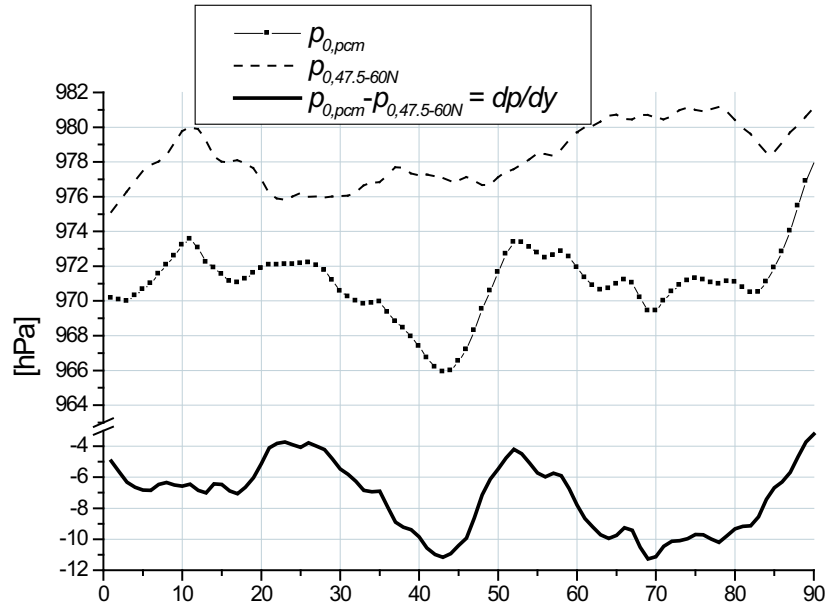


Fig. 3.4: The time series of the 11-day running mean of $p_{0,pcm}$, $p_{0,47.5-60N}$ and Δp for the winter 1988-89.

Figure 3.5 shows, for the winter of 1988-89, the time series of the 11-day running mean of $-\Delta p$, together with the zonal-mean zonal wind at 1000 hPa averaged between 55-65°N (denoted as $[u]_{1000hPa,55-65N}$), which is used here as a measure for the zonal wind near the surface around 60°N. The correlation between these time series is very high (0.94). Variations in $-\Delta p$ clearly correspond to variations in $[u]_{1000hPa,55-65N}$. Maxima of $-\Delta p$ occur simultaneously with maxima of $[u]_{1000hPa,55-65N}$ at day 43, 64, 70 and 78, and minima of $-\Delta p$ occur simultaneously with minima of $[u]_{1000hPa,55-65N}$ at day 26, 52, 66 and 75. The same conclusions can be drawn for all winters from 1979 to 1993: the correlation between the time series of $-\Delta p$ and $[u]_{1000hPa,55-65N}$ is high (the 14-winter average and the sample standard deviation are, respectively, 0.86 and 0.08), and extremes of $-\Delta p$ coincide with extremes of $[u]_{1000hPa,55-65N}$. This indicates, that variations in Δp are (geostrophically) coupled to variations in $[u]_{1000hPa,55-65N}$. Therefore, Δp appears to be a good measure for the meridional surface pressure gradient around 60°N.

Winter	standard deviation $p_{0,pcm}$ [hPa]	standard deviation $p_{0,47.5-60N}$ [hPa]	r
1979-80	5.5	1.5	3.8
1980-81	4.3	1.4	3.1
1981-82	3.0	1.8	1.6
1982-83	3.2	2.3	1.4
1983-84	3.7	2.2	1.7
1984-85	5.2	3.3	1.6
1985-86	2.7	2.2	1.2
1986-87	4.4	2.4	1.8
1987-88	3.1	2.6	1.2
1988-89	2.2	1.8	1.2
1989-90	3.4	1.4	2.4
1990-91	2.9	1.5	1.9
1991-92	3.4	1.4	2.5
1992-93	4.2	2.4	1.7
Average (sample standard deviation)	3.7 (0.9)	2.0 (0.5)	1.9 (0.7)

Table 3.2 The standard deviations of the time series of $p_{0,pcm}$ and $p_{0,47.5-60N}$ and their ratio (denoted as r) for the NH winters 1979-93

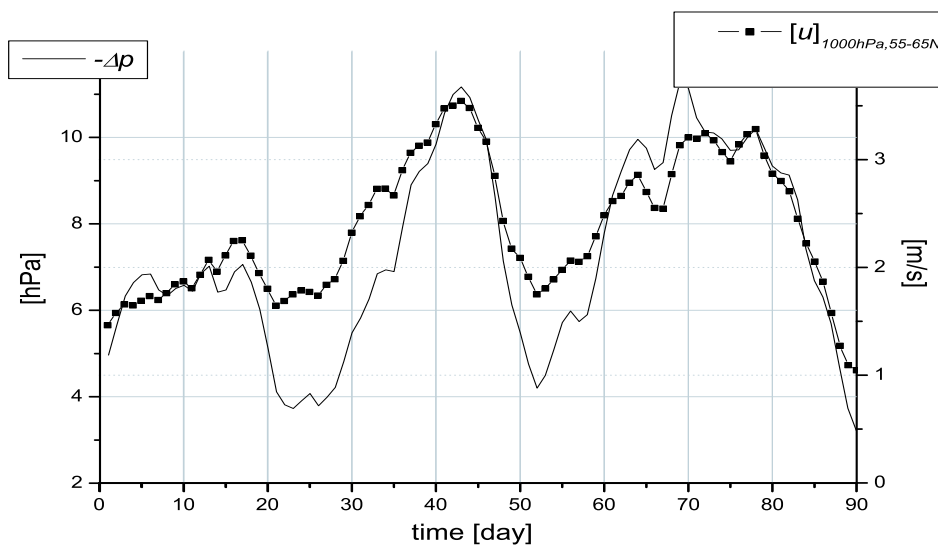


Fig. 3.5: The time series of the 11-day running mean of $-\Delta p$ and $[u]_{1000hPa,55-65N}$ for the winter 1988-89.

3.3.4 Forces governing the meridional transport at 60°N

The results in the previous subsections indicate that in the NH extratropical winters, low-frequency variations in the stratospheric meridional mass flux out of the polar cap induce, with a time delay of about one day, variations in the tropospheric meridional mass flux into the polar cap. The resulting variations in the meridional pressure gradient cause variations in the zonal wind near the surface through geostrophic adjustment. In an attempt to gain more understanding of a possible mechanism of the coupling between the stratospheric and tropospheric winds, the forces governing the meridional motions at 60°N in the stratosphere and lower troposphere will be investigated. To this end, the different terms of the zonally averaged zonal momentum equation will be investigated. After neglecting non-quasi-geostrophic terms, this equation can be expressed as (Peixoto and Oort 1992, p. 387):

$$\frac{\partial[u]}{\partial t} = F_c + F_m + F_f , \quad (3.4a)$$

where

$$F_c = f[v] , \quad (3.4b)$$

and

$$F_m = -\frac{1}{a \cos^2 \varphi} \frac{\partial \left([u'v'] \cos^2 \varphi \right)}{\partial \varphi} . \quad (3.4c)$$

F_f is the frictional force, φ is latitude, u is the zonal wind, v is meridional wind, a is the radius of the earth and f is the Coriolis parameter. The square brackets denote the zonal-mean value, the prime denotes the deviation from that value. The equation expresses that the zonal-mean zonal wind tendency is balanced by the Coriolis force (F_c), the convergence of the eddy momentum flux (F_m) and the zonal frictional force (F_f). Variations in F_m are associated with variations in wave activity. The frictional force F_f may include surface drag, turbulent exchange of momentum and drag due to cumulus convection, and cannot be calculated directly. It will be computed as a residual by:

$$F_{f^*} \equiv \frac{\partial[u]}{\partial t} - F_c - F_m . \quad (3.5)$$

Rearranging Eq. (3.4a) to:

$$[v] = \frac{\left(\frac{\partial[u]}{\partial t} - F_m - F_f \right)}{f}, \quad (3.6)$$

shows that the zonal-mean meridional wind is balanced by three terms.

Figure 3.6 shows the time series of the 11-day running mean of $[v]$, $(\partial[u]/\partial t)/f$, $-F_m/f$, and $-F_{f^*}/f$ for the winter of 1988-89, at 60°N and averaged over the stratosphere (i.e., between 0 hPa and 270 hPa). It shows that F_{f^*} and $(\partial[u]/\partial t)$ are small compared to F_m . Therefore, in the stratosphere the Coriolis force associated with the zonal-mean meridional wind is nearly balanced by the convergence of the eddy momentum flux.

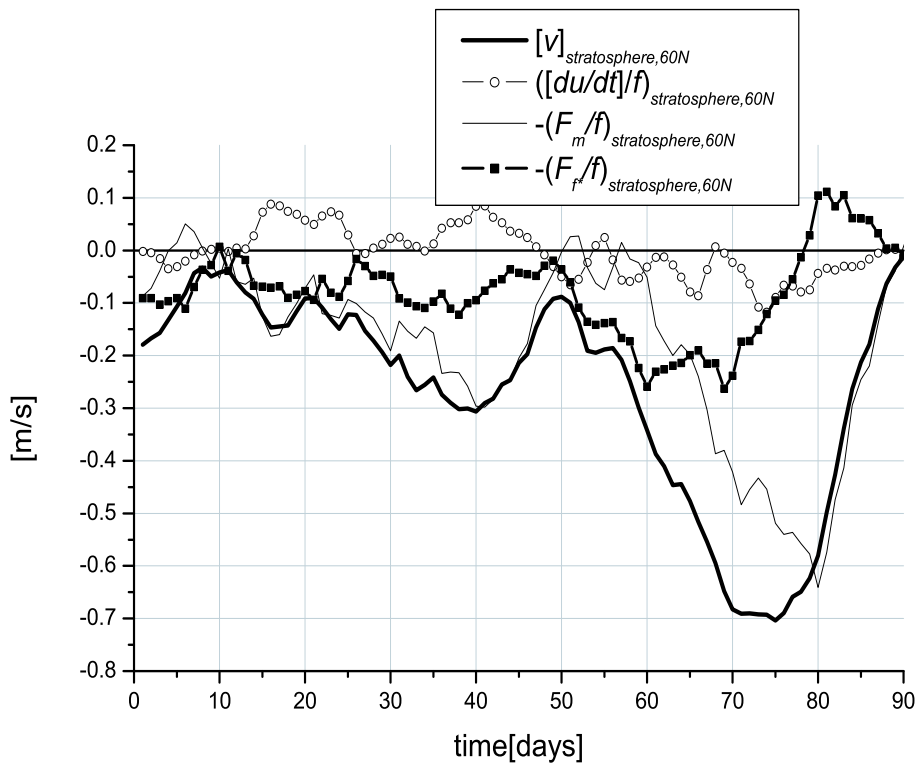


Fig. 3.6: The time series of the 11-day running mean of $[v]$, $(\partial[u]/\partial t)/f$, $-F_m/f$, and $-F_{f^*}/f$ for the winter 1988-89, all at 60°N and averaged over the stratosphere (i.e. between 0 hPa and 270 hPa).

Figure 3.7 shows the same quantities near the surface, at 1000 hPa. It shows that the two dominant forces near the surface are F_c and F_{f^*} , indicating that near the surface the Coriolis force on the zonal-mean meridional wind is nearly balanced by the zonal frictional force. Averaging the quantities of Eq. (3.6) between the surface and 500 hPa (the “lower troposphere”) for the winter 1988-89 reveals that also in this layer the Coriolis force on the zonal-mean meridional wind is nearly balanced by the frictional force (*not shown*).

Repeating this analysis for the other winters from 1979 to 1993 shows that in all these winters at 60°N in the stratosphere the Coriolis force on the zonal-mean meridional wind is nearly balanced by the convergence of the eddy momentum flux, whereas in the lower troposphere it is nearly balanced by the (residual) zonal frictional force.

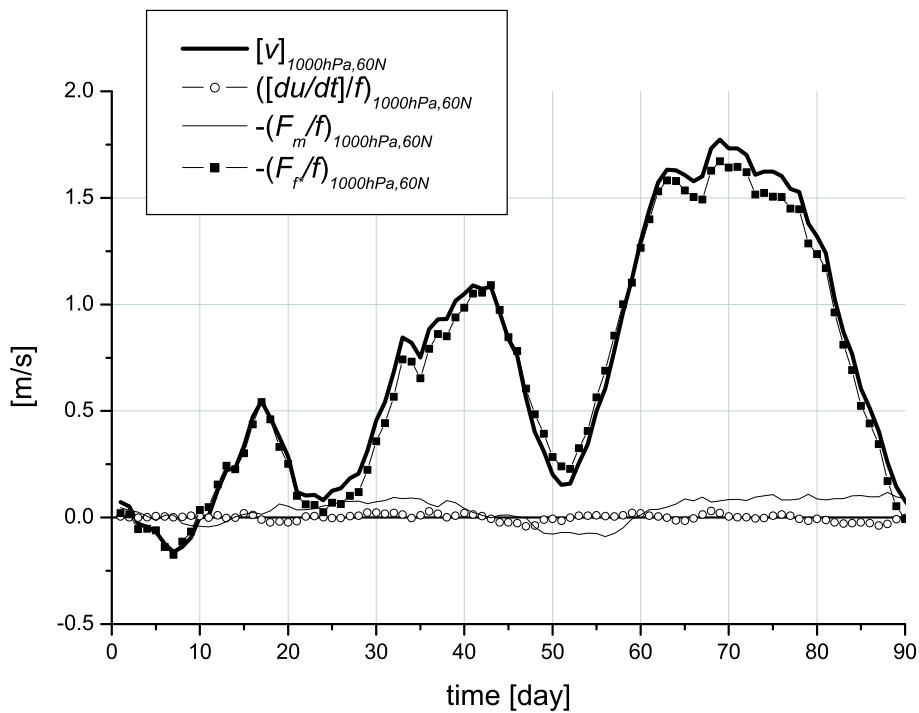


Fig. 3.7: Same as in Fig. 3.6, at 1000 hPa.

3.4 Summary and discussion

In this Chapter the coupling between low-frequency variations in the stratospheric meridional wind and in the zonal wind near the surface in the NH extratropical winters from 1979 to 1993 has been investigated. The meridional wind at 60°N is generally equatorward in the stratosphere and poleward in the troposphere (Fig. 3.2). Low-frequency variations in the stratospheric equatorward mass flux tend to be followed by similar variations in the tropospheric poleward mass flux with an average lag of about 0.8 days (subsection 3.3.2). The resulting variations in the analysed polar cap mean surface pressure explain most of the variations in the analysed meridional surface pressure gradient around 60°N (subsection 3.3.3). The latter variations are (geostrophically) coupled to the variations in the zonal wind near the surface around 60°N (subsection 3.3.3). In the stratosphere the Coriolis force on the zonal-mean meridional wind is nearly balanced by the convergence of the eddy momentum flux, and in the lower troposphere by the zonal frictional force (subsection 3.3.4).

These results indicate the existence of a mechanism for the coupling between low-frequency variations in the meridional wind (or: mass transport) in the stratosphere and the zonal wind near the surface. Here we will describe this mechanism for an increase in the meridional mass transport, but it also applies to a decrease. An increase in the stratospheric meridional mass flux out of the polar cap is followed, with a delay of about one day, by an increase in the tropospheric meridional mass flux into the polar cap. Because of this delay, the magnitude of the stratospheric mass flux out of the polar cap is larger than that of the tropospheric mass flux into the polar cap and, consequently, the polar cap mean surface pressure decreases. This leads to an increased meridional pressure gradient and, by geostrophy, to an increased zonal wind in the lower troposphere around the southern boundary of the polar cap (60°N). In the new equilibrium situation at low levels the larger eastward zonal Coriolis force associated with the larger poleward meridional wind is balanced by an increased westward frictional force that is due to an increased zonal wind. Also, the increased equatorward Coriolis force associated with the increased zonal wind, is balanced by an increased poleward meridional pressure gradient.

According to the proposed mechanism, the zonal wind in the lower troposphere should positively correlate with the strength of the equatorward meridional mass flux in the stratosphere. The results for the 1000 hPa zonal-mean zonal wind around 60°N (Fig. 3.5) and the stratospheric equatorward mass flux at 60°N (Fig. 3.3) show that, in the winter 1988-89, this is indeed the case. Averaged over all winters the correlation coefficient between these two quantities is 0.75. This correlation itself, of course, does not inform about cause and effect. Since the meridional mass flux in the stratosphere is nearly equal to that in the troposphere,

there exists also a strong correlation between the zonal wind in the lower troposphere and the meridional mass flux in the troposphere. However, the observation in the present study that, in the extratropical northern winter hemisphere, the meridional mass flux variations in the stratosphere generally precede those in the troposphere, suggests that it is the meridional motion in the stratosphere rather than that in the troposphere that induces variations in the lower tropospheric zonal wind.

To explain the rapid transfer of zonal wind variations from the lower stratosphere to the lower troposphere, as observed by, e.g., Baldwin and Dunkerton (1999), the presented mechanism lacks a link between variations in the zonal wind and in the meridional wind in the stratosphere. The stratospheric zonal wind variations can induce variations in the momentum flux by altering the propagation and dissipation of planetary waves (e.g., Shindell *et al.* 2001). The observation in the present study that in the stratosphere the meridional wind is nearly balanced by the convergence of the eddy momentum flux, suggests the presence of a link between the stratospheric zonal and meridional wind variations.

Although the one-day time lag found in the present study appears to be very small compared to the 3-week propagation time of disturbances from 10 hPa to the surface as found by Baldwin and Dunkerton (1999), it can still be argued that it could be the proposed mechanism that explains the observed downward propagation. Firstly, the downward propagating speed found by Baldwin and Dunkerton (1999) tends to increase strongly when the troposphere is reached, so that their time lag between the stratosphere-averaged and the troposphere-averaged disturbances would be much shorter than three weeks. Secondly, one should bear in mind that the disturbances described by Baldwin and Dunkerton (1999) are related to the *zonal* wind variations, whereas the one-day time lag found in our study corresponds to the lag between the stratospheric and tropospheric *meridional* mass fluxes. The possible link between the zonal and meridional wind variations in the stratosphere, on which we have speculated above, could introduce an extra lag time to the one-day time lag of the meridional mass fluxes. Finally, the time lag between the stratospheric and tropospheric disturbances could also be modulated by other mechanisms (see section 3.1).

Stratospheric meridional transport is often considered in the Transformed Eulerian Mean (TEM) framework. However, in the present Chapter the Eulerian framework has been applied, because it uses the zonal-mean meridional wind [v], which can, unlike the TEM meridional velocity v^* , be directly coupled to the surface pressure tendency (see Eq. 3.2). The surface pressure tendency has been used to study the effect of the time lag between stratospheric and tropospheric meridional mass fluxes on the surface zonal wind.

In conclusion, this study has given evidence for the existence of a mechanism by which the stratosphere influences the lower tropospheric zonal wind through variations in a meridional cell.

3.5 Appendix: Simple model of the upper and lower level meridional flow

A very simple model of the lag between the upper level and lower level meridional transport as diagnosed in subsection 3.3.2, is presented. The atmosphere is separated into an upper layer (index 1) and a lower layer (index 2), and in a region a from 60-90°N and a region b south of 60°N, with the same area as region a . For simplicity it is assumed that both layers have equal pressure thickness ΔP . The model consists of simplified versions of the zonally averaged zonal and meridional momentum equations (see e.g., Holton 1992, p. 316), applied to lower layer 2. The zonal momentum equation is approximated as a balance between the Coriolis force on the zonal-mean meridional wind and the frictional force:

$$f[v_2] = F_f = k[u_2], \quad (3.7)$$

where the second part of Eq. (3.7) expresses the approximation of F_f in terms of the zonal-mean zonal wind $[u_2]$; k is a constant of proportionality (it would be more realistic to express the friction in terms of $[u_2]^2$ rather than $[u_2]$, but for reasons of simplicity a linear relation is assumed). In Eq. (3.7) the zonal wind tendency and the convergence of the eddy momentum flux have been neglected, which is supported by the results at the end of subsection 3.3.4. The meridional momentum equation is approximated by a balance between the meridional surface pressure gradient force and the Coriolis force on the zonal-mean zonal wind:

$$(p_{0a} - p_{0b})/(\rho Y) = -f[u_2], \quad (3.8)$$

where ρ denotes density and Y , the length scale for this gradient, is taken as the distance between the two latitudes which separate, respectively, regions a and b in two equal-area parts; p_{0a} and p_{0b} denote the area mean surface pressure in, respectively, region a and b . More precisely, $[u_2]$ is balanced by the mean pressure gradient in layer 2 rather than by the surface pressure gradient. The mean pressure gradient is determined by the surface pressure gradient as well as by the temperature difference between regions a and b . However, as mentioned later, in this model it are the pressure time variations rather than the pressure itself that are relevant. In the model, variations in temperature are not considered and, therefore, the variations in the pressure gradient are approximated by the variations in the surface pressure gradient.

Further, under the assumptions of hydrostatic equilibrium and that there is no mass flux across the southern boundary of region b , the conservation of mass implies that the surface pressure tendencies in the equal areas a and b can be expressed as:

$$\partial p_{0a}/\partial t = -\partial p_{0b}/\partial t = \Delta P([v_1] + [v_2])/d, \quad (3.9a)$$

where

$$d = \frac{a(1 - \sin 60^\circ)}{\cos 60^\circ}, \quad (3.9b)$$

and a is the radius of the Earth. Combining Eqs. (3.7) and (3.8) into one equation for $[v_2]$ and substituting the time-derivative of the resulting equation into Eq. (3.9), gives an expression relating $[v_1]$ and $[v_2]$:

$$\partial[v_2]/\partial t = -([v_1] + [v_2])/\tau, \quad (3.10)$$

where the time constant τ is equal to $(\rho Y f^2 d)/(2k \Delta P)$. The value of k is estimated from Eq. (3.7), assuming that $[v_2]/[u_2] = 0.1$, and f is computed at 60°N . Adopting $\Delta P = 500$ hPa and $\rho = 1$ kg/m³, and computing Y and d as described above, a value for τ of 0.4 day is obtained. To determine the lag between $[v_1]$ and $[v_2]$, the $[v_1]$ is assumed to vary harmonically with time with a period T , i.e., $[v_1] = v_{10} \cos(2\pi t/T)$. For reasons of simplicity, the attention here is restricted to oscillations for which T is much larger than $2\pi\tau$. This applies to a large part of the variations of the 11-day running mean filtered data of this study. For these oscillations, the solution of Eq. (3.10) is $[v_2] = -v_{10} \cos(2\pi(t - \tau)/T)$. Thus, $[v_2]$ lags $[v_1]$ by a period τ .

The lag time between $[v_1]$ and $[v_2]$ as diagnosed in subsection 3.3.2 is about 0.8 day. Although this value is twice the value estimated with this very simple model, it nevertheless indicates that the lag between $[v_1]$ and $[v_2]$ can, at least qualitatively, be described by two balances of forces, namely in the zonal direction a balance between the Coriolis force on the zonal-mean meridional wind and the frictional force on the zonal-mean zonal wind (Eq. (3.7)), and in the meridional direction a geostrophic balance (Eq. (3.8)).

It should be noted that the stratospheric wave forcing, which determines the meridional mass flux variations in the upper layer 1, is not considered in this model. In the model the latter variations are prescribed, rather than modelled as a response to wave forcing, and the response of only the meridional mass flux in the lower layer 2 is calculated.

Acknowledgements

We thank Peter van Velthoven for helpful suggestions. Comments of two anonymous reviewers helped improve the manuscript, and are greatly appreciated.

Chapter 4

Stratosphere-troposphere exchange in an extratropical cyclone, calculated with a Lagrangian method *

A Lagrangian technique is developed and applied to calculate stratosphere-troposphere exchange in an extratropical cyclone. This exchange is computed from the potential vorticity or PV along trajectories, calculated from ECMWF circulation data. Special emphasis is put on the statistical significance of the results. The computed field of the cross-tropopause flux is dominated by elongated patterns of statistically significant large downward and small upward fluxes. The downward fluxes mainly occur in the lower part of the considered tropopause folds. The upward fluxes are found near the entrance of the folds, in the tropopause ridges. The ratio between the area averaged downward and upward cross-tropopause fluxes increases with increasing strength of the cyclone. Since the largest fluxes are shown to occur in the regions with the largest wind shear, where PV-mixing is thought to cause large cross-tropopause fluxes, the results are expected to be reliable, at least in a qualitative sense. The position of a tropopause fold along the northwest coast of Africa is confirmed by total ozone observations. The results indicate that the applied Lagrangian technique is an appropriate tool for diagnosing stratosphere-troposphere exchange.

* This Chapter is a slightly revised version of: Sigmond, M., J. Meloen, and P.C. Siegmund, 2000: Stratosphere-troposphere exchange in an extratropical cyclone, calculated with a Lagrangian method. *Ann. Geophys.*, **18**, 573-582.

4.1 Introduction

Understanding and quantifying human impact on the climate system is one of the most challenging questions in atmospheric sciences. The importance of stratosphere-troposphere exchange (STE) for understanding this impact is widely acknowledged (e.g., Holton *et al.* 1995). The transport of specific anthropogenic emissions from the ground to the stratosphere is believed to be the main cause of stratospheric ozone depletion (WMO 1995), whereas the increasing aircraft emissions in the tropopause region could have a substantial impact on climate and the atmospheric composition (IPCC 1999).

The global scale STE is realised by a mean meridional cell, which is called the Brewer-Dobson circulation. The cell consists of upward cross-tropopause transport in the tropics, poleward drift in the stratosphere towards the winter pole, and downward transport into the extratropical winter troposphere (Brewer 1949, Dobson 1956).

At smaller scales, however, STE is not dominated by mean circulations, but by synoptic scale eddy processes, such as tropopause folds associated with cut-off lows, that can lead to rapid exchange of air across the tropopause (Holton *et al.* 1995). Therefore, apart from downward cross-tropopause transport, upward cross-tropopause transport occurs in the extratropics, which can bring anthropogenic species directly into the extratropical lower stratosphere (e.g., Hoerling *et al.* 1993). Knowledge of the instantaneous bi-directional cross-tropopause fluxes rather than the time-mean net flux is, in the presence of a cross-tropopause gradient of a chemical species, necessary to determine the fluxes of this species across the tropopause (Gettelman and Sobel 2000). Moreover, since the anthropogenic species are emitted non-uniformly in time and space, the knowledge of the distribution of the instantaneous cross-tropopause flux (CTF) is essential for modelling the human impact on the climate.

Many efforts have been made to determine the CTF. In these studies, Eulerian diagnostic methods have been dominant. The CTF is generally computed with one of the versions of the diagnostic formula derived by Wei (1987) (hereafter called the Wei- x formula, where x is the vertical coordinate, see later). Hoerling *et al.* (1993) diagnosed the net global-scale CTF by applying Wei's equation to twice-daily global circulation data with a horizontal resolution of $3.75^\circ \times 3.75^\circ$. Siegmund *et al.* (1996) investigated the STE with a more accurate numerical method and with circulation data at higher temporal and spatial resolution. They calculated the magnitudes of the upward and downward cross-tropopause fluxes separately. They found that for an accurate estimation of the local and instantaneous CTF, the spatial and temporal resolution should be at least $1^\circ \times 1^\circ$ and 6 hours, respectively. To cope with practical problems of time and space differencing, a complicated numerical scheme is applied.

Siegmund *et al.* (1996) as well as Gettelman and Sobel (2000) both used the Wei- p formula (where p denotes pressure) and found strong dipole structures in the computed CTF field.

Wirth and Egger (1999) examined five different methods to diagnose the CTF in a cut-off low. They found that both the Wei- p and the Wei- θ formula (where θ denotes potential temperature) are unreliable. In these formulas, the CTF is a small residual of three relatively large terms, so that small errors in the individual terms can result in a large relative error in the computed CTF. A third method examined by Wirth and Egger (1999) is the Wei- PV formula, where potential vorticity is taken as the vertical coordinate. The advantage of this method is that if the tropopause is defined as a PV -surface, the formula consists of only one term. The method therefore does not suffer from the problem of strong cancellation, provided that the PV -sources can be calculated with reasonable accuracy.

Apart from these Eulerian diagnostic methods, Wirth and Egger also examined a Lagrangian method, by starting multiple trajectories on the tropopause. The pressure difference between the endpoint of a trajectory and the tropopause at that point is then considered as a measure for the STE in the considered time interval.

Wernli and Davies (1996) describe how their Lagrangian method can be applied for diagnosing the CTF in an extratropical cyclone. Coherent ensembles of trajectories with a period of 10 days, which cross the tropopause (defined as the 2 PVU surface, $1 \text{ PVU} = 10^{-6} \text{ K m}^2 \text{ kg}^{-1} \text{ s}^{-1}$), are identified. Only a small part (5-25%) of these trajectories indicate significant STE (i.e., reside within the stratosphere (troposphere) during (at least) the first four days and within the troposphere (stratosphere) for (at least) the last four days). Although this method is an appropriate tool for studying the spatial structure of STE in an extratropical cyclone, it does not give a numerical estimate of the CTF.

In the present study a Lagrangian technique is used to calculate STE in an extratropical cyclone. Although this technique is to some extent similar to that applied by Wirth and Egger (1999), there are several new aspects in it. The main concept of our method is the evaluation along trajectories of the air mass flux across several PV -surfaces. Unlike in previous studies, the errors in the calculated data will be discussed. In section 4.2 the method, input data and the trajectory model will be described. The results will be presented in section 4.3, discussed in section 4.4 and summarised in section 4.5.

4.2 Method and data

4.2.1 Calculation of the air mass flux across a *PV*-surface

In the present study Wei's (1987) general formula is used with *PV* as the vertical coordinate. The air mass flux across a *PV*-surface per unit surface area (F) is then given by:

$$F = -\frac{1}{g} \frac{\partial p}{\partial PV} \frac{dPV}{dt}, \quad (4.1)$$

where g is the acceleration due to gravity. The unit of F is $\text{kg m}^{-2} \text{s}^{-1}$. For consistency, it is desired that positive values of F near the tropopause would denote transport from the troposphere to the stratosphere in all cases. In order to accomplish this, Eq. (4.1) should be altered in the case of tropopause folds. A tropopause is folded where the *PV*-surface is multi-valued with respect to pressure, i.e., at a particular longitude and latitude where 3 heights are found where $PV = \text{constant}$. Consider the tropopause fold as in Fig. 4.1, where the air is transported from the troposphere to the stratosphere in all parts of the fold. Since the surface is turned upside down in the middle part of the fold, $\partial p / \partial PV$ is positive in that part. Calculating F with Eq. (4.1) would then give a negative F through this middle surface, whereas a positive value is desired. This problem can be solved by calculating F as:

$$F = \frac{1}{g} \left| \frac{\partial p}{\partial PV} \right| \frac{dPV}{dt}, \quad (4.2)$$

so that the sign of F is determined by the sign of dPV/dt . Positive values of F are then always associated with transport from the troposphere to the stratosphere.

To compute the right-hand side of Eq. (4.2), we calculate the *PV* and $|\partial p / \partial PV|$ along trajectories. Computed in this way, *PV* and $|\partial p / \partial PV|$ should be considered as gridbox averaged values. An example of the *PV* along a trajectory is shown in Fig. 4.2. As can be inferred from Fig. 4.2, the *PV* is partially fluctuating due to noise. The instantaneous dPV/dt is therefore not reliable. In order to reduce this noise, the *PV* should be averaged over a certain period. F is therefore approximated as:

$$\tilde{F} = \frac{1}{g} \overline{\left| \frac{\partial p}{\partial PV} \right|} \overline{\frac{dPV}{dt}}, \quad (4.3)$$

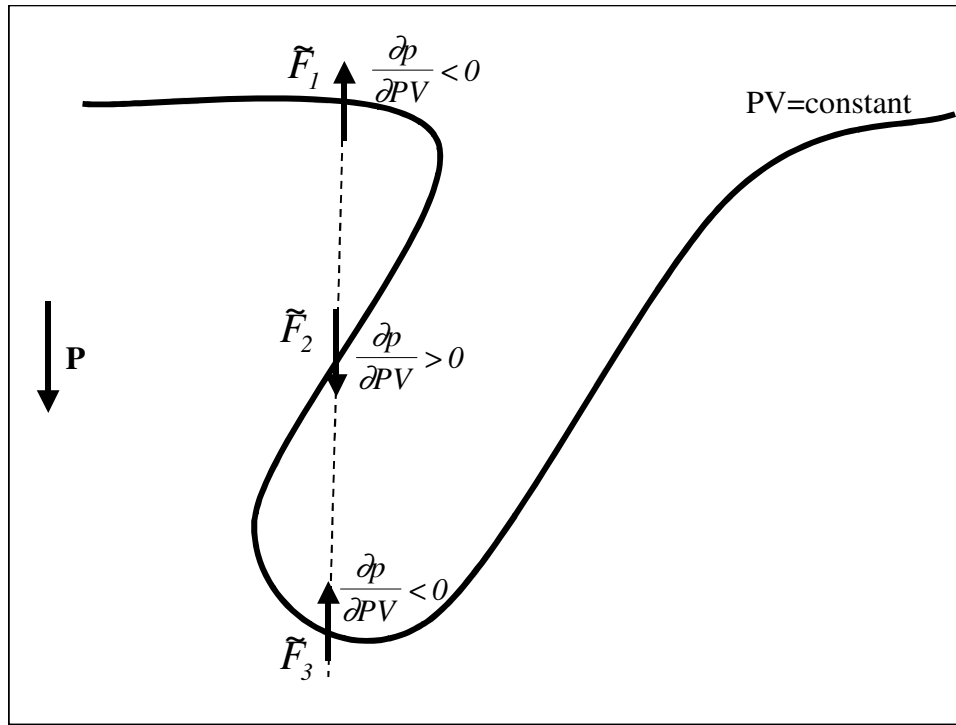


Fig. 4.1: Illustration of a tropopause fold.

where $\overline{dPV/dt}$ is the mean dPV/dt in the 12-hour time interval obtained by a linear least square regression of the PV along the trajectory versus time, and $\overline{|\partial p/\partial PV|}$ is the mean of $|\partial p/\partial PV|$ along the 12-hour trajectory.

The value of \tilde{F} is calculated for each gridpoint of the 3D-domain (described in section 4.3), by calculating PV and $|\partial p/\partial PV|$ along the 6-hour forward and backward trajectory that start at the gridpoint. The value of \tilde{F} is then attributed to the gridpoint and the starting time of the trajectories. To compute the flux \tilde{F} in a tropopause fold at a particular latitude and longitude, the fluxes through the three surfaces where $PV=\text{constant}$ are summed so that Eq. (4.3) becomes:

$$\tilde{F} = \tilde{F}_1 + \tilde{F}_2 + \tilde{F}_3 \quad , \quad (4.4)$$

where subscript 1 denotes calculation at the top of the fold, 2 at the middle tropopause and 3 at the bottom of the fold (see Fig. 4.1).

According to Eq. (4.2), an air mass flux across a PV -surface implies a material change of PV . The PV of a single air parcel can be changed by diabatic heating gradients and friction (Hoskins *et al.* 1985). In addition, the gridbox mean PV (which is considered in this study) can be changed by mixing (Shapiro 1980). The computed fluxes also suffer from noise due to

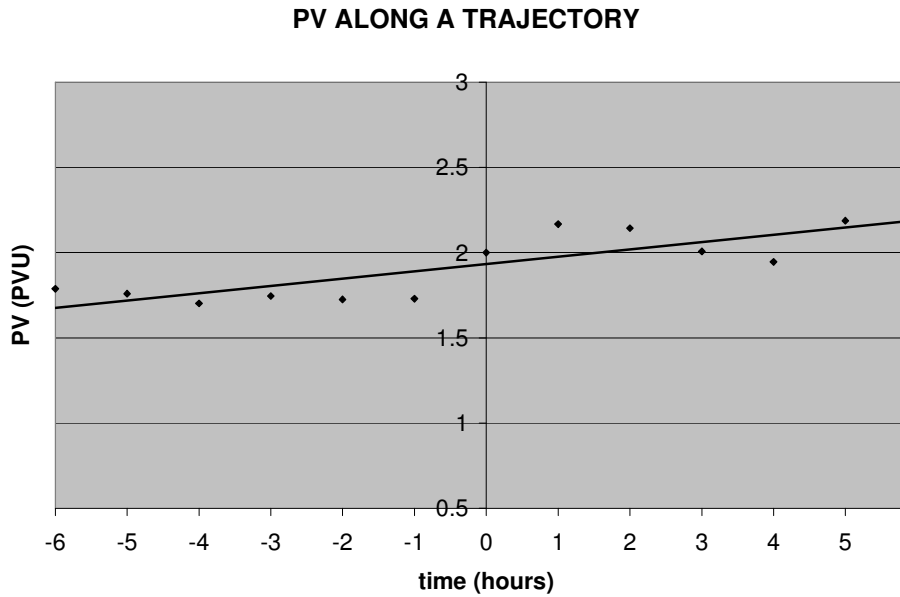


Fig. 4.2: Determination of the 12-hour mean dPV/dt with a linear regression of PV versus time. The trajectory model gives output data every hour. ($1 \text{ PVU} = 10^{-6} \text{ K m}^2 \text{ kg}^{-1} \text{ s}^{-1}$).

errors in the atmospheric dataset, the computed trajectories and the numerical method to calculate PV .

\tilde{F} is called statistically significant if the probability that \tilde{F} differs from zero is more than 99%. Hereto a Student's t -test is applied to the value of \tilde{F} and its standard deviation, where the standard deviation of \tilde{F} is computed from the standard deviations of $\overline{dPV/dt}$ and $|\partial p / \partial PV|$.

4.2.2 Trajectory model

To calculate the trajectories, we have used the KNMI trajectory model (as described by Scheele *et al.* 1996). This model calculates the three-dimensional displacement of air parcels for each timestep δt using the iterative scheme after Petterssen (1940). In the present study $\delta t = 10$ minutes. The input circulation data are obtained from the ECMWF (see subsection 4.2.3). Spatial interpolation (linear in the horizontal and linear in the vertical with $\log(p)$) and temporal interpolation (quadratic) are applied to the input data. In the present study three-dimensional rather than isentropic trajectories are calculated in order to include diabatic effects in the calculations of \tilde{F} . Moreover, the three-dimensional trajectories are believed to be more accurate as is concluded, e.g., by Stohl *et al.* (1995). To calculate the PV at place X and at time t , the PV is first calculated at the three data input times closest to time t at place X and is then quadratically interpolated to the time t .

4.2.3 ECMWF-data

For this study we use ECMWF circulation and temperature data of the first five days of a forecast run, which is initialised on 13 April 1998, 12 GMT. The data are at a $1^\circ \times 1^\circ$ horizontal grid, at 31 vertical levels. Around the tropopause the vertical resolution is about 25 hPa. The model data are stored every 6 hours. Forecast data rather than analysed data are used in order to have a physically consistent data set, in which the modelled quantities (in particular the PV) are not disturbed by the addition of new observations. Since the difference between the +96 hour model forecast of the 500-hPa geopotential height field for 12 GMT on 17 April 1998 and the verifying analyses is very small, the forecast data give a realistic representation of the synoptic-scale processes in the considered period.

4.3 Results

The air mass flux across a PV -surface (\bar{F}) is calculated for an extratropical cyclone over the North Sea between 14 and 17 April 1998. \bar{F} is calculated on two different three-dimensional grids with a horizontal resolution of $1^\circ \times 1^\circ$: one with PV as the vertical coordinate (fluxes are calculated across the 1, 1.5, 2, 3, 4, 6, 8 and 10 PVU surfaces) and one with pressure as the vertical coordinate (from 600 hPa to 100 hPa, with a vertical resolution of 25 hPa). The horizontal domain is the area between 35°W and 25°E and between 20°N and 75°N .

4.3.1 Synoptic situation

The solid lines in Fig. 4.3 show the 500-hPa geopotential height field for the period between 14 and 17 April 1998. On April 14 the cyclone has already reached maturity, on April 16 the strength of the cyclone is maximal and on April 17 the cyclone has weakened considerably. The centre of the cyclone as seen on the 500-hPa geopotential height map hardly moves; it lies at the northern part of the North Sea during the entire period considered.

4.3.2 Geographical distribution of the flux across PV -surfaces

The tropopause is generally defined as a surface of constant PV . The values mostly used vary between 1.5 and 3.5 PVU. When the tropopause is defined as the 2 PVU surface, which is an often-used value, the flux across that surface can be considered as the cross-tropopause flux.

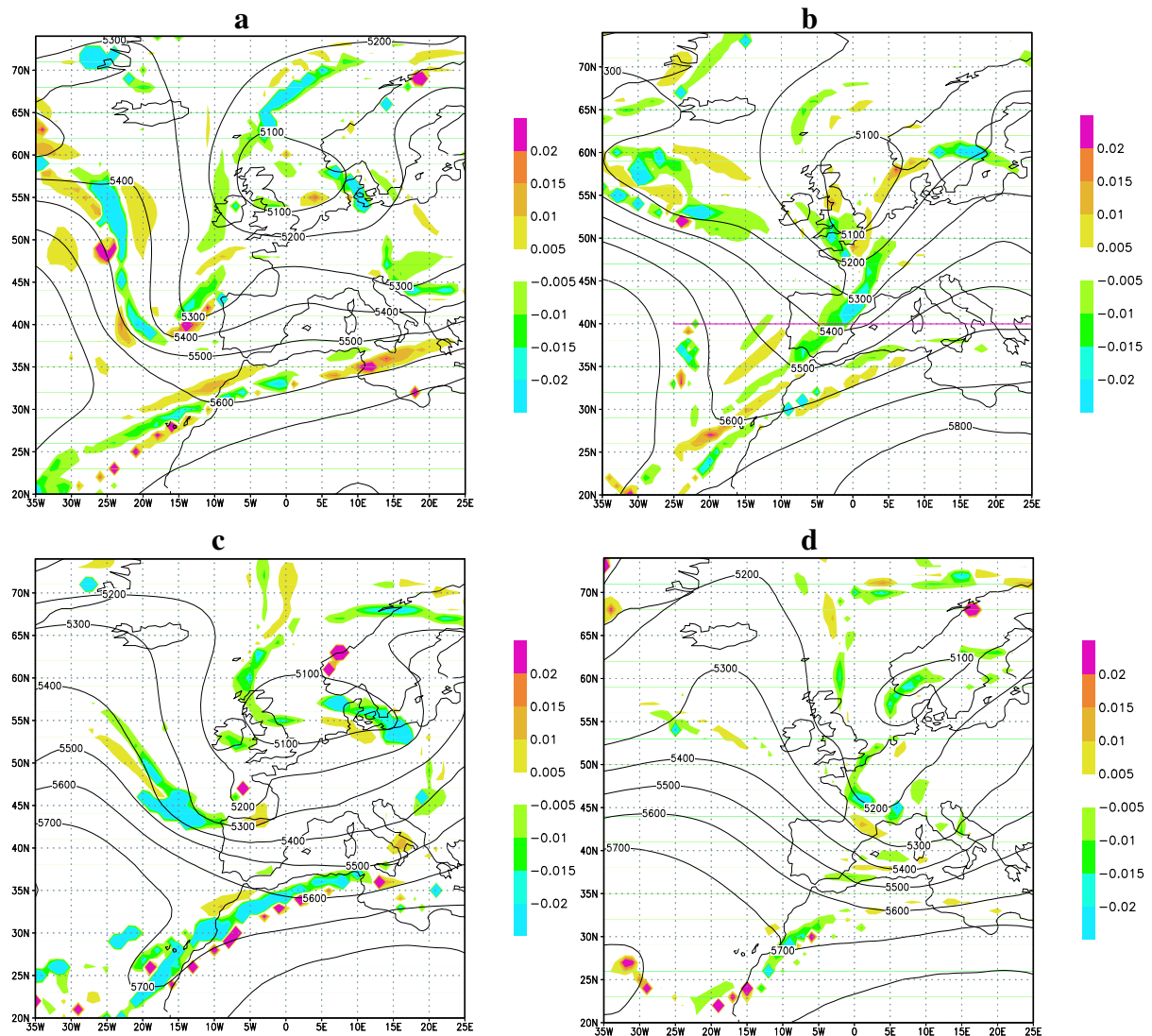


Fig. 4.3: \tilde{F} across the 2 PVU surface (shaded, in $\text{kg m}^{-2} \text{s}^{-1}$) together with the 500 hPa geopotential height (contours, in m). Positive values denote transport from the troposphere to the stratosphere. Shown is \tilde{F} for (a) 14 April, (b) 15 April, (c) 16 April and (d) 17 April 1998, all at 12 GMT.

Figure 4.3 also shows the field of \tilde{F} across the 2 PVU surface for the four different days. The field is dominated by elongated patterns of large downward and small upward fluxes. During the entire period a region with large downward fluxes far south of the cyclone centre (along the northwest coast of Africa) is visible. On April 14 and April 16 (Fig. 4.3a,c), a region with large upward fluxes can be found just south of this region. Two other regions with large downward fluxes are present on April 14: one north of the cyclone centre and one southwest of the cyclone centre, west of the 500-hPa trough. On April 15 the latter region has separated into two regions, one west and one south of the cyclone centre, in the middle of the 500-hPa trough. The region with large downward fluxes north of the centre on the 14th has moved eastward towards southeast Scandinavia. On April 16 a region with large downward fluxes is again identified southwest of the cyclone centre. Two other bands with large

downward fluxes are present: the first just east of the cyclone centre, the other starting in the cyclone centre and then curling to the north. On April 17 the large downward fluxes southwest of the cyclone have vanished. The regions with large downward fluxes occur near the cyclone centre and just south of it.

The flux across the PV -surfaces decreases with increasing PV . The $|\partial p/\partial PV|$ -field and thus the \tilde{F} -field across PV -surfaces lower than 2 PVU is very noisy (*not shown*).

Figure 4.4 shows \tilde{F} across the 2 PVU surface on 14 April at 12 GMT with significance criterion, as described in subsection 4.2.1. Although the three areas with large downward fluxes can still be identified, it is clear that in large parts of these areas the computed fluxes are not significant. This can be understood as follows. Along trajectories passing a tropopause fold, PV is changing relatively rapid. dPV/dt along those trajectories is relatively large but noisy. As a result, the signal to noise ratio along a trajectory passing a fold is generally low and consequently the computed \tilde{F} is often not statistically significant, i.e., the probability that the real flux differs from zero is less than 99%. In other areas where the flux is statistically insignificant, the flux itself is very small. In the entire domain 87% of the gridpoints in Fig. 4.4 have significant fluxes, 88% have significant dPV/dt and 99% have significant $|\partial p/\partial PV|$. Similar values are found for the other days.

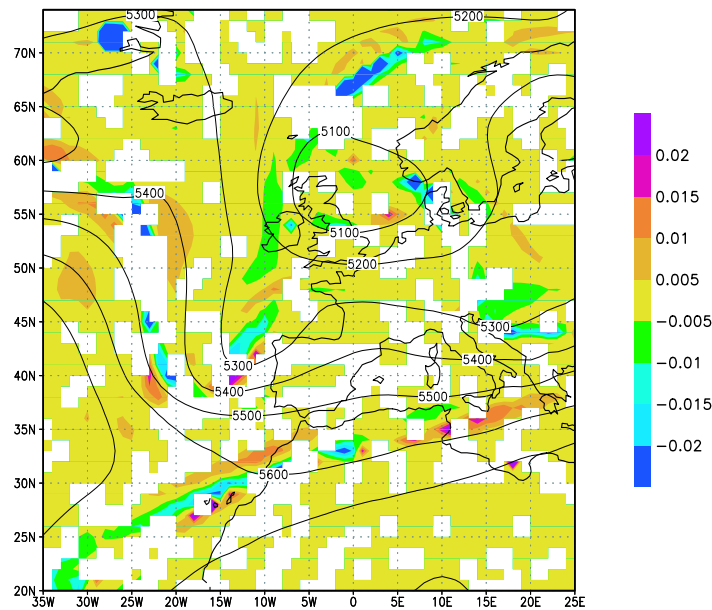


Fig. 4.4: \tilde{F} across the 2 PVU surface (shaded, in $\text{kg m}^{-2} \text{s}^{-1}$) together with the 500 hPa geopotential height (contours, in m) on 14 April 12 GMT, with significance criterion. Where \tilde{F} is statistically insignificant, the corresponding gridbox has been left blank.

4.3.3 Decomposition of the flux

In order to gain understanding of the structures in the \tilde{F} -field, \tilde{F} across the 2 PVU surface on 14 April is decomposed in dPV/dt (Fig. 4.5a) and $|\partial p/\partial PV|$ (Fig. 4.5b). After comparing Fig. 4.5a,b with Fig. 4.3a, one can conclude that a condition for large (downward) fluxes is a large $|\partial p/\partial PV|$. A large dPV/dt does not imply a large flux when $|\partial p/\partial PV|$ is small. In the south-western part of Iceland, for example, a large dPV/dt but small $|\partial p/\partial PV|$ is present, which results in a small flux. When $|\partial p/\partial PV|$ is small, the vertical distance between the different PV -surfaces is small so that a large PV -change does not imply that much air has crossed a PV -surface.

The $|\partial p/\partial PV|$ -field at the 2 PVU surface appears to be directly coupled to the pressure field at this surface (Fig. 4.5c), i.e., the tropopause height. The $|\partial p/\partial PV|$ and thus the flux is large in the areas where the tropopause pressure gradient is large (i.e., where the tropopause slopes) and in small-scale areas where the tropopause pressure itself is high (i.e., where the tropopause height is small), which can be understood from Fig. 4.6. These conditions are valid in the tropopause folds, where the slope of the tropopause is very large (see Fig. 4.1), and at the edge of a more extended lowering of the tropopause in the centre of a cyclone.

4.3.4 Vertical cross-sections of the air mass flux across PV -surfaces

In order to obtain a clearer understanding of the structure of the field of \tilde{F} in tropopause folds, vertical cross-sections of \tilde{F} across these folds have been calculated. Figure 4.7 shows a cross-section of \tilde{F} on 15 April 12 GMT along 40°N, with pressure as the vertical coordinate. A region with large downward fluxes on the eastside of the tropopause trough and a region with smaller upward fluxes in the tropopause ridges west and east of this trough are clearly distinguished. Many insignificant fluxes are found below the 1 PVU surface, where $|\partial p/\partial PV|$ is very large and noisy, resulting in a low signal to noise ratio. In most other tropopause folds (*not shown*), the region with the largest downward fluxes is also found on the eastside; in some folds this maximum is found in the middle of the fold, but not in the western part. The presence of regions with upward fluxes in tropopause ridges is also found to be a returning feature.

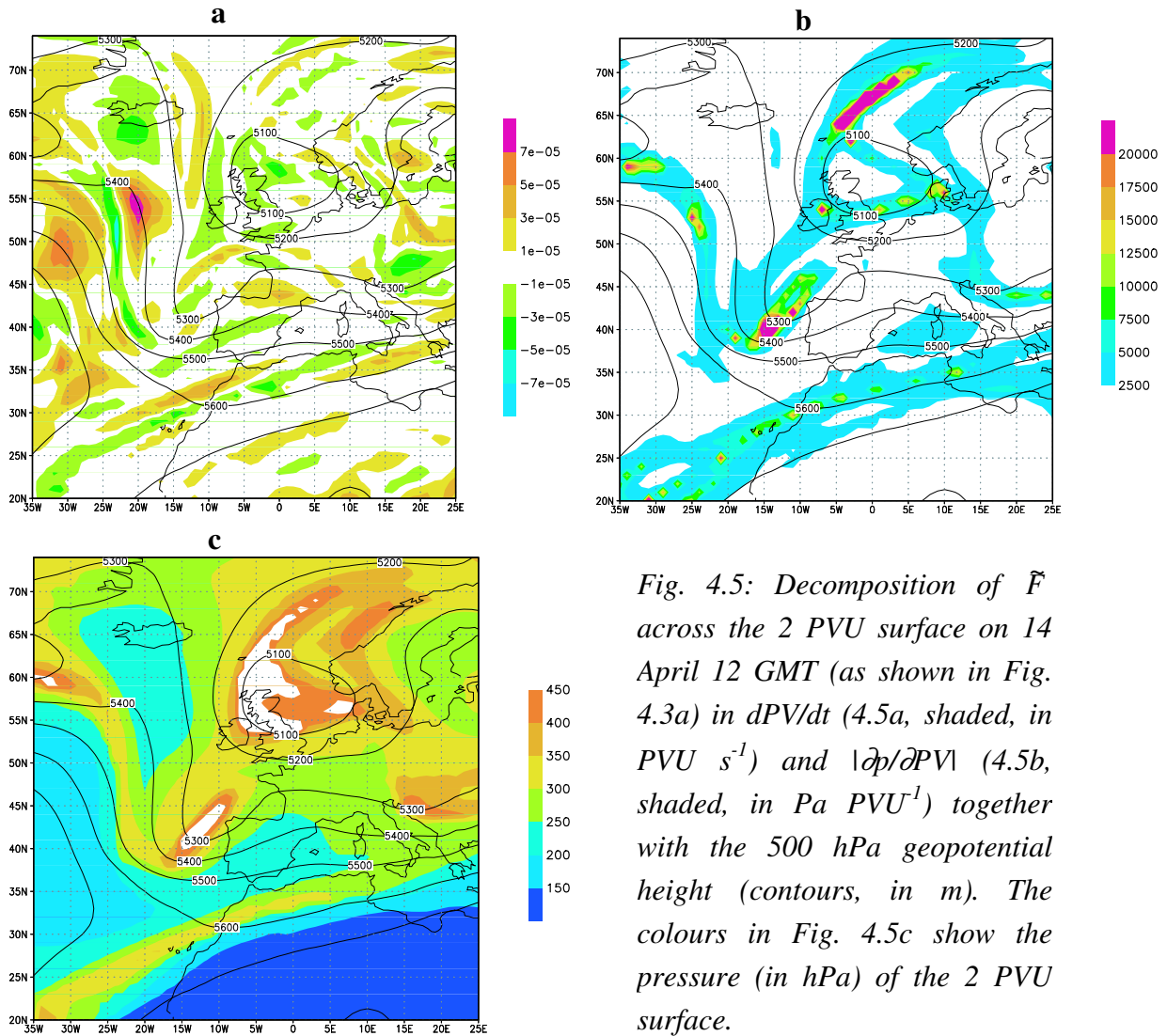


Fig. 4.5: Decomposition of \tilde{F} across the 2 PVU surface on 14 April 12 GMT (as shown in Fig. 4.3a) in dPV/dt (4.5a, shaded, in $PVU s^{-1}$) and $|\partial p/\partial PV|$ (4.5b, shaded, in $Pa PVU^{-1}$) together with the 500 hPa geopotential height (contours, in m). The colours in Fig. 4.5c show the pressure (in hPa) of the 2 PVU surface.

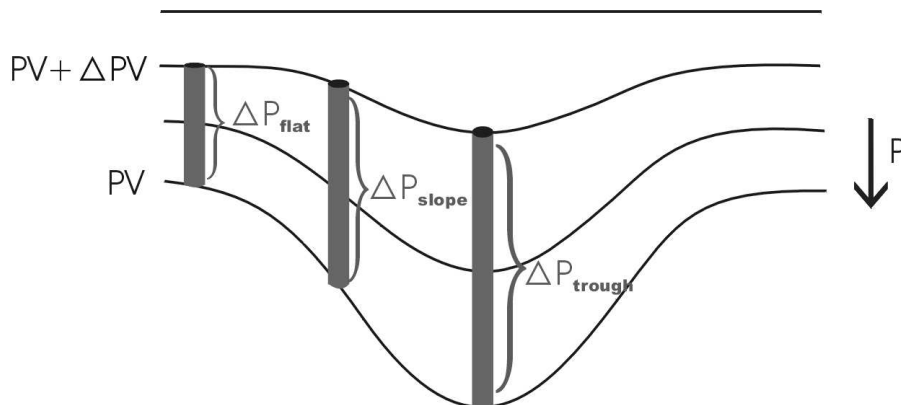


Fig. 4.6: Illustration of $|\partial p/\partial PV|$ around a tropopause trough. $|\partial p/\partial PV|$ at a sloping tropopause and at a tropopause trough is generally larger than $|\partial p/\partial PV|$ at a flat tropopause.

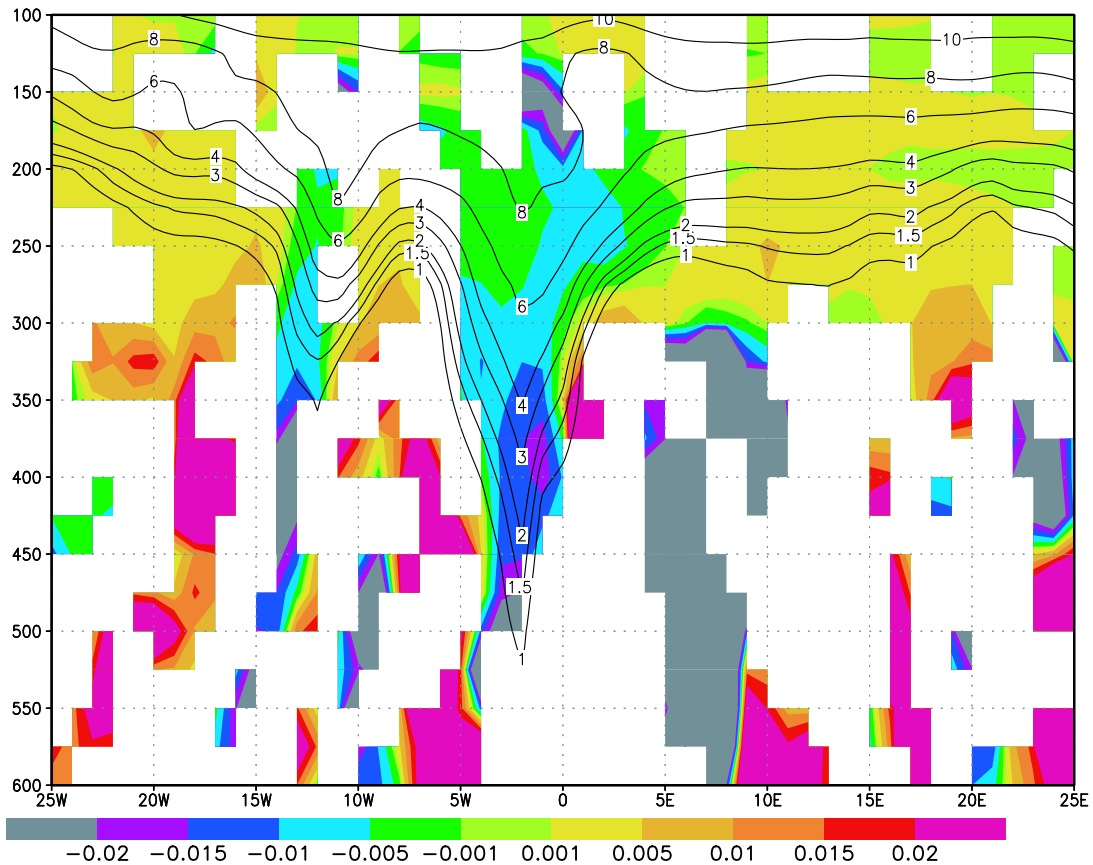


Fig. 4.7: Vertical cross-section of \tilde{F} (shaded, in $\text{kg m}^{-2} \text{s}^{-1}$) on 15 April 12 GMT along 40°N (which is the red line in Fig. 4.3b), with significance criterion (i.e., spaces are left blank where \tilde{F} is statistically insignificant), with pressure as the vertical coordinate, together with isolines of PV (in PVU).

The found maximum in downward fluxes in tropopause folds is expected to be a reliable result for the following reason. A tropopause fold can be looked at as a small-scale lowering of the tropopause. Above a lowered tropopause, the PV is anomalously high. According to the definition of PV, this would mean an anomalously high positive relative vorticity and an anomalously high $\partial\theta/\partial p$ in this PV-anomaly. The wind speed is therefore highest on both sides of the PV-anomaly, as can be verified from ECMWF-data for April 15 as seen in Fig. 4.8. The wind maxima cause a large shear in the surrounding areas. This wind shear causes strong mixing of air masses in the tropopause fold. Since the PV-gradient is relatively high in this region, this mixing of air masses implies a strong PV-mixing. Comparing Fig. 4.8 with Fig. 4.7, one can clearly see that the fluxes are largest in the regions where the wind shear is maximal. In these regions, PV-mixing is thought to cause the large fluxes. The large downward fluxes found in tropopause folds are therefore thought to be a reliable result, at least in a qualitative sense.

Cross section between 40.0N 335.0E and 40.0N 385.0E
on 13- 4-1998 at 12 Z + 48 on model levels

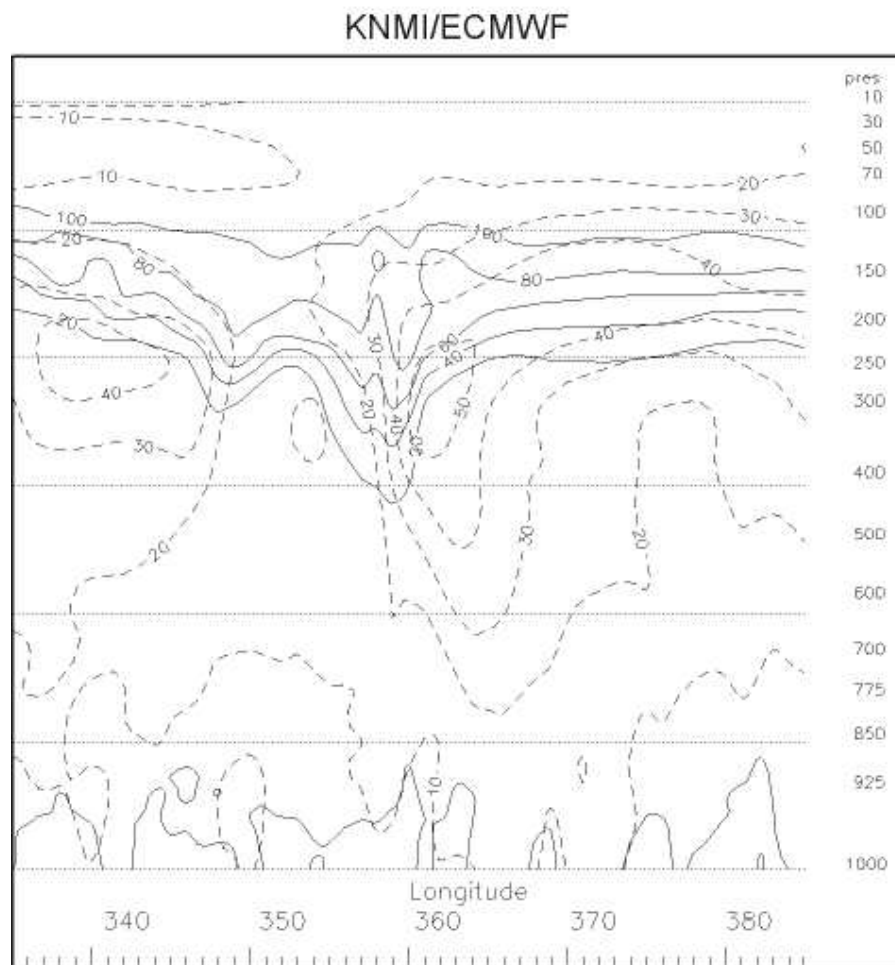


Fig. 4.8: Vertical cross-section of the wind speed (dotted lines, in $m s^{-1}$) on 15 April 12 GMT along $40^{\circ}N$ (which is the red line in Fig. 4.3b), with pressure as the vertical coordinate (in hPa), together with some isolines of PV (solid lines, in $PVU \cdot 10$).

The tropopause fold found along the northwest coast of Africa is thought to lie on a peculiar position. To validate the position of this tropopause fold, GOME (Global Ozone Monitoring Experiment) total ozone columns have been considered. These data (*not shown*) show a maximum in the total ozone column, which implies a lowering of the tropopause, virtually along the tropopause fold. The found tropopause fold with its large downward fluxes along the northwest coast of Africa is therefore expected to be a reliable result.

4.3.5 Area-averaged upward and downward fluxes

As is described in the introduction, the ratio between the upward and downward fluxes should be known in order to calculate the cross-tropopause fluxes of chemical species. To make an impression of this ratio, all upward and downward fluxes (without significance criterion) are added separately and are then averaged over the entire domain (see Table 4.1). In this calculation, fluxes larger than $0.1 \text{ kg m}^{-2} \text{ s}^{-1}$ and smaller than $-0.1 \text{ kg m}^{-2} \text{ s}^{-1}$ are assumed to be non-physical and are set to $0.1 \text{ kg m}^{-2} \text{ s}^{-1}$ and $-0.1 \text{ kg m}^{-2} \text{ s}^{-1}$, respectively. It is striking to see that the ratio R is smallest on April 16, when the strength of the cyclone is maximal, and largest on April 17, when the cyclone has weakened. The ratio between the area averaged upward and downward cross-tropopause fluxes appears to decrease with increasing strength of the cyclone.

TIME	F_{down}	F_{down}	F_{net}	R
98041412	1.69E-03	-2.24E-03	-5.44E-04	0.757
98041512	1.40E-03	-1.78E-03	-3.83E-04	0.785
98041612	1.52E-03	-2.39E-03	-8.77E-03	0.633
98041712	1.29E-03	-1.10E-03	1.84E-04	1.167

Table 4.1: Domain-averaged upward (F_{up}), downward (F_{down}) and net (F_{net}) fluxes (in $\text{kg m}^{-2} \text{ s}^{-1}$) and the ratio of the domain-averaged upward and downward fluxes ($R = |F_{up}/F_{down}|$) across the 2 PVU surface for 14, 15, 16 and 17 April 1998, 12 GMT.

4.4 Discussion

In this section the parameterisation of PV -mixing in the ECMWF-model and the method for calculating the flux across a PV -surface will be discussed. In subsection 4.4.3, the found ratios between the area-averaged upward and downward fluxes will be compared with those found in previous studies.

4.4.1 Parameterisation of PV -mixing in the ECMWF-model

As was described in subsection 4.2.1, one of the sources of the gridbox mean PV (and thus the stratosphere-troposphere exchange as calculated in this study) is PV -mixing. In the real atmosphere, the PV of a single air parcel can only be changed by diabatic heating gradients

and friction. In a numerical (prognostic) model, the change of PV due to mixing is a result of the model formulation of subgrid-scale processes. A restriction of a model is that it can not calculate the evolution of the properties of every single air parcel in the atmosphere explicitly. Instead, the quantities are calculated on a grid with a finite spatial resolution. The quantities calculated in a model are therefore gridbox mean rather than local quantities. The same applies to the PV computed along a trajectory. Therefore, in the absence of diabatic heating gradients and friction, mixing of air masses with different PV can lead to a change in the gridbox mean PV , although the PV of the individual air parcels is conserved.

The PV -change computed from gridbox mean circulation data is given by (for simplicity the 2-dimensional situation is considered):

$$\frac{d\overline{PV}}{dt} \equiv \frac{\partial\overline{PV}}{\partial t} + \overline{u} \frac{\partial\overline{PV}}{\partial x} + \overline{v} \frac{\partial\overline{PV}}{\partial y} = - \left[\frac{\partial\overline{u'PV'}}{\partial x} + \frac{\partial\overline{v'PV'}}{\partial y} \right], \quad (4.5)$$

where the overbar denotes gridbox mean values and the prime denotes deviations from those mean values. The right-hand side of this equation, the divergence of the eddy PV -flux, is a subgrid process, which is not computed explicitly. Instead, subgrid processes are parameterised in terms of the known gridbox mean quantities. In the ECMWF-model, the subgrid-scale fluxes of the model variables that determine the PV (vorticity, divergence and temperature) are parameterised, rather than the eddy PV -flux itself. The quality of these parameterisations in the ECMWF-model determines the quality of the results of this study. A second, possibly even more important contribution to the divergence of the eddy PV -flux is model numerical diffusion.

4.4.2 Method for calculating the flux across a PV -surface

Calculation of the fluxes

Because of numerical errors due to finite time and space differencing, finding an appropriate method for diagnosing the local and instantaneous flux across a PV -surface is not straightforward. Siegmund *et al.* (1996) have introduced the “advection method”, in which the space terms are selectively averaged over time in an Eulerian framework. In this Chapter we have circumvented these time differencing problems by working in a Lagrangian framework. The main remaining problem is that the data suffer from noise. Instant values of dPV/dt can therefore be unreliable. To cope with this problem, a certain kind of averaging is necessary. The instant flux in a gridpoint has therefore been computed from data along 6-hour forward and backward trajectories starting at the gridpoint.

A second approximation that has been made concerns the calculation of the PV along the trajectories. The gridbox averaged PV , used in numerical atmospheric models, should be calculated according to:

$$\overline{PV} = \overline{\frac{\partial\theta}{\partial p}(\zeta + f)} = \overline{\frac{\partial\theta}{\partial p}}(\overline{\zeta + f}) + \overline{\left(\frac{\partial\theta}{\partial p}\right)'(\zeta + f)}, \quad (4.6)$$

where the overbar denotes the gridbox mean value and the accent denotes the deviation from that value. In our calculation of \overline{PV} we were forced to neglect the second term on the right hand side, since the ECMWF-model only provides gridbox mean quantities.

Averaging period

The averaging period for the calculation of \tilde{F} (Eq. 4.3) has been varied to see how this affects the results. With decreasing period, the reduction of the noise in the results, which was made by averaging, decreases and less values of \tilde{F} are statistically significant. As a suitable time period for averaging dPV/dt and $|\partial p/\partial PV|$, 12 hours is found. Averaging over a longer period does not decrease the noise substantially, but artificially smoothes out the cross- PV fluxes.

Comparison with the Lagrangian flux calculation of Wirth and Egger (1999)

As described in the introduction, Wirth and Egger (1999) also used a Lagrangian method to diagnose the cross-tropopause air mass flux. Although the concept of their method is similar to the method applied in this study, there are some noteworthy differences. The similarity is that in both methods a quantity is considered along a trajectory, which is the PV in the present study and the pressure in their study. The pressure difference between the endpoint of a trajectory that started at the tropopause and the tropopause at that endpoint is then taken by Wirth and Egger (1999) as a measure of the cross-tropopause flux.

A difference with our method is that every three hours a reinterpolation of their trajectories to a regular grid is performed in order to avoid a too strong accumulation or dilution of points, which introduces some smoothing. Our method circumvents this problem by calculating forward and backward trajectories starting at a gridpoint and attributing the computed flux to this gridpoint. A second difference is that Wirth and Egger (1999) compute the cross-tropopause flux from information at only the begin and the end of the trajectory, whereas in the present study the averaged PV -rate of change along the trajectory, estimated by

a linear least square method, and the trajectory-mean value of $|\partial p/\partial PV|$ are used to calculate the flux. Our results are, therefore, expected to be less subjected to noise.

4.4.3 Comparison of F_{up}/F_{down} with previous studies

Table 4.2 shows different values of R ($=|F_{up}/F_{down}|$) found in different studies with different methods. Before comparing our values with the other values from Table 4.2, one should realise that R can be strongly case-dependent. In our results, the largest downward fluxes have been found in tropopause folds. From Table 4.2 it appears that R decreases if fewer fluxes outside the tropopause fold are taken into account in the calculation of R . In Spaete *et al.* (1994) and Lamarque and Hess (1994), R is calculated in a relatively small area around, respectively, a tropopause fold and an extratropical cyclone, whereas in our case, R is calculated averaged over a larger area around an extratropical cyclone. Siegmund *et al.* (1996), finally, computed R for a whole month and for a much larger area. The domain-averaged upward (F_{up}) and downward (F_{down}) fluxes are comparable to the values found by Lamarque and Hess ($1.68 \times 10^{-3} \text{ kg m}^{-2} \text{ s}^{-1}$ and $2.12 \times 10^{-3} \text{ kg m}^{-2} \text{ s}^{-1}$, respectively) and Spaete *et al.* ($5.79 \times 10^{-3} \text{ kg m}^{-2} \text{ s}^{-1}$ and $2.31 \times 10^{-3} \text{ kg m}^{-2} \text{ s}^{-1}$, respectively).

Source	R	Averaging period	Averaging area	Method	model
Spaete <i>et al.</i> (1994)	0.4	1 day	Area around tropopause fold, travelling with system	Wei- θ across 3 PVU	Mesoscale
Lamarque and Hess (1994)	0.79	4 days	Area around extratropical cyclone travelling with system	Wei-PV across 2 PVU	Mesoscale
Siegmund <i>et al.</i> (1996)	0.97	Month	28°N - 90°N	Wei-p across 3.5 PVU	ECMWF, first guess data
Present study	0.63-1.17	(12 hours)	35°W-25°E 20°N-75°N	Trajectories, Wei-PV across 2 PVU	ECMWF, first guess data

Table 4.2: Calculations of R ($=|F_{up}/F_{down}|$) from previous studies and the present study

4.5 Conclusions

In this Chapter a Lagrangian method for diagnosing the air mass flux across PV -surfaces, in particular across the tropopause, has been applied. Several aspects of the method are new compared to previous studies. The flux is computed from the PV and $|\partial p/\partial PV|$ along 12-hour trajectories that pass the gridpoint for which the flux is estimated. The trajectories are computed from ECMWF circulation data. The error in the flux across PV -surfaces is quantified and used to determine the statistical significance of the flux.

The computed field of the air mass flux across PV -surfaces is dominated by elongated patterns of statistically significant large downward and small upward fluxes. The downward fluxes mainly occur in regions of a tropopause fold, whereas the upward fluxes are found near tropopause ridges. The area-averaged upward (F_{up}) and downward (F_{down}) fluxes, which both lie between 1 and $2.5 \times 10^{-3} \text{ kg m}^{-2} \text{ s}^{-1}$, are comparable to the values found by previous investigators. The ratio between the area averaged upward and downward cross-tropopause fluxes appears to decrease with increasing strength of the cyclone.

The results are thought to be reliable, at least in a qualitative sense, because the largest downward fluxes in the tropopause fold occur in regions with maximum wind shear, where PV -mixing is thought to cause stratosphere-troposphere exchange. The geographical agreement between tropopause folds with large downward fluxes and the high total ozone values is good. Although several approximations have been made in the applied new Lagrangian method, this method appears to be an appropriate tool for diagnosing dPV/dt in general and stratosphere-troposphere exchange in particular.

Acknowledgements

We thank Rinus Scheele for his support he gave concerning the KNMI trajectory model. We also would like to thank Geert-Jan Roelofs and Anastasios Kentarchos (both from the Institute of Marine and Atmospheric Research, Utrecht University, the Netherlands) for their helpful suggestions. Comments of two anonymous reviewers helped improve the manuscript, and were greatly appreciated.

Chapter 5

Summary and outlook

In this concluding Chapter the main results of the study presented in this thesis will be summarised. In addition, an outlook on future research will be given.

5.1 Summary

In this thesis some aspects of the coupling between the stratosphere and the troposphere have been investigated. A variety of models and methods has been used to investigate stratosphere-troposphere coupling issues on different time-scales. In particular, the following five questions have been addressed:

1. *What is the effect of CO₂ doubling in the troposphere on the middle atmosphere?*
2. *What is the effect of CO₂ doubling in the middle atmosphere on the troposphere?*
3. *How well has the middle atmosphere to be represented in General Circulation Models to capture the middle atmospheric influence on the tropospheric climate and climate change?*
4. *Through which dynamical mechanism does the stratosphere influence the troposphere?*
5. *How can Lagrangian methods be used to quantify stratosphere-troposphere exchange?*

1. What is the effect of CO₂ doubling in the troposphere on the middle atmosphere?

This question has been addressed in Chapter 2. Hereto, the climate effects of separate middle atmospheric and tropospheric CO₂ doubling have been investigated by performing 30-year model experiments with the middle atmosphere General Circulation Model MA-ECHAM4. It has been shown that in the largest part of the atmosphere, the response to a uniform CO₂ doubling is approximately equal to the sum of the separate responses to middle atmospheric and tropospheric CO₂ doubling. Hence, in these regions, the changes in the uniformly doubled CO₂ climate could be attributed either to tropospheric or to middle atmospheric CO₂ doubling. The stratospheric meridional overturning circulation, also called the residual or Brewer-Dobson circulation, was found to increase in response to a uniform CO₂ doubling. This increase is mainly due to tropospheric CO₂ doubling. Thus, the results indicate that tropospheric climate change induces significant stratospheric climate change. In the uniformly

doubled CO₂ climate, the increased downward motions in the Arctic lower stratosphere (associated with the increased residual circulation) induce a dynamical heating that is slightly larger than the radiative cooling due to CO₂ doubling. Consequently, the Arctic lower stratosphere warms and the stratospheric meridional temperature gradient north of 60°N reduces, which is consistent with the weakening of the zonal winds in the Arctic middle atmosphere. In summary, the results indicate that CO₂ doubling in the troposphere causes significant stratospheric climate changes. It can explain the largest part of the strengthening of the stratospheric residual circulation and associated temperature and zonal wind changes.

2. What is the effect of CO₂ doubling in the middle atmosphere on the troposphere?

This question has also been addressed with the model experiments presented in Chapter 2. During NH winter, the simulated uniformly doubled CO₂ climate is characterised by an increase of the tropospheric NH mid-latitude westerlies and a poleward shift of the tropospheric SH westerlies. The zonal wind response to uniform CO₂ doubling was found to be approximately equal to the sum of the zonal wind responses to separate tropospheric and middle atmospheric CO₂ doubling in the largest part of the atmosphere, including the tropospheric mid-latitudes. Thus, it is possible to attribute the tropospheric mid-latitude zonal wind responses in the uniformly doubled CO₂ climate either to tropospheric or to middle atmospheric CO₂ doubling. The middle atmospheric CO₂ doubling causes significant increases in the tropospheric NH mid-latitude westerlies, in contrast to the tropospheric CO₂ doubling. Thus, the simulated strengthening of the tropospheric NH mid-latitude westerlies in the doubled CO₂ climate can be attributed to middle atmospheric CO₂ doubling. This result indicates a crucial role of the middle atmospheric climate change in the increase of the tropospheric NH mid-latitude westerlies in the uniformly doubled CO₂ climate. In contrast, the poleward shift of the tropospheric SH westerlies in NH winter in response to uniform CO₂ doubling has been attributed to tropospheric CO₂ doubling.

3. How well has the middle atmosphere to be represented in General Circulation Models to capture the middle atmospheric influence on the tropospheric climate and climate change?

This question has also been addressed in Chapter 2. It was stimulated by the finding that in a middle atmosphere GCM stratospheric climate change induces significant tropospheric climate change, and by the observation that until recently, in many General Circulation Models the region above 10 hPa was only represented by one model layer. Although this question has been addressed in several previous studies, no unambiguous answer has been found yet. The middle atmosphere GCM MA-ECHAM4 has been used to contribute to this issue. Hereto, the CO₂ has been doubled only in the region between 10 and 0.01 hPa. The results show that CO₂ doubling in this region already causes significant increases of the tropospheric NH mid-latitude westerlies, suggesting that CO₂ doubling above 10 hPa

significantly contributes to the strengthening of the tropospheric NH mid-latitude westerlies in the uniformly doubled CO₂ climate. Thus, this result indicates that the inclusion in GCM's of the region between 10 and 0.01 hPa seems necessary for producing reliable tropospheric climate predictions.

4. Through which dynamical mechanism does the stratosphere influence the troposphere?

This question has been addressed in Chapter 3. It has been postulated in previous studies that the stratosphere could dynamically influence the troposphere through variations in a meridional circulation cell. The study presented in Chapter 3 is one of the first in which the occurrence of such a mechanism in circulation data is investigated. Hereto, ECMWF reanalysis data for the NH extratropical winters from 1979 to 1993 have been analysed. The following results indicate a mechanism that couples extratropical meridional mass flux variations in the stratosphere to variations in the extratropical zonal wind in the lower troposphere:

- In all NH extratropical winters from 1979 to 1993 low-frequency variations in the stratospheric meridional mass flux are followed by similar variations in the tropospheric meridional mass flux, with a lag of about one day. This lag has also been obtained qualitatively with a very simple model based on the zonally averaged zonal and meridional momentum equations. The lag has implications for the polar cap averaged surface pressure. An increase in the stratospheric meridional mass flux out of the polar cap is followed, with a delay of about one day, by an increase in the tropospheric meridional mass flux into the polar cap. Because of this delay, the magnitude of the stratospheric mass flux out of the polar cap is larger than that of the tropospheric mass flux into the polar cap and, consequently, the polar cap mean surface pressure decreases. The opposite applies for a decrease in the stratospheric meridional mass flux.
- The resulting low-frequency variations in the polar cap averaged surface pressure explain most of the variations in the meridional surface pressure gradient around 60°N.
- The latter variations are geostrophically coupled to the variations in the zonal wind near the surface around 60°N.
- In the NH mid-latitude stratosphere the Coriolis force on the zonal-mean zonal meridional wind is nearly balanced by the convergence of the eddy momentum flux, and in the lower troposphere by the zonal frictional force.

5. How can Lagrangian methods be used to quantify stratosphere-troposphere exchange?

This question has been addressed in Chapter 4. Previous studies have shown that most Eulerian methods to quantify local and instantaneous stratosphere-troposphere exchange (STE) appear to be inaccurate because they suffer from cancellation of large terms. Therefore, recently a number of Lagrangian methods have been introduced. One of them has been introduced and applied to an extratropical cyclone in Chapter 4 of this thesis. The cross-tropopause air mass flux has been computed from the potential vorticity along trajectories that pass the grid point for which the flux is to be estimated. The trajectories have been computed with ECMWF circulation data. The results from the application of this method to an extratropical cyclone have given confidence in the reliability of the method for the following reasons:

- The computed field of the cross-tropopause fluxes, as well as the ratio between the area-averaged downward and upward fluxes are consistent (or at least not in conflict with) results from previous studies.
- The largest downward fluxes in the tropopause folds have been shown to occur in regions with maximum wind shear, where mixing is thought to cause large stratosphere-troposphere exchange.

5.2 Outlook

The results presented in this thesis have contributed to our understanding of stratosphere-troposphere coupling in the present climate, and its relation to climate change. Nevertheless, several new important questions have emerged, which should be addressed in the future.

Stratosphere-troposphere coupling and climate change

Climate change affects life on Earth. Therefore, the understanding and attribution of recent climate trends, and the prediction of future climate changes are major issues in current science. As has been mentioned in Chapter 1, the observed recent positive trend of the Arctic Oscillation index (and, consequently, the increase of the tropospheric NH mid-latitude westerlies) can explain much of recent NH mid-latitude trends. In Chapter 2 the increase of the tropospheric NH mid-latitude westerlies in response to increasing greenhouse gases has been attributed to middle atmospheric CO₂ doubling. The results are consistent with the hypothesis that the stratospheric climate change induces tropospheric climate change through wave-mean flow interactions. However, the exact mechanism has remained unclear, and further research is needed. In particular, the causes of the surface pressure distribution change in response to increasing greenhouse gases should be investigated. The results presented in Chapter 2 do not confirm the hypothesis for the causes of these changes suggested by some

previous authors (e.g., Shindell *et al.* 2001). A recent study by Carnell and Senior (2002) suggests that sea surface temperature changes could play a major role, but this hypothesis is not supported by the results presented in Section 2.7.1 of this thesis.

Such an explanation for the surface pressure response to increasing CO₂ concentrations would shed more light on the following paradox. Because of the expected high latitude low level warming amplification (due to the ice-albedo feedback) in response to increased CO₂ concentrations, the lower tropospheric meridional temperature gradient is expected to decrease. Due to the thermal wind relationship, the zonal wind change is expected to decrease with height, whereas we find increased tropospheric westerlies. However, the tropospheric zonal wind is determined not only by the meridional temperature gradient and associated vertical zonal wind gradient, but also by the surface pressure distribution. In our simulations, the effect of the changes in these two quantities is an increase of the zonal wind throughout the troposphere. It is desirable to investigate the causes of the surface pressure pattern change in more detail, so that the tropospheric NH mid-latitude response to increasing greenhouse-gas concentrations can be understood better.

General circulation model studies

Even when, as in the present study, large computer resources are available, an atmospheric modeller should make choices. It is not clear if the conclusions drawn from the uniform and non-uniform CO₂ doubling experiments presented in Chapter 2 also would apply if other model configurations would be used. The robustness of the results could be tested by investigating the sensitivity of the results to the following choices:

- *Horizontal and vertical resolution.* General circulation models solve the primitive equations on grid boxes with a particular horizontal and vertical size. The simulations presented in Chapter 2 have been performed at T42 horizontal resolution (about $2.8^\circ \times 2.8^\circ$) and at 39 model levels from the surface up to 0.01 hPa. It would be interesting to investigate the sensitivity of the results to changes in the horizontal and vertical resolution. In particular, the importance of a good vertical resolution in the middle and upper atmosphere is of interest. A recent study by Gillett *et al.* (2003b) has demonstrated that the AO-index increase (and, consequently, the tropospheric NH mid-latitude zonal wind increase and related temperature response) in response to increasing greenhouse-gases is largely underestimated by several general circulation models. They suggest that such a discrepancy could result from a lack of stratospheric resolution, which is supported by the results presented in Chapter 2. Our results have suggested that CO₂ doubling between 10 and 0.01 hPa significantly contributes to the strengthening of the tropospheric NH mid-latitude westerlies in the uniformly doubled CO₂ climate. However, from our simulations it can not be determined whether the upper atmosphere above 0.01 hPa must be represented adequately to capture all middle and upper atmospheric influences on the troposphere.

- *Coupling with an ocean model.* The atmospheric GCM used in our study has not been interactively coupled to an ocean model. Instead, monthly climatological sea surface temperature fields have been prescribed. It would be interesting to investigate if our conclusions also apply when the atmospheric GCM would be interactively coupled to an ocean model. In particular, the stratospheric residual circulation appears to be very sensitive to sea surface temperatures (e.g., Rind *et al.* 2002).
- *Coupling with an atmospheric chemistry model.* A recent modelling study (Shindell *et al.* 1998) has suggested that the recovery of the ozone layer is delayed because of increasing greenhouse gases. Stratospheric ozone depletion cools the polar vortex, since less ozone absorbs less solar radiation. In our simulations, these climate-chemistry interactions could not be simulated, since the atmospheric general circulation model has not been coupled to a chemistry model. Instead, responses to CO₂ doubling have been investigated in simulations where the ozone field was prescribed. Recently, the MA-ECHAM4 model has been coupled to a chemistry model (Manzini *et al.* 2003). It would be interesting to investigate whether the conclusions of Chapter 2 also apply in that configuration.

Since the stratosphere-troposphere coupling is strongest during NH winter, Chapter 2 has focussed on this season. An other interesting question for future research would be to investigate whether similar conclusions apply for SH winter.

Stratosphere-troposphere coupling mechanisms in the present climate

In Chapter 3 evidence has been presented for the presence of a mechanism that couples low-frequency variations in the stratospheric meridional wind and in the surface level zonal wind during 1979-93 NH extratropical winters. Several questions have raised that could be addressed in the future:

- *Is the mechanism also present in other seasons and in the Southern Hemisphere?*
- *Which mechanism can explain the rapid transfer of zonal wind variations from the lower stratosphere to the lower troposphere?* The mechanism presented in Chapter 3 links variations in the stratospheric *meridional* wind to variations in the lower tropospheric zonal wind, but lacks a link between variations in the zonal wind and in the meridional wind in the stratosphere. Although indications have been presented for such a link, more evidence is desirable.
- *Is the mechanism also present in ERA-40 data?* The meridional mass fluxes have been calculated using the ERA-15 data set, which extends up to 10 hPa. Recently, the new ERA-40 data set has become available, which extends up to 0.1 hPa. In Chapter 3, it has been suggested that uncertainties in the calculation of the stratospheric meridional mass flux are caused by the lack of meridional wind information above 10 hPa in the

ERA-15 data set. Since the new ERA-40 data set extends up to 0.1 hPa, it contains much more information on the meridional wind above 10 hPa. Therefore, the stratospheric meridional mass fluxes can, in principle, be calculated more precisely with this new data set. Consequently, confidence in the presence of a lag between the low-frequency variations in the meridional mass flux variations in the stratosphere and those in the troposphere could be increased by identifying such a lag in the ERA-40 data set.

- *Why do the low-frequency meridional mass flux variations in the stratosphere precede those in the troposphere?* A priori, the opposite situation (troposphere preceding the stratosphere) can not be excluded, but this is not found in our results. Three possible answers are:
 - a) The driving forces of meridional mass transport vary much more and are much larger in the stratosphere than in the troposphere.
 - b) The frictional force, which is large only in the lower troposphere, plays a crucial role in generating the lag, by delaying the tropospheric response to surface pressure changes generated by stratospheric meridional mass flux variations. This could be investigated further with idealized model experiments in which the lower tropospheric frictional force is varied.
 - c) The lag is a reflection of a different mechanism or a combination of several mechanisms.

Quantification of stratosphere-troposphere exchange

The reliability of the Lagrangian method to calculate stratosphere-troposphere exchange introduced in Chapter 4 has been investigated in several studies. The results of the application to an extratropical cyclone presented in Chapter 4 indicate that the method is reliable, at least in a qualitative sense. Meloen *et al.* (2001) have applied the method to a SH subtropical cyclone, and also found that the geographical distribution of the computed cross-tropopause mass fluxes was consistent with what was expected from physical arguments. In addition, they computed the probability density functions of the computed fluxes. They suggested that the method is more reliable than previous methods, since the distributions were narrower than those computed with other methods in previous studies. The larger tails of the distributions evaluated with the other methods indicate that they suffer more from numerical noise. Using ozone soundings and the relationship between ozone concentration and potential vorticity, they showed results that increase the confidence in the reliability of the calculated fluxes. The Lagrangian technique was part of an intercomparison study of models and methods to quantify stratosphere-troposphere exchange performed by Meloen *et al.* (2003). They showed that the results from our Lagrangian method applied to a 12-day case study compare well with those from other, but conceptually different Lagrangian methods. Cristofanelli *et al.* (2003) compared the results of different methods with observations of several atmospheric trace

gases. They found that the Lagrangian methods based on trajectories simulated the event reasonably well. However, these methods sometimes failed to capture the presence of stratospheric air in the troposphere, which they attributed to the fact that convection and turbulence schemes are missing in these models.

The results presented in Chapter 4 show that the largest downward fluxes occur in tropopause folds, where mixing is expected to cause large stratosphere-troposphere exchange (STE). However, relatively little attention has been given to other sources of STE, such as diabatic heating gradients, which could be an interesting subject for future research.

Since several studies indicate that the method presented in Chapter 4 is reliable, it can be further exploited. For example, it can be used to calculate climatologies of STE, like has been done by Sprenger and Wernli (2002). They applied an other Lagrangian technique to the ERA-15 data set, and identified regions where large upward and large downward cross-tropopause fluxes occur. Application of such techniques to data sets with a longer duration, like the new ERA-40 data set, could be used to investigate whether a trend in the STE has occurred. Such trends could confirm the finding of several recent modelling studies (see section 1.6) that the stratospheric Brewer-Dobson circulation, the circulation that drives the large scale STE, strengthens in response to increasing greenhouse gases.

References

Andrews, D.G., J.R. Holton, and C.B. Leovy, 1987: Middle atmosphere dynamics, Academic Press, Orlando, 490 pp.

Andrews, D.G., 2000: *An introduction to atmospheric physics*. Cambridge University Press, 229 pp.

Baldwin, M.P., and T.J. Dunkerton, 1999: Propagation of the Arctic Oscillation from the stratosphere to the troposphere. *J. Geophys. Res.*, **104**, 30937-30946.

Baldwin, M.P., and T.J. Dunkerton, 2001: Stratospheric harbingers of anomalous weather regimes. *Science*, **294**, 581-584.

Baldwin, M.P., L.J. Gray, T.J. Dunkerton, K. Hamilton, P.H. Haynes, W.J. Randel, J.R. Holton, M.J. Alexander, I. Hirota, T. Horinouchi, D.B.A. Jones, J.S. Kinnersley, C. Marquardt, K. Sato, and M. Takahashi, 2001: The quasi-biennial oscillation. *Rev. of Geophys.*, **39**, 179-229.

Black, R.X., 2002: Stratospheric forcing of surface climate in the Arctic Oscillation. *J. Climate*, **15**, 268-277.

Boville, B.A., 1984 : The influence of the Polar Night Jet on the Tropospheric Circulation in a GCM. *J. Atmos. Sc.*, **41**, 1132-1142.

Brewer, A.M., 1949: Evidence for a world circulation provided by the measurements of helium and water vapour distribution in the stratosphere. *Q.J.R. Meteorol. Soc.*, **75**, 351-363.

Brühl, C., 1993: Atmospheric effects of stratospheric aircraft. Rep 1992 Models and Measurements Workshop (Prather M., Remsberg E., eds.) *NASA Ref Publ. 1292 II*.

Butchart, N., and A.A. Scaife, 2001: Removal of chlorofluorocarbons by increased mass exchange between the stratosphere and troposphere in a changing climate. *Nature*, **410**, 799-802.

Carnell, R.E., and C.A. Senior, 2002: An investigation into the mechanisms of changes in mid-latitude mean sea level pressure as greenhouse gases are increased. *Clim. Dyn.*, **18**, 533-543.

Charney J.G., and P.G. Drazin, 1961: Propagation of planetary-scale disturbances from the lower into the upper atmosphere. *J. Geophys. Res.*, **66**, 83-109.

Christiansen, B., 1999: Stratospheric vacillations in a general circulation model. *J. Geophys. Res.*, **56**, 1858-1872.

Christiansen, B., 2001: Downward propagation from the stratosphere to the troposphere: Model and reanalysis. *J. Geophys. Res.*, **106**, 27307-27322.

- Cristofanelli, P., P. Bonasoni, W. Collins, J. Feichter, C. Forster, P. James, A. Kentarchos, P.W. Kubik, C. Land, J. Meloan, G.J. Roelofs, P. Siegmund, M. Sprenger, C. Schnabel, A. Stohl, L. Tobler, L. Tositti, T. Trickl, and P. Zanis, 2003: Stratosphere-to-troposphere transport: a model and method evaluation. *J. Geophys. Res.*, **108**, 8525, doi:10.1029/2002JD002600.
- Dobson, G.M.B., 1956: Origin and distribution of polyatomic molecules in the atmosphere. *Proc. Roy. Meteor. Soc.*, **A236**, 187-193.
- Eskes, H.J., A.J. Segers, and P.F.J. van Velthoven, 2003: Ozone forecasts of the stratospheric polar vortex splitting event in September 2002, *J. Atmos. Sci.*, submitted.
- Farman, J.C., B.G. Gardiner, and J.D. Shanklin, 1985: Large losses in total ozone in Antarctica reveal seasonal ClO_x/NO_x interaction. *Nature*, **315**, 207-210.
- Fels, S.B., J.D. Mahlman, M.D. Schwarzkopf, and R.W. Sinclair, 1980: Stratospheric sensitivity to perturbations in ozone and carbon dioxide: Radiative and dynamical response. *J. Atmos. Sci.*, **37**, 2265-2297.
- Fyfe, J.C., G.J. Boer, and G.M. Flato, 1999: The Arctic and Antarctic Oscillations and their projected changes under global warming. *Geophys. Res. Lett.*, **26**, 1601-1604.
- Gottelman, A., and A.H. Sobel, 2000: Direct diagnoses of stratosphere-troposphere exchange. *J. Atmos. Sci.*, **57** 3-16.
- Gibson, J.K., P. Kallberg, S. Uppala, A. Hernandez, A. Normura, and E. Serran, 1997: ERA description, ECMWF Re-Analysis Project Report Series 1, ECMWF Reading RG2 AX, UK, 72pp.
- Gillett, N.P., M.R. Allen, and K.D. Williams, 2002: The role of stratospheric resolution in simulating the Arctic Oscillation response to greenhouse gases. *Geophys. Res. Lett.*, **29**, 1500-1503.
- Gillett, N.P., M.R. Allen, K.D. Williams, 2003a: Modelling the atmospheric response to doubled CO₂ and depleted stratospheric ozone using a stratosphere-resolving coupled GCM. *Q. J. R. Meteorol. Soc.*, **29**, 947-966.
- Gillett, N. P., F. W. Zwiers, A. J. Weaver, P. A. Stott, 2003b: Detection of human influence on sea level pressure, *Nature*, **422**, 292-294.
- Hartley, D.E., J. Villarín, R.X. Black, C.A. Davis, 1998: A new perspective on the dynamical link between the stratosphere and troposphere. *Nature*, **391**, 471-474.
- Hartmann, D.L., J.M. Wallace, V. Limpasuvan, D.W.J. Thompson, J.R. Holton, 2000: Can ozone depletion and global warming interact to produce rapid climate change? *Proc. Natl. Acad. Sci.*, **97**, 1412-1417.
- Haynes, P.H., and T.G. Shepherd, 1989: The importance of surface pressure changes in the response of the atmosphere to zonally symmetric thermal and mechanical forcing. *Q. J. R. Meteorol. Soc.*, **115**, 1181-1208.

- Haynes, P.H., C.J. Marks, M.E. McIntyre, T.G. Shepherd, K.P. Shine, 1991: On the “downward control” of extratropical diabatic circulation by eddy-induced mean zonal forces. *J. Atmos. Sci.*, **48**, 651-678.
- Hines, C.O., 1997a: Doppler spread parameterization of gravity wave momentum deposition in the middle atmosphere. Part 1: Basic formulation. *J. Atmos. Sol. Terr. Phys.*, **59**, 371-386.
- Hines, C.O., 1997b: Doppler spread parameterization of gravity wave momentum deposition in the middle atmosphere. Part 2: Broad and quasi monochromatic spectra and implementation. *J. Atmos. Sol. Terr. Phys.*, **59**, 387-400.
- Hoerling, M.P., T.K. Schaack, and A.J. Lenzen, 1993: A global analysis of stratospheric-tropospheric exchange during northern winter. *Mon. Wea. Rev.*, **121**, 162-172.
- Hoinka, K.P., 1998: Statistics of the global tropopause pressure. *Mon. Wea. Rev.*, **126**, 3303-3325.
- Holton, J.R., and C. Mass, 1976: Stratospheric vacillation cycles. *J. Atmos. Sci.*, **33**, 2218-2225.
- Holton, J.R., 1992: An introduction to dynamic meteorology, Third Edition. Academic Press, San Diego New York Boston London Sydney Tokyo Toronto, 511pp.
- Holton, J.R., P.H. Haynes, M.E. McIntyre, A.R. Douglass, R.B. Rood, and L. Pfister, 1995: Stratosphere-troposphere exchange. *Rev. Geophys.*, **33**, 403-439.
- Hoskins, B.J., M.E. McIntyre and A.W. Robertson, 1985: On the use and significance of isentropic potential vorticity maps. *Q.J.R. Meteorol. Soc.*, **111**, 877-946.
- IPCC (Intergovernmental Panel on Climate Change), 1999: special report on ‘Aviation and the global atmosphere’, Cambridge University Press.
- IPCC (Intergovernmental Panel on Climate Change), 2001: The Scientific Basis. Contribution of Working Group I to the Third Assessment Report of the Intergovernmental Panel on Climate Change [Houghton, J.T., Y.Ding, D.J. Griggs, M. Noguer, P.J. van der Linden, X. Dai, K. Maskell, and C.A. Johnson (eds.)]. Cambridge University Press, Cambridge, United Kingdom and New York, NY, USA, 881pp.
- Kelly, P.M., P.D. Jones, and J. Penqun, 1996: The spatial response of the climate system to explosive volcanic eruptions. *Int. J. Climatol.*, **16**, 537-550.
- Kodera, K., K. Yamazaki, M. Chiba, K. Shibata, 1990: Downward propagation of upper stratospheric mean zonal wind perturbation to the troposphere. *Geophys. Res. Lett.*, **17**, 1264-1266.
- Kodera, K., M. Chiba, K. Yamazaki and K. Shibata, 1991: A Possible influence of the polar night stratospheric jet on the subtropical tropospheric jet. *J. Meteor. Soc. Japan*, **69**, 715-720.

- Kuroda, Y., and K. Kodera, 1999: Role of planetary waves in the stratosphere-troposphere coupled variability in the northern hemisphere winter. *Geophys. Res. Lett.*, **26**, 2375-2378.
- Lamarque, J. and P.G. Hess, 1994: Cross-tropopause mass exchange and potential vorticity budget in a simulated tropopause folding. *J. Atmos. Sci.*, **51**, 2246-2269.
- Mahfouf, J.F., D. Cariolle, J.F. Royer, J.F. Geleyn, and B. Timbal, 1994: Response of the Meteo-France climate model to changes in CO₂ and sea surface temperature. *Clim. Dyn.*, **9**, 345-362.
- Manzini, E., N.A. McFarlane, and C. McLandress, 1997: Impact of the Doppler spread parameterization on the simulation of the middle atmosphere circulation using the MAECHAM4 general circulation model. *J. Geophys. Res.*, **102**, 25751-25762.
- Manzini, E., and N.A. McFarlane, 1998: The effect of varying the source spectrum of a gravity wave parameterization in a middle atmosphere general circulation model. *J. Geophys. Res.*, **103**, 31523-31539.
- Manzini, E., B. Steil, C. Brühl, M.A. Giorgetta, and K. Krüger, 2003: A new interactive chemistry-climate model. II. Sensitivity of the middle atmosphere to ozone depletion and increase in greenhouse gases: Implications for recent stratospheric cooling. *J. Geophys. Res.*, in press.
- Matsuno, T., 1970: Vertical propagation of stationary planetary waves in the winter Northern Hemisphere, *J. Atmos. Sci.*, **27**, 871-883.
- McFarlane, N.A., 1987: The effect of orographically excited gravity wave drag on the general circulation of the lower stratosphere and troposphere. *J. Atmos. Sci.*, **44**, 1775-1800.
- Meloan, J., P.C. Siegmund, and M. Sigmond, 2001: A Lagrangian computation of stratosphere-troposphere exchange in a tropopause folding event in the subtropical Southern Hemisphere. *Tellus*, **53**, 367-378.
- Meloan, J., P. Siegmund, P. van Velthoven, H. Kelder, M. Sprenger, H. Wernli, A. Kentarchos, G. Roelofs, J. Feichter, C. Land, C. Forster, P. James, A. Stohl, W. Collins, and P. Cristofanelli, 2003: Stratosphere-troposphere exchange: a model and method intercomparison. *J. Geophys. Res.*, **108**, 8526, doi:10.1029/2002JD002274.
- Paeth, H., A. Hense, R. Glowienka-Hense, S. Voss, and U. Cubasch, 1999: The North Atlantic Oscillation as an indicator for greenhouse-gas induced regional climate change. *Clim. Dyn.*, **15**, 953-960.
- Peixoto, J.P., and A.H. Oort, 1992: *Physics of climate*. Springer-Verlag, New York Berlin Heidelberg, 520pp.
- Petterssen, S., 1940: *Weather Analysis and Forecasting*. McGraw-Hill, p. 221-223.
- Quiroz, R.S., 1977: Tropospheric-stratospheric polar vortex breakdown of January 1977. *Geophys. Res. Lett.*, **4**, 151-154.

- Rind, D., R. Suozzo, N.K. Balachandran, and M.J. Prather, 1990: Climate change and the middle atmosphere. Part I: The doubled CO₂ climate. *J. Atmos. Sci.*, **47**, 475-494.
- Rind, D., D. Shindell, P. Lonergan, and N.K. Balachandran, 1998: Climate change and the middle atmosphere. Part III: The doubled CO₂ climate revisited. *J. Clim.*, **11**, 876-894.
- Rind, D., P. Lonergan, N.K. Balachandran, and D. Shindell, 2002: 2 × CO₂ and solar variability influences on the troposphere through wave-mean flow interactions. *J. Meteor. Soc. Japan*, **80**, 811-830.
- Roeckner, E., K. Arpe, L. Bengtsson, M. Christoph, M. Claussen, L. Dümenil, M. Esch, M. Giorgetta, U. Schlese, and U. Schulzweida, 1996: The atmospheric general circulation model ECHAM4: Model description and simulation of present day climate. *MPI Rep.*, **218**, 90 pp., Hamburg, Germany.
- Rosenlof, K.H., and J.R. Holton, 1993: Estimates of the stratospheric residual circulation using the downward control principle. *J. Geophys. Res.*, **98**, 10465-10479.
- Scaife, A.A., N. Butchart, M. Bourqui, J. de Grandpre, S. Hare, J. Kettleborough, U. Langematz, E. Manzini, F. Sassi, K. Shibata, D. Shindell and M. Sigmond, 2003: Model intercomparison of climate change in troposphere-stratosphere mass exchange, *in preparation*.
- Scheele, M.P., P.C. Siegmund and P.F.J. van Velthoven, 1996: Sensitivity of trajectories to data resolution and its dependence on the starting point: in or outside a tropopause fold. *Meteorol. Appl.*, **3**, 267-273.
- Shapiro, M.A., 1980: Turbulent mixing within tropopause folds as a mechanism for the exchange of chemical constituents between the stratosphere and troposphere. *J. Atmos. Sci.*, **37**, 994-1004.
- Shindell, D.T., D. Rind, and P. Lonergan, 1998: Increased polar stratospheric ozone losses and delayed eventual recovery owing to increasing greenhouse-gas concentrations. *Nature*, **392**, 589-592.
- Shindell, D.T., R.L. Miller, G. Schmidt, and L. Pandolfo, 1999: Simulation of recent northern winter climate trends by greenhouse-gas forcing. *Nature*, **399**, 452-455.
- Shindell, D.T., G.A. Schmidt, R.L. Miller, and D. Rind, 2001: Northern Hemisphere winter climate response to greenhouse gas, ozone, solar, and volcanic forcing. *J. Geophys. Res.*, **106**, 7193-7210.
- Siegmund, P.C., P.F.J. van Velthoven and H. Kelder, 1996: Cross-tropopause transport in the extratropical northern winter hemisphere, diagnosed from high-resolution ECMWF data. *Q.J.R. Meteorol. Soc.*, **122**, 1921-1941.
- Sigmond, M., J. Meloen, and P.C. Siegmund, 2000: Stratosphere-troposphere exchange in an extratropical cyclone, calculated with a Lagrangian method. *Ann. Geophys.*, **18**, 573-582.

- Sigmond, M., P.C. Siegmund, and H. Kelder, 2003a: Analysis of the coupling between the stratospheric meridional wind and the surface level zonal wind during 1979-93 Northern Hemisphere extratropical winters. *Clim. Dyn.*, **21**, 211-219, doi: 10.1007/s00382-003-0328-2.
- Sigmond, M., P.C. Siegmund, H. Kelder, E. Manzini, 2003b: A simulation of the separate climate effects of middle atmosphere and troposphere CO₂ doubling. *J. Climate*, submitted.
- Spaete, P., D.R. Johnson and T.K. Schaack, 1994: Stratospheric-tropospheric mass exchange during the Presidents' day storm. *Mon. Wea. Rev.*, **122**, 424-439.
- Sprenger, M., and H. Wernli, 2003: A northern hemispheric climatology of cross-tropopause exchange for the ERA15 time period (1979-1993). *J. Geophys. Res.*, **108**, 8521, doi:10.1029/2002JD002636.
- Stohl, A., G. Wotawa, P. Seibert and H. Kromp-Kolb, 1995: Interpolation errors in wind fields as a function of spatial and temporal resolution and their impact on different types of kinematic trajectories. *J. Appl. Meteorol.*, **35**, 2149-2165.
- Thompson, D.W.J., and J.M. Wallace, 1998: The Arctic Oscillation signature in the wintertime geopotential height and temperature fields. *Geophys. Res. Lett.*, **25**, 1297-1300.
- Thompson, D.W.J., and J.M. Wallace, 2000: Annular modes in the extratropical circulation. Part I: Month-to-month variability. *J. Climate*, **13**, 1000-1016.
- Thompson, D.W.J., J.M. Wallace, and G.C. Hegerl, 2000: Annular modes in the extratropical circulation. Part II: Trends. *J. Climate*, **13**, 1018-1036.
- Thompson, D.W.J., and J.M. Wallace, 2001: Regional climate impacts of the Northern Hemisphere Annular Mode. *Science*, **293**, 85-89.
- Thompson, D.W.J., M.P. Baldwin, and J.M. Wallace, 2002: Stratospheric connection to Northern Hemisphere wintertime weather: implications for prediction. *J. Climate*, **15**, 1421-1428.
- Trenberth, K.E., 1991: Climate diagnostics from global analyses: Conservation of mass in ECMWF Analyses. *J. Climate*, **4**, 707-722.
- Wallace, J.M., 2000: North Atlantic Oscillation/Northern Hemisphere annular mode, 2000: One phenomenon, two paradigms. *Q. J. Roy. Met. Soc.*, **126**, 791-805.
- Wei, M.-Y., 1987: A new formulation of the exchange of mass and trace constituents between the stratosphere and Troposphere. *J. Atmos. Sci.*, **44**, 3079-3086.
- Wernli, H., and H.C. Davies, 1997: A Lagrangian-based analysis of extratropical cyclones. I: The method and some applications, *Q.J.R.Meteorol. Soc.*, **123**, 467-489.

Wirth, V. and J. Egger, 1999: Diagnosing extratropical synoptic-scale stratosphere-troposphere exchange: A case study. *Q.J.R. Meteorol. Soc.*, **125**, 635-655.

WMO, 1995: 'Scientific assessment of ozone depletion: 1994'. Global ozone research and monitoring project, Report No. 37 World Meteorological Organization, Geneva, Switzerland.

Nawoord

Zo begin je met je promotieonderzoek en voordat je het weet leg je de laatste hand aan je proefschrift. De laatste jaren zijn echt voorbij gevlogen. Ik heb me bezig mogen houden met interessant klimaatonderzoek in een stimulerende, interessante onderzoeksomgeving. Bovendien heb ik erg genoten van de mogelijkheden om mijn werk te presenteren op internationale conferenties (Den Haag, Mar del Plata, Utrecht, Nice, Sapporo) en van het bezoeken van - en samenwerken met collega's in Hamburg, Bracknell en Bologna. Met veel goede herinneringen kan ik terugkijken op deze mooie tijd.

Vijf jaar geleden begon ik mijn afstudeeronderzoek op het onderwerp stratosfeer-troposfeer-uitwisseling. De negen maanden die ik hieraan spendeerde bevielen mij zo goed dat ik het aanbod om aan de Technische Universiteit Eindhoven promotieonderzoek te gaan doen met beide handen aangreep. Aangezien de meeste klimaatexpertise op het KNMI ligt, heb ik veruit de meeste onderzoekstijd in De Bilt doorgebracht.

Terugkijkend valt me op dat ik de resultaten van mijn onderzoek steeds gemakkelijker aan familie en vrienden heb kunnen uitleggen. Dit kwam niet zozeer doordat mijn didactische vaardigheid of de wetenschappelijke kennis van mijn toehoorders toenam, maar eerder doordat het onderwerp steeds concreter werd. Vijf jaar geleden begon ik mijn onderzoek met het zoeken naar een verklaring voor het feit dat de potentiële vorticeiteit langs trajectoriën fluctueert. Vervolgens heb ik samen met anderen een methode ontwikkeld om stratosfeer-troposfeeruitwisseling te kwantificeren. In een volgend onderzoek heb ik geanalyseerd via welk mechanisme variaties in de stratosfeer invloed hebben op variaties in de troposfeer en dus, indirect, op het weer zoals we dat ervaren. De resultaten van mijn laatste onderzoek bevestigen vermoedens dat de versterking van de troposferische westenwinden (die in de winter zorgen voor een opwarming van West-Europa) grotendeels toegeschreven kan worden aan stratosferische klimaatveranderingen.

Het resultaat van die jaren onderzoek heeft u in uw handen. Een groot aantal mensen heeft in meer of mindere mate bijgedragen aan dit onderzoek. Een aantal onder hen wil ik hier bedanken:

Allereerst Peter Siegmund. Het vooruitzicht van jou als begeleider was vier jaar geleden één van de redenen om te kiezen voor dit promotieonderzoek. Al tijdens mijn stageperiode heb ik ervaren dat je een geboren talent hebt om mensen te begeleiden in het onderzoek. Je komt met interessante ideeën, je motiveert, je corrigeert en je creëert altijd genoeg tijd voor je studenten. Een betere begeleider kon ik me niet wensen, bedankt!

Mijn eerste promotor Hennie Kelder wil ik bedanken voor de mogelijkheid die je hebt gecreëerd om dit onderzoek te kunnen doen. Bedankt voor de vrijheid en het vertrouwen dat je me hebt gegeven, en de interesse die je hebt getoond. Ook Frans Sluijter (mijn tweede

promotor) en Leon Kamp wil ik bedanken voor de getoonde interesse en de nuttige commentaren.

Voorts ben ik Hans Cuijpers veel dank verschuldigd. Als kamergenoot en modelondersteuner heb je veel bijgedragen aan het soepele verloop van het onderzoek. Dank je voor je hulp en succes met je nieuwe baan! Peter van Velthoven wil ik bedanken voor de nuttige discussies over - en commentaren op mijn onderzoek. Ondanks het feit dat je altijd druk bent heb je altijd tijd vrij kunnen maken. Rinus Scheele mag ik ook niet vergeten te bedanken voor de hulp die ik heb gekregen bij het runnen van het trajectoriënmodel.

Ook met Rob van Dorland, Klearity Tourpali, Geert-Jan Roelofs, Cor Schuurmans, Maarten van Aalst, Bram Bregman, Neal Butchart en Adam Scaife heb ik nuttige, interessante discussies gevoerd.

I would like to thank Elisa Manzini for giving me the possibility to work with a state-of-the-art General Circulation Model. Thanks also for the interesting discussions and your hospitality during my trips to Hamburg and Bologna!

Natuurlijk wil ik alle collega's uit de gezelligste groep van het KNMI (AS) bedanken. Het lunchgroepje (o.a. Bas, Dirk, Ernst, Gabriella, Gé, Hans, Jeroen, Jojanneke, Jos, Mijke, Paul, Pieter, Renske, Twan) maakte de lunches tot een aangename onderbreking van de werkdag. Michel wil ik nog bedanken voor de hulp voor wat betreft TUE-zaken.

Mijn voormalige 'Zeister achterban' (Wim, Martin, Bart, Johan) is ook de laatste jaren 'hondstrouw' (inside joke) gebleken. Daarnaast wil ik ook Peet, Henry en mijn andere vrienden bedanken voor jullie vriendschap en interesse in wat ik doe.

Tot slot wil ik mijn ouders, oma's en zus bedanken voor jullie onmisbare steun.

Curriculum vitae

Op 12 juni 1976 zag ik te Arnhem het levenslicht. Als kleine jongen werd al duidelijk dat ik iets exacts moest gaan doen. Buslijnummers en digitale horloges intrigeerden me al op zeer jonge leeftijd. Tijdens onze lange autoreizen naar Zuid-Europa wist ik mijn ouders menigmaal te verbazen door alle kwantificeerbare reisgegevens op te schrijven en vervolgens in oneindig grote tabellen te verwerken (gelukkig ben ik inmiddels van deze ‘ziekte’ genezen). In 1994 haalde ik mijn VWO-diploma aan het Christelijk Lyceum Arnhem, om vervolgens te beginnen met de studie natuurkunde aan de Universiteit Utrecht. Na een jaar haalde ik mijn propedeuse en ben ik verder gegaan met de bovenbouwstudie Meteorologie en Fysische Oceanografie, waarbij mijn interesse vooral uitging naar de klimaatfysica. De eerste drie maanden van 1998 heb ik doorgebracht in het Engelse Reading, waar ik aan de lokale universiteit vakken in deze richting volgde. Het laatste jaar van mijn studie (1998-1999) mocht ik stage lopen op het KNMI, temidden van een leuke groep. Dit smaakte naar meer. Toen mij een promotieplaats werd aangeboden aan de Technische Universiteit Eindhoven met als standplaats het KNMI, hoefde ik niet lang na te denken. De afgelopen vier jaar heb ik met veel plezier interessant onderzoek mogen doen, wat geresulteerd heeft in dit proefschrift.

Stellingen behorend bij het proefschrift:

“On the coupling between the stratosphere and the troposphere”

Michael Sigmond, 27 oktober 2003

- I. De met een klimaatmodel gesimuleerde versterking van de troposferische westenwinden op de gematigde breedten van het noordelijk halfrond in de winter ten gevolge van het versterkte broeikaseffect kan grotendeels toegeschreven worden aan stratosferische klimaatverandering (*dit proefschrift, hoofdstuk 2*).
- II. De met een klimaatmodel gesimuleerde versterking van de Brewer-Dobsoncirculatie op het noordelijk halfrond in de winter ten gevolge van het versterkte broeikaseffect kan grotendeels toegeschreven worden aan troposferische klimaatverandering (*dit proefschrift, hoofdstuk 2*).
- III. Ter verbetering van klimaatmodellen is de laatste jaren de nadruk gelegd op het verhogen van de horizontale resolutie, terwijl het verhogen van de verticale resolutie in de hogere luchtlagen ten onrechte onderbelicht is gebleven (*dit proefschrift, hoofdstuk 2*).
- IV. Het systeem troposfeer-stratosfeer kan wat betreft relatieve massa vergeleken worden met het systeem hond-staart. Dat de hond met z'n staart kwispelt wisten we al lang, maar dat de staart ook met de hond kwispelt is pas de laatste jaren duidelijk geworden (*dit proefschrift, hoofdstuk 1,2,3*).
- V. De invloed van de stratosfeer op het Nederlandse weer is groter dan die van El Niño.
- VI. De verwachte versterking van de Brewer-Dobsoncirculatie als gevolg van de toename van broeikasgassen in de atmosfeer zal het herstel van de ozonlaag waarschijnlijk enigszins versnellen.
- VII. De droge, hete Europese zomer van 2003 kan niet rechtstreeks worden toegeschreven aan het versterkte broeikaseffect.
- VIII. Tijdens de basisopleiding van wetenschappers wordt te weinig aandacht besteed aan de mondelinge en schriftelijke presentatie van onderzoeksresultaten.
- IX. Welvaart leidt tot individualisering, maar individualisering hoeft niet tot welzijn te leiden.
- X. De laatste stap van het verstand is het erkennen dat er (op ieder moment) oneindig veel dingen zijn die (dan) het verstand te boven gaan (B. Pascal, *Pensées*).